U.S. Department of Transportation
Federal Railroad Administration

Office of Research, Development and Technology
Washington, DC 20590

Unsaturated Characteristics of Fouled Ballast to Support In Situ Identification of Fouling Using Ground Penetrating Radar – Phase I

DOT/FRA/ORD-22/09

Final Report | February 2022

NOTICE

This document is disseminated under the sponsorship of the Department of Transportation in the interest of information exchange. The United States Government assumes no liability for its contents or use thereof. Any opinions, findings and conclusions, or recommendations expressed in this material do not necessarily reflect the views or policies of the United States Government, nor does mention of trade names, commercial products, or organizations imply endorsement by the United States Government. The United States Government assumes no liability for the content or use of the material contained in this document.

NOTICE

The United States Government does not endorse products or manufacturers. Trade or manufacturers' names appear herein solely because they are considered essential to the objective of this report.

REPORT DOCUMENTATION PAGE

Form Approved
OMB No. 0704-0188

1. REPORT DATE *(DD-MM-YYYY)*	**2. REPORT TYPE**	**3. DATES COVERED** *(From - To)*
February 2022	Technical Report	September 2018–August 2020

4. TITLE AND SUBTITLE

Unsaturated Characteristics of Fouled Ballast to Support In Situ Identification of Fouling Using Ground Penetrating Radar – Phase I

5a. CONTRACT NUMBER

5b. GRANT NUMBER

5c. PROGRAM ELEMENT NUMBER

5d. PROJECT NUMBER

5e. TASK NUMBER

5f. WORK UNIT NUMBER

6. AUTHOR(S)

Stacey E. Kulesza 0000-0003-3283-6235
Michelle L. Barry 0000-0002-0947-5307
Robert R. Sherwood 0000-0001-9737-4508
Anibal Santos 0000-0002-8888-0799

7. PERFORMING ORGANIZATION NAME(S) AND ADDRESS(ES)

Kansas State University, 1701C Platt St, 2118 Fiedler Hall, Manhattan, KS 66506
University of Arkansas, 210 Administration Building, Fayetteville, AR 72701

8. PERFORMING ORGANIZATION REPORT NUMBER

KSU-UoA-2020-Phase-I

9. SPONSORING/MONITORING AGENCY NAME(S) AND ADDRESS(ES)

U.S. Department of Transportation
Federal Railroad Administration
Office of Railroad Policy and Development
Office of Research, Development and Technology
Washington, DC 20590

10. SPONSOR/MONITOR'S ACRONYM(S)

11. SPONSOR/MONITOR'S REPORT NUMBER(S)

DOT/FRA/ORD-22/09

12. DISTRIBUTION/AVAILABILITY STATEMENT

This document is available to the public through the FRA website.

13. SUPPLEMENTARY NOTES

COR: Hugh Thompson

14. ABSTRACT

This research established a protocol for sample preparation and testing between a large suction water characteristic curve (SWCC) device and a large-scale direct shear (LSDS) device using clean ballast and fouling material collected from mainline track. This allowed for comparisons of strength and volumetric behavior at volumetric water contents from the SWCCs. Preliminary results indicate the characteristics of the fouling material control the unsaturated characteristics of fouled ballast. Meaningful changes in peak stress were observed at different volumetric water contents in 5 percent fouled specimens, where the water contents were bound by the SWCC measurements.

15. SUBJECT TERMS

Ballast stability detection technology, suction water characteristic curves, SWCC, large-scale direct shear, LSDS, ballast, fouling, track

16. SECURITY CLASSIFICATION OF:			**17. LIMITATION OF ABSTRACT**	**18. NUMBER OF PAGES**	**19a. NAME OF RESPONSIBLE PERSON**
a. REPORT	**b. ABSTRACT**	**c. THIS PAGE**			Hugh B. Thompson
					19b. TELEPHONE NUMBER *(Include area code)* (202) 493-6383

Standard Form 298 (Rev. 8/98)
Prescribed by ANSI Std. Z39.18

METRIC/ENGLISH CONVERSION FACTORS

ENGLISH TO METRIC

LENGTH (APPROXIMATE)

1 inch (in)	=	2.5 centimeters (cm)
1 foot (ft)	=	30 centimeters (cm)
1 yard (yd)	=	0.9 meter (m)
1 mile (mi)	=	1.6 kilometers (km)

AREA (APPROXIMATE)

1 square inch (sq in, in^2)	=	6.5 square centimeters (cm^2)
1 square foot (sq ft, ft^2)	=	0.09 square meter (m^2)
1 square yard (sq yd, yd^2)	=	0.8 square meter (m^2)
1 square mile (sq mi, mi^2)	=	2.6 square kilometers (km^2)
1 acre = 0.4 hectare (he)	=	4,000 square meters (m^2)

MASS - WEIGHT (APPROXIMATE)

1 ounce (oz)	=	28 grams (gm)
1 pound (lb)	=	0.45 kilogram (kg)
1 short ton = 2,000 pounds (lb)	=	0.9 tonne (t)

VOLUME (APPROXIMATE)

1 teaspoon (tsp)	=	5 milliliters (ml)
1 tablespoon (tbsp)	=	15 milliliters (ml)
1 fluid ounce (fl oz)	=	30 milliliters (ml)
1 cup (c)	=	0.24 liter (l)
1 pint (pt)	=	0.47 liter (l)
1 quart (qt)	=	0.96 liter (l)
1 gallon (gal)	=	3.8 liters (l)
1 cubic foot (cu ft, ft^3)	=	0.03 cubic meter (m^3)
1 cubic yard (cu yd, yd^3)	=	0.76 cubic meter (m^3)

TEMPERATURE (EXACT)

[(x-32)(5/9)] °F = y °C

METRIC TO ENGLISH

LENGTH (APPROXIMATE)

1 millimeter (mm)	=	0.04 inch (in)
1 centimeter (cm)	=	0.4 inch (in)
1 meter (m)	=	3.3 feet (ft)
1 meter (m)	=	1.1 yards (yd)
1 kilometer (km)	=	0.6 mile (mi)

AREA (APPROXIMATE)

1 square centimeter (cm^2)	=	0.16 square inch (sq in, in^2)
1 square meter (m^2)	=	1.2 square yards (sq yd, yd^2)
1 square kilometer (km^2)	=	0.4 square mile (sq mi, mi^2)
10,000 square meters (m^2)	=	1 hectare (ha) = 2.5 acres

MASS - WEIGHT (APPROXIMATE)

1 gram (gm)	=	0.036 ounce (oz)
1 kilogram (kg)	=	2.2 pounds (lb)
1 tonne (t)	=	1,000 kilograms (kg)
	=	1.1 short tons

VOLUME (APPROXIMATE)

1 milliliter (ml)	=	0.03 fluid ounce (fl oz)
1 liter (l)	=	2.1 pints (pt)
1 liter (l)	=	1.06 quarts (qt)
1 liter (l)	=	0.26 gallon (gal)
1 cubic meter (m^3)	=	36 cubic feet (cu ft, ft^3)
1 cubic meter (m^3)	=	1.3 cubic yards (cu yd, yd^3)

TEMPERATURE (EXACT)

[(9/5) y + 32] °C = x °F

QUICK INCH - CENTIMETER LENGTH CONVERSION

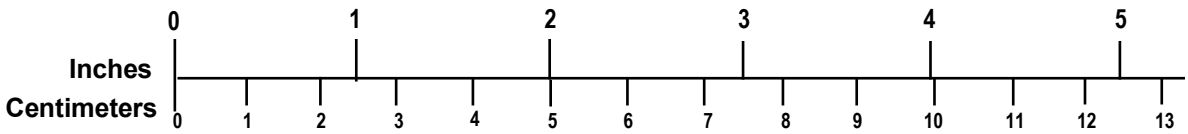

QUICK FAHRENHEIT - CELSIUS TEMPERATURE CONVERSIO

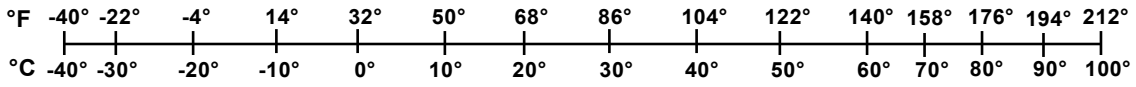

For more exact and or other conversion factors, see NIST Miscellaneous Publication 286, Units of Weights and Measures. Price $2.50 SD Catalog No. C13 10286

Updated 6/17/98

Acknowledgements

The authors would like to acknowledge project partner, Robert Banister, for providing feedback on the technical approach and sample selection. The authors would also like to acknowledge Hugh Thompson of the Federal Railroad Administration and Ted Sussmann of the Volpe National Transportation Systems Center for their advice and support during this project. Finally, thank you to BNSF Railway, MetroLink, and Mill Creek Quarry for donating project materials.

Contents

Illustrations

Tables

Executive Summary

From September 2018 through August 2020, the Federal Railroad Administration funded Kansas State University and the University of Arkansas to establish the electromagnetic, suction, and strength characteristics of fouled ballast as a function of the fouling material, volumetric water content, and density. The testing in Phase I was divided into two parts: Kansas State University (Manhattan, KS) was responsible for the suction characteristics, and the University of Arkansas (Fayetteville, AR) was responsible for preliminary strength measurements.

Researchers used a total of 14 fouling materials in this research, 12 samples were collected from mainline track in the Midwest and 2 were collected from track in California. Seven of the 14 samples were clean sands with similar particle size distributions and 2 samples contained silt (i.e., a silty sand and a sandy silt). Five samples were suspected to contain coal dust based on where they were collected and a thermogravimetric analysis verified this. Seven representative samples were chosen for analysis and discussed in the body of this report, while the appendix presents the information for the remaining seven samples. Additionally, a quarry in Oklahoma that sources Class I ballast supplied clean, granitic ballast.

Suction water characteristic curves (SWCCs) were determined for the fouling materials. The influence of coal dust on the SWCC parameters was identified. Although three of the coal samples classified as silty, clayey sand (SC-SM) and two as low plasticity clay (CL), the SWCC results were more variable. The specimen that had the highest percentage of coal also had the highest water holding capacity. Phase I marked the first time that the unsaturated characteristics of fouling materials were measured in this way and it provided a means of differentiating the unique features of fouling materials that otherwise would traditionally appear similar based on geotechnical classification. Theoretical SWCCs were simulated based on the results of the fouling material. A custom large-volume cell was developed for measuring the SWCCs of fouled ballast and was validated with the fouled ballast numerical results. The research team found that the characteristics of the fouling material appear to control the unsaturated behavior (i.e., water holding capacity) of the fouled ballast. This has important implications for Phase II where the team will vary the percent fouling as well as test additional ballast mineralogies and fouling materials.

Sample preparation and testing methodologies protocols between the large SWCC measurement device and the large-scale direct shear (LSDS) were determined to ensure directly comparable results. An 85 percent maximum relative density was possible in the SWCC cell. A similar preparation protocol was matched in the LSDS specimens to achieve a similar initial packing. Specimens in the LSDS tests were prepared at the saturated volumetric water content, based on the SWCC of the fouling materials, and could air dry to the residual water content while running tests at the points in between. This allowed for comparisons of strength and volumetric behavior at volumetric water contents measured with the SWCC device. As determined in both the LSDS and SWCC, it is more meaningful to track the water content of the fouling materials than the bulk of the fouled ballast. The fouling materials influence the water holding capacity of the fouled ballast and will also likely be the main indicator of ballast strength in Phase II. Based on preliminary LSDS results, researchers found that one stress level was sufficient to describe the influence of fouling and moisture on strength. An observation of meaningful changes in peak stress took place at different volumetric water contents in 5 percent fouled specimens, where the

SWCC measurements were used to bound the water contents, although additional testing is needed to draw distinct conclusions.

SWCC results on specimens without coal dust closely matched established SWCC parameters from the literature. There is limited information about the SWCC of soil fouled with coal dust, as most research has focused on pure coal dust. Thus, these findings are new. Experimental and numerical SWCC results highlight how the parent fouling material controls the water holding capacity of fouled ballast, an important finding regarding electromagnetic properties to be measured in Phase II. The research team established the experimental setup and specimen preparation procedures for specimens in the large SWCC cell and the LSDS to ensure congruence between the two experiments to establish the electromagnetic, suction, and strength characteristics of fouled ballast.

1. Introduction

This report includes the Phase I results of Kansas State University's suction water characteristic curves (SWCC) of ballast fouling materials, as well as a proof of concept new testing protocol for SWCC of fouled ballast specimens. The report also includes results from the University of Arkansas' new protocol for large-scale direct shear (LSDS) testing of fouled ballast specimens at a target water contents. The Federal Railroad Administration (FRA) funded this research from September 2018 through August 2020. The research team conducted the experiments at Kansas State University in Manhattan, KS, and the University of Arkansas in Fayetteville, AR.

Project partners collected the fouling materials from track in the Midwest and California. The University of Arkansas obtained additional clean ballast from a quarry in Oklahoma, which serves as a major ballast source for track in that region. Kansas State University measured SWCCs on 14 ballast fouling materials using a 66.0 mm tall by 61.8 mm diameter flow cell and using the transient water release and imbibition method (TRIM) at a constant density. The SWCCs of fouled ballast specimens were predicted using the results from the fouling material SWCCs and a large particle correction procedure. Kansas State University developed a custom 178 mm tall by 255 mm diameter flow cell for measuring SWCCs of fouled ballast (with aggregate sizes up 42.5 mm, nominal diameter) compacted to a target ballast density. The University of Arkansas measured the shear stress and volumetric response of clean and fouled ballast specimens compacted to the same target ballast density, percent fouling, and observed range of volumetric water contents from the SWCC. In this study, researchers want to link the mechanical response with the SWCCs to better understand the controlling factors of strength loss due to ballast fouling that are identifiable by electromagnetic measurements. This report provides a summary of Phase I results and how these results were used to develop the Phase II experimental procedures for achieving the objective.

1.1 Background

FRA and the rail industry have recognized the potential of using ground penetrating radar (GPR) for providing real time, automatic mapping of ballast condition to identify the need for remediation [1]. Although extensive research on GPR for identifying fouled ballast exists, the focus of previous studies is on experimental setup, selecting the antenna frequencies, and time-based versus frequency-based analyses [2] [3] [4] [5]. Others have quantified the degree and type of ballast fouling in controlled experimental conditions [6] [7]; however, GPR measurements are a function of the material dielectric constant, which is heavily influenced by the moisture and fouling conditions [8] [9]. The influence of both moisture and the type of parent fouling material on the dielectric constant can make field interpretations difficult.

Sahin et al. [10] showed that correlations between dielectric constant and the SWCC can aid reliable, quantitative GPR evaluation of volumetric water content in road base materials. SWCCs define the constitutive relationship between moisture condition and matric suction of geomaterials (e.g., like fouled ballast). The SWCC is also correlated with engineering behavior (e.g., permeability, strength, and stiffness). SWCCs are influenced by factors associated with fouling such as grain size distribution, density, and mineralogy [11] [12] [13] [14]. This research established the water holding capacity of ballast fouling material. As ballast nominal size limits the use of traditional experimental methods, this research also focused on novel equipment for measuring the water holding capacity of fouled ballast and sample preparation between two

different devices. There is a need to quantify how the fouling material and changes in moisture affect the strength and stability of the ballast. There are anecdotal cases of fouled ballast that show no detectible changes in track geometry and no loss of support, despite the reduced drainage capacity. Therefore, the University of Arkansas also measured the shear stress and volumetric response of clean and fouled ballast specimens prepared at the same ballast density and percent fouling as the SWCC experiments and at a range of target water contents. This research established the protocol for Phase II testing of SWCCs of fouled ballast and linking them to the corresponding mechanical response and electromagnetic signatures.

1.2 Objectives

The objective of this research is to establish the electromagnetic, suction, and strength characteristics of fouled ballast as a function of the fouling material, moisture content, and density. This will improve our fundamental understanding of ballast degradation characteristics, non-destructive identification of fouled ballast in the field, and ultimately improve the performance and safety of the track structure.

1.3 Overall Approach

Conducting laboratory experiments allowed the characterization of fouling materials and obtaining geotechnical properties including particle size distribution, Atterberg limits, and Unified Soil Classification System (USCS) group classification. This study established the sample preparation protocol with the fouled ballast in two different devices and the results were used to guide Phase II to achieve the primary objective. Specifically, researchers conducted the following tests to establish the unsaturated characteristics of the fouled ballast:

- SWCCs were obtained for fouling materials using a small-cell and TRIM. A large cell was then developed and validated and is capable of obtaining SWCCs for fouled ballast.
- The strength of fouled ballast was determined using a large-scale direct shear machine under similar moisture, density, and fouling conditions tested in the large-cell TRIM testing.

1.4 Scope

This work includes 7 SWCC tests on fouling materials, 2 SWCC tests on fouled ballast, 14 simulated SWCCs of fouled ballast, 6 LSDS tests on clean ballast, and 8 LSDS tests on fouled ballast with moisture. Additional experimental results are included in the appendices. The work focused on one type of ballast and likely does not include all fouling materials.

1.5 Organization of the Report

Section 2 provides a brief literature review of unsaturated geomaterials and experimental methods. Section 3 describes the methodology, Section 4 includes results and analysis, and Section 5 provides the Phase I conclusions and how this study will guide Phase II. Results of the material characteristics of all samples are include in Appendix A. Additional SWCC experiments not included for clarity are found in Appendix B.

2. Unsaturated Materials

Studies show that as clean ballast become fouled the behavior degrades and it becomes complex. Fouled ballast can be dry in persistently arid regions and it can be saturated during rain events or flooding [15]. Clay fouled ballast can behave elastically when dry and then plastically when wet [16]. Often fouled ballast are exposed to fluctuating environmental conditions keeping the material in an unsaturated state of drying or wetting [15] [17]. Materials similar to fouled ballast (e.g., in gradation and/or mineralogy) experience negative pore water pressure under these drying and wetting conditions [18] [19]. The general nature of unsaturated material gives insight to this complexity, but little research has been done to quantify the unsaturated characteristics of fouled ballast [20] [21].

2.1 Soil Water Characteristic Curves

The SWCC relates the stress states of unsaturated soil (i.e., matric suction) to its moisture conditions (i.e., volumetric water content) [22]. A SWCC is generally sigmoidal in shape but can be unimodal or bimodal. The SWCC describes three phases of an unsaturated soil: the saturated condition, transition phase (i.e., drying, or wetting condition), and residual condition. SWCCs can be measured as a material dries or wets; this research focused on the drying phase, future research may consider wetting and any measured hysteresis. SWCCs also quantify four parameters: saturated volumetric water content, air entry, distribution of pore size, and the residual volumetric water content. The SWCC (i.e., shown as a solid black ‘S’ shaped line) in Figure 1 shows the three phases. The four parameters are also labeled. The saturated volumetric water content is the volume of water within the saturated soils pore network, divided by the total sample volume. Geomaterial pores have the matric potential to retain the full volume of this water over a range of suction heads. The pore networks matric potential gives rise to the saturated phase in the SWCC. Eventually the materials potential to stay saturated is overcome and the SWCC begins to break to the left as air begins to displace the pore water. The suction head at which this break occurs is the air entry value. The air entry value is evaluated at the intersection of two straight lines plotted tangent to 1) the saturated phase of the SWCC and 2) the slope of the transition phase. Therefore, air entry is the start of the transition phase (i.e., in this case, the draining phase).

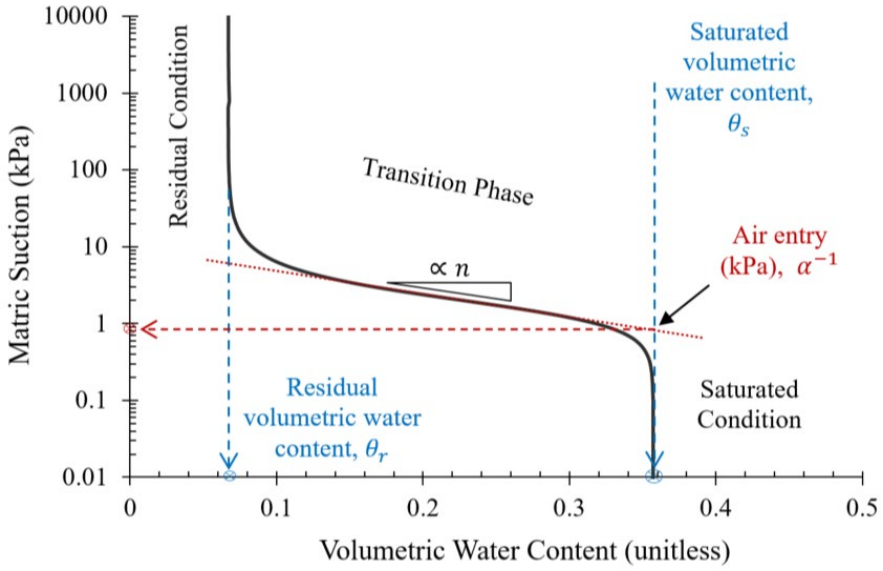

Figure 1. Typical SWCC with measured parameters

The draining phase is the central portion of the SWCC; the slope may be shallow (as shown in Figure 1) or steeper. Liquid and gas phases are continuous through the pore network during the transition phase; the continuity within each fluid phase facilitates the flow of each fluid: liquid water can flow out of the sample where liquid water is continuous and air into the sample where air is continuous. This flow takes place within a range of suction values in excess of air entry. The slope of the transition phase is characteristic of the samples pore size distribution. SWCCs with a small slope in the transition phase (i.e., nearly horizontal) are characteristic of samples having a narrow pore size distribution. In response, the samples moisture condition will transition from the saturated condition to the residual condition over a narrow range of suction values. The residual condition is characterized by a discontinuous liquid phase and continuous gas phase within the pore network. During the residual phase, liquid water stops draining out of a sample, however, it may still leave the sample in the vapor state [11]. Material in the residual condition will be highly sensitive to addition of water, readily taking in (imbibing) water whenever and wherever water is available (e.g., rain event). The volumetric water content and suction corresponding to the start of the residual phase are the residual volumetric water content and the residual suction pressure, respectively.

The SWCC is a function of many soil parameters controlling the pore network (e.g., material gradation and density). As particle sizes decrease and dry density increases, the air entry and residual pressures and residual volumetric water content typically increase [12] [23] [24]. As a result, the SWCC can be very distinctive in its form (i.e., shape and placement) depending on the soil parameters. Wayllace and Lu [25] proposed a TRIM which was used in this research to determine the SWCC. The SWCC is created using inverse modeling of data measured from the TRIM, measured hydraulic parameters, and a hydraulic model. The van Genuchten model was used in this research [26]. The van Genuchten model fits the behavior of most soils and is commonly used to evaluate unsaturated soil behavior [19] [25] [27], including the unsaturated characteristics of highly fouled ballast [21]. The van Genuchten model is:

$$\boldsymbol{\theta(\psi) = \theta_r + (\theta_s - \theta_r)\left(\frac{1}{1 + (\alpha * \psi)^n}\right)^m}$$

where, $\theta(\psi)$ is the SWCC, θ_s is the saturated volumetric water content, θ_r is the residual volumetric water content, α, n, and m are fitting parameters, and ψ (kPa) is any soil suction. The van Genuchten SWCC model uses the residual volumetric water content as a fitting parameter. The residual phase of the SWCC should not be used for interpretation of the soil's behavior outside of it being the "maximum amount of water in a soil that will not contribute to liquid flow" [11]. While the van Genutchten model was utilized in Phase I it is anticipated that other models that can account for dual porosity will need to be explored depending on the degree of fouling in Phase II. Dual porosity was not considered in the fouled samples in Phase I because the experimental samples tested were highly fouled (i.e., 50% by mass) so that the results could be compared to the simulated SWCCs. Cui [21] similarly measured the unsaturated characteristics of the "interlayer" between ballast and subgrade which resembled a highly fouled (~40% by mass) ballast. Cui also compared the water retention curves of fines with the interlayer. Though the results were limited, they support the findings of one fouling material tested in this research.

2.2 Large-scale Direct Shear Testing

An extensive amount of literature regarding strength testing of large aggregates and aggregate mixes is available within the rail and geotechnical communities. For brevity, the discussion here only includes select examples that guided the decisions and testing methodology used in this study. Previous studies on ballast strength focused on large-scale direct shear (LSDS) testing [28] [29], and triaxial shear testing [30] [31] [32]. LSDS tests are simple and straightforward to conduct and analyze, and the device allows for rotation of the principal planes, which is an important characteristic of field loading conditions. However, LSDS testing can overestimate the strength of granular materials because the forced horizontal failure plane may not represent the weakest plane. While triaxial testing allows for identification of the weakest failure plane, the results can be influenced by penetration of the membrane confining the sample and the test cannot replicate the smooth rotation of the principal planes. Therefore, this study focused on LSDS testing as a step towards large-scale direct simple shear (LSDSS) in Phase II.

Direct shear devices consist of a shear box, either circular or square in cross-section that is divided into two halves by a horizontal plane. There are several different device configurations. Studies have shown that these configurations can affect the specimen boundary conditions and thus, the observed behavior [33] [34], although there is little discussion or guidance on this in the American Society for Testing and Materials (ASTM) standards. The specimen size is also an important parameter, as specimen size to maximum particle size ratios below that specified in ASTM 3080 have been shown to falsely exhibit significant apparent cohesion [29] [35] [36] [37].

Previous LSDS testing has considered both clean and fouled ballast specimens [28] [38] [39]. As discussed in Selig and Waters [40], ballast breakdown accounts for up to 76 percent of the fouling on average, with an estimated 13 percent coming from infiltration from subballast, 7 percent due to infiltration from the ballast surface, 3 percent from subgrade intrusion, and 1 percent due to tie wear. The degree or percentage of fouling affects both the settlement and strength characteristics of the ballast material. Huang et al. [38] described three critical phases

for ballast fouling (Figure 2). Phase I is represented by a clean or only slightly fouled ballast sample where most ballast aggregate particles are in contact with one another and little effect of fouling is observed. Phase II is characterized by a higher degree of fouling within the voids leading to some of the fouling material being present at the ballast contacts and a significant reduction in the strength; however, most of the aggregate-to-aggregate contacts are still maintained. Phase III represents the condition when the voids are completely filled with fouling material and most of the aggregate-to-aggregate contacts are eliminated. The third phase has been criticized as it is not likely to occur in real field track conditions and will not be examined in this study. The threshold where critical strength loss occurs as fouling moves from Phase I to Phase II is of particular interest and is currently not well understood as it relates to the unsaturated characteristics.

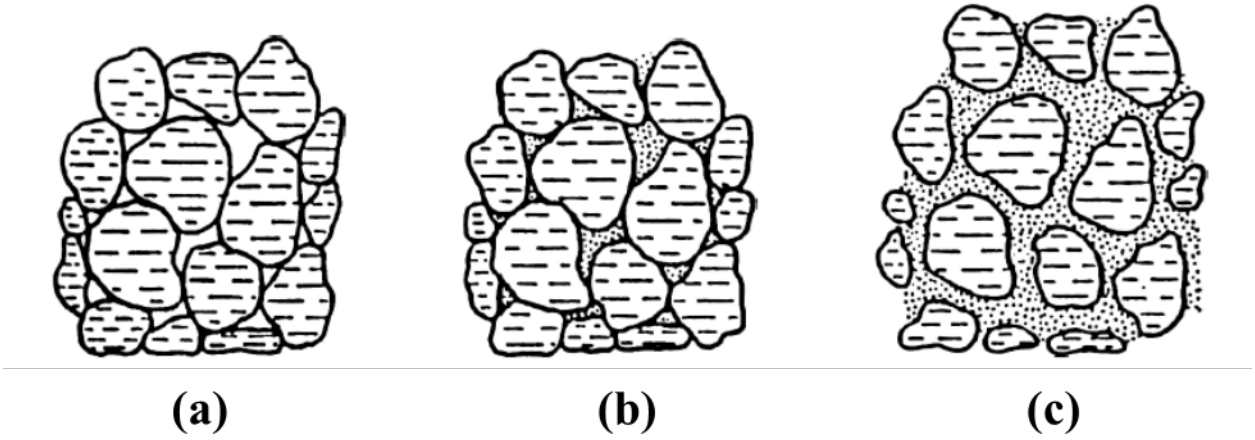

Figure 2. Schematic representation of critical fouling phases for (a) Phase I, (b) Phase II, and (c) Phase III

The percentage of fouling, as proposed by Sevi et al. [40], is the ratio of the dry weight of material passing the 9.5 mm (3/8 in.) sieve to the dry weight of the total sample. This is the primary index used and reported in this study. Huang et al. [38] tested clean, coal fouled, and mineral fouled ballast at various degrees of fouling and moisture conditions and showed that clean ballast had the highest shear strength and fouling of only 5 percent was shown to reduce the strength (i.e., mostly through a reduction in friction angle). The coal fouling led to the highest reduction in strength and wet fouling generally resulted in lower strengths than dry fouling. For 25 percent wet coal dust fouling, the strength results of the fouled ballast were equivalent to the properties of the coal dust itself. Tutumluer et al. [28] showed that 25 percent coal fouling by weight was enough to fill all the voids in the ballast which further explains why this behavior was more aligned with the Phase III condition. More testing is needed, however, to further explain the Phase I and II behaviors. Note that the dimensions of the shear box used in many of the tests by previous researchers were below the particle to specimen size threshold required in ASTM D3080. Estaire and Santana [29] state that the use of smaller shear boxes can produce an increase in shear strength of 40 to 60 percent. This should be considered when comparing tests from the literature. All the tests in this study were within the specified particle size to specimen size ratios according to ASTM 3080. The fouling and moisture conditions tested also aim to further explore the Phase I to II behavior thresholds.

3. Methods

BNSF Railway (BNSF), Metrolink, and Martin Marietta donated the materials for this research. A testing protocol was developed for measuring SWCCs of fouling material and to enable measurements on fouled ballast using a new experimental device. A testing protocol was developed for the LSDS tests to ensure percent fouling, density, and water content matched those of the fouled ballast SWCC tests.

3.1 Materials

All materials were collected via excavation from mainline track or donated directly from a quarry. The clean granitic ballast was from a quarry in Oklahoma. Seven one-gallon samples of processed ballast breakdown were also used. Processed ballast breakdown is ballast fouling material (i.e., materials that passed at 3/8" sieve) that have been washed to determine the percent of fines (i.e., material passing the No. 200 sieve), as per routine ballast inspection. Nine additional 5-gallon samples of fouled ballast were also used. The fouled ballast samples were a combination of ballast, ballast breakdown, and fines (i.e., clay, silt, and coal). The fouling materials sieved from the fouled ballast samples collected from mainline track in the Midwest were dark grey in color suggesting the presence of dark colored fines such as coal. The fouling materials from the California samples were light brown and two smelled strongly of fertile soil. Each sample was sieved into constituents where appropriate (i.e., clean ballast separated from fouling materials). Washing the ballast removed any fouling material adhered to the ballast. All materials were oven dried for at least 24 hours at 108 °C to ensure there was no residual moisture prior to testing.

3.1.1 Material Characterization & Classification

Each sample was characterized with the following: grain size distribution [41] [42], Atterberg limits as required [43], specific gravity [44], and saturated hydraulic conductivity [45] [46]. Each fouling material was classified using the USCS. Ballast aggregate gradation was designed to meet American Railway Engineering and Maintenance-of-Way Association (AREMA) #4A gradation standards [47]. Ballast fouling conditions were regulated by controlling the percent mass passing the No. 3/8" sieve, noted as percent fouling. Each fouled ballast was classified using the Selig Fouling Index,

$$\boldsymbol{F_1 = P_4 + P_{200}}$$

where P_4 is the percent mass passing the No. 4 sieve (4.75 mm), and P_{200} is the percent mass passing the No. 200 sieve (0.075 mm) [40].

Fouling materials suspected of coal content were characterized using thermogravimetric analysis (TGA) [48]. TGA was conducted on the portion of each material passing the No. 40 sieve. Approximately 10 milligrams was heated in the TGA apparatus from ambient temperature to 850 °C at 10 °C per minute. A platinum massing tray was used to hold the material in the furnace, and the testing system was continually purged with nitrogen gas to prevent ignition of materials. The balance purge flow and sample purge flow rates were set to 20 mL min.-1 and 80 mL min.-1, respectively. Mass change of the sample, due to materials volatizing, was recorded as a function of time and temperature. The first order derivative of the mass change vs. temperature was analyzed to identify temperatures which induced the greatest change in mass. These values

of the greatest mass change were compared to the literature on coal to validate presence of coal. The percent mass of volatile matter was calculated over temperatures which volatize coal (i.e., the area under a percent-mass vs. temperature curve between 300 and 800 °C).

3.2 TRIM Testing

The TRIM test [25] was used to measure SWCCs on all the fouling materials and fouled ballast samples. The size of the flow-cell that came standard with the TRIM was 66.0 mm tall and 61.8 mm in diameter (i.e., small cell). The small cell was used to test the fouling materials. A custom cell was used to measure SWCCs of samples with ballast aggregate. The custom large flow cell was 178 mm tall and 255 mm in diameter. Cell dimensions limit aggregate size to 42.5 mm [49] which is appropriate for AREMA #4 graded ballast, where the largest nominal particle size is 38.1 mm [47]. Figure 3 shows the small and large cells used in this research.

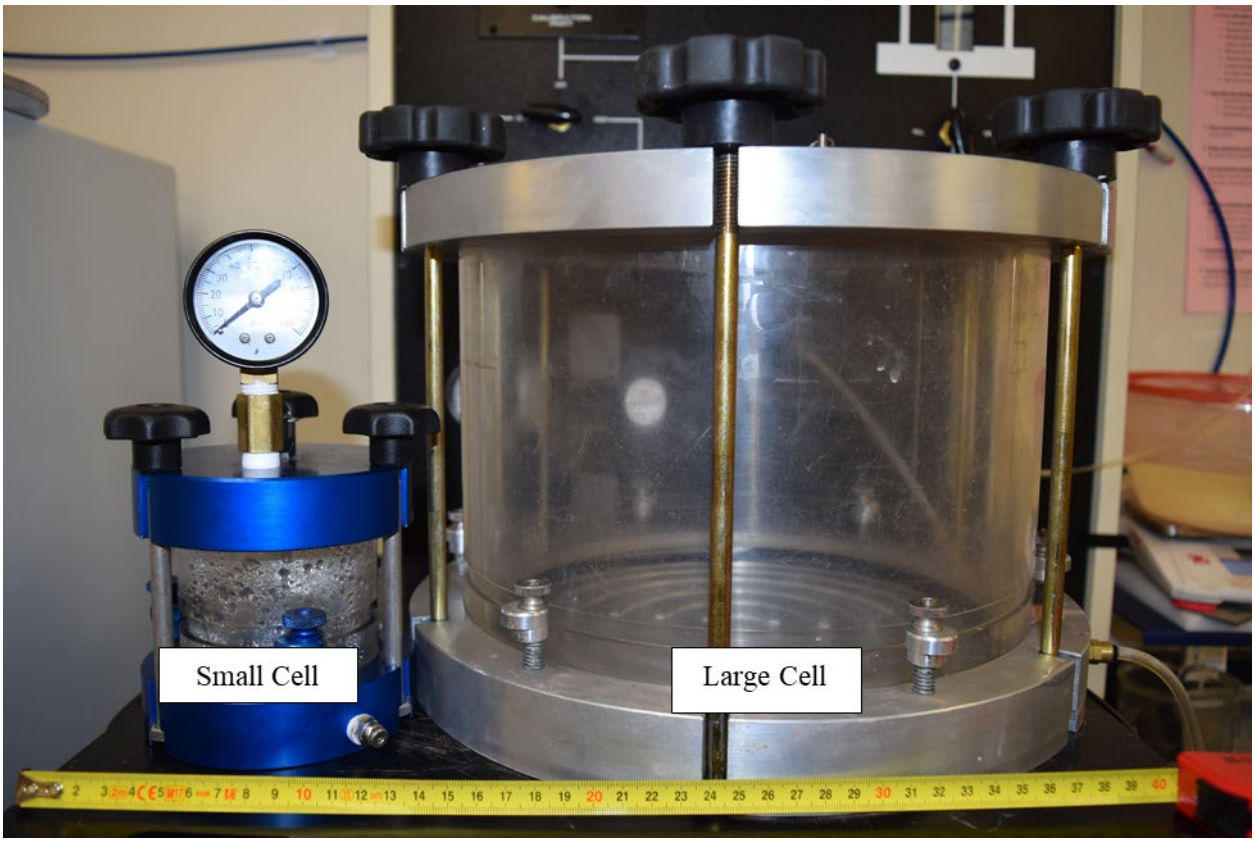

Figure 3. TRIM flow cells

3.2.1 Specimen Preparation

Fouling material samples were prepared in the small cell by compacting 170.0 gram (g) of dry ballast fouling material into the small cell and to a target dry density of 1.65 g/cm^3. This target value of dry density was selected by taking the average of the minimum dry density of the coarser materials (i.e., processed ballast breakdown) and maximum dry density of the finer materials (i.e., ballast fouling material removed from fouled ballast samples). Specimens were compacted dry in three lifts to a target final height. Fouled ballast specimens were prepared in the large flow cell using dry ballast and dry fouling material. Materials were added in five lifts;

each lift had a thickness of approximately 38.1 mm. Each lift was compacted to a target dry density of 1.73 g/cm^3 which correlates to a ballast relative density of 85 percent. Results shown herein were at very high fouling indexes so they could be compared with theoretical SWCCs. A proof of concept SWCC was measured following the sample preparation procedure described for LSDS (see Section 3.4.1) to ensure the sample density matched. Specimens were prepared to the target ballast density in three lifts and the appropriate amount of fouling material was added in each lift. Specimens were tamped in each lift with a flat plate with the same diameter as the cell.

3.2.2 Testing Procedure

Two high air entry (HAE) ceramic discs were used in the TRIM: a one-bar (~ 100 kPa) high-flow disc and a three-bar (~ 300 kPa) standard disc. The one-bar disc had a higher permeability which facilitated faster testing for sand samples. The three-bar disc had a higher air entry which enabled the use of higher testing pressures for testing clay and silt fouling samples. The hydraulic properties for each HAE disc are listed in Table 1. Saturation of the HAE discs was confirmed by mass. The surface dry mass of each disc was measured at intervals of 4+ hours, and saturation was confirmed by a stable saturated-surface-dry mass.

Table 1. Hydraulic properties of HAE porous discs [50]

Air Entry (bar)	θ_r	θ_s	α (1/cm)	n	K_s(cm/s)
1	0.07	0.45	0.0008	7	8.6E-06
3	0.07	0.34	0.00015	7	2.5E-07

During specimen saturation, water was drawn from the mass balance reservoir via suction. The suction applied to the sample was regulated through the pressure panel and never permitted to exceed 14 in. Hg (~ 47 kPa) to avoid breaking the HAE disc. The total mass of water imbibed by the sample was recorded to determine the saturated volumetric water content of each sample; this was a hydraulic parameter used for modeling SWCCs. The transient outflow was measured using two pressures. Pressures used during the first step ranged between 0.6 kPa and 7 kPa. The second pressure step was never permitted to exceed 90 percent of the air entry value of the HAE discs. From experience, pressures of 80 kPa and 250 kPa were most appropriate for the second step when using the one-bar and three-bar HAE discs, respectively. Each pressure step was terminated after the flux of water leaving the sample had reduced to 0.05 g/hr in the small cell and 0.1 gram per hour in the large cell. Specimens were tested only in the drying state. Quantifying hysteresis was determined to be outside of the scope of this project, but it may be of interest in Phase II. Outflow testing took 3 to 12 days per sample. Transient outflow data were corrected for diffused air displacement, as well as evaporation.

A minimum of 100 data points were sampled from the corrected outflow data and used as an objective function for modeling SWCCs via an inverse method. More points were sampled from areas of rapid mass change to preserve the shape of the curve. Figure 4 shows an example of the objective function. The transparent ‘x’ markers are the sampled data points. This specimen had a saturated volumetric water content of approximately 37.0 percent. The second pressure step quickly drained the specimen to a near residual state. The horizontal part of each step shows that the volumetric water content had stabilized prior to changing the testing pressure. The volumetric

water content was measured following each test to provide the residual volumetric water content, an upper boundary for the SWCC inverse model. Saturated hydraulic conductivity was also measured on three representative fouling materials following TRIM testing.

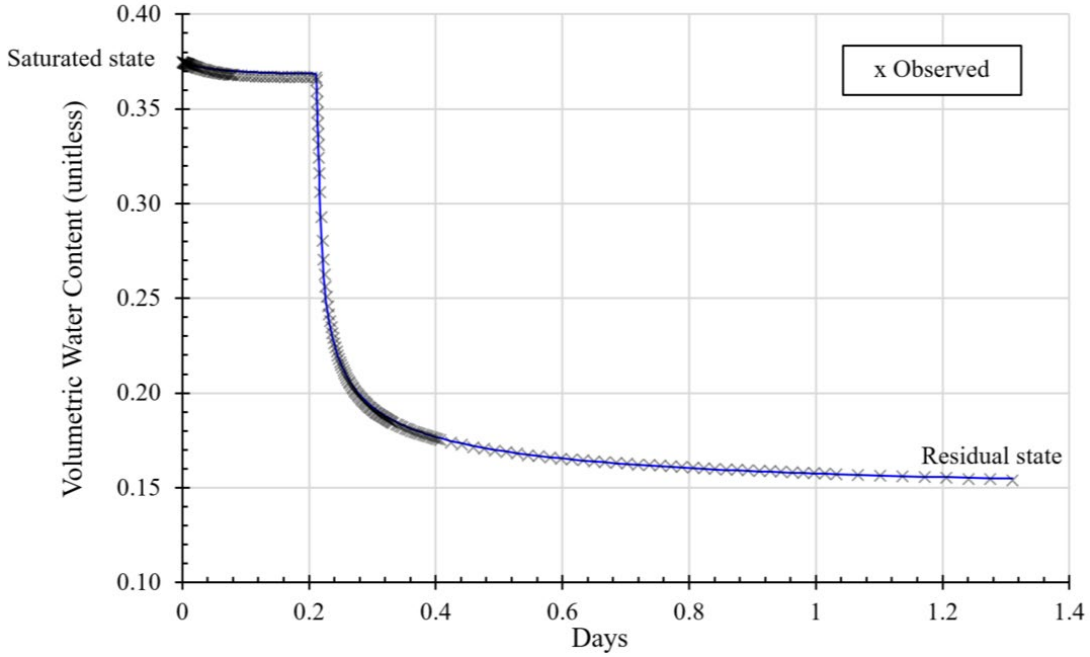

Figure 4. Example objective function from TRIM

Inverse modeling of SWCC's was performed using Hydrus one-dimensional software and the van Genuchten-Mualem model [26]. The van Genuchten model was previously defined. The hydraulic conductivity function is

$$\boldsymbol{K(h) = K_s \frac{\left[1 - |\alpha h|^{n-1}(1 + |\alpha h|^n)^{-m}\right]^2}{(1 + |\alpha h|^n)^{m/2}}}$$

where $K(h)$ is the hydraulic conductivity function, K_s is the saturated hydraulic conductivity (cm/s), h is the suction head (cm), n, m, and α and are empirical fitting parameters. Corrected outflow data, soil sample properties, and HAE disc properties were used for inverse modeling. All data for each HAE disc was taken from Table 1, except for the saturated hydraulic conductivity. The HAE disc saturated hydraulic conductivity was measured during each leak test in accordance with ASTM D5856 [46]. Data describing the fouling material included: porosity, sample dimensions, and bounded hydraulic model parameters (i.e., θ_s, θ_r, K_s, n, and α). The hydraulic model and the imported data were used to solve a numerical solution of Richards' Equation [51] to predict the transient outflow of the sample. Hydraulic parameters (i.e., θ_s, θ_r, K_s, n, and α) were optimized between each iteration, minimizing variation between the two objective functions. Fitting parameters were verified with final measurements where appropriate (i.e., volumetric water contents and saturated hydraulic conductivity) and by comparing the final parameters to similar materials found in the literature. Uniqueness was confirmed by checking model dependency on the initial hydraulic parameters. If the model converged on the same results using different initial values of θ_s, θ_r, K_s, n, and α, then results were considered unique [25].

3.3 Theoretical SWCC of Fouled Ballast

Fouling conditions were selected using criteria from the Bouwer-Rice Large Particle Correction Procedure [52]. The procedure requires that ballast voids be filled with fouling material and that the dry density of fouling material in the ballast voids be the same as the fouling material tested in the TRIM. The minimum amount of fouling material to meet these criteria at a relative density of 85 percent (i.e., corresponding to the maximum relative density achievable in the TRIM and LSDS) was 32.5 percent, which was rounded to 35 percent. Additional curves with 50 and 60 percent fouling were chosen arbitrarily. A test specimen at each fouling degree was molded in the lab to confirm constructability; bulk density and voids in ballast were measured in accordance with ASTM C29, method A [53]. Twenty-one SWCCs were calculated for highly fouled ballast using the Bouwer-Rice Large Particle Correction Procedure [52] where the volumetric water content of a fouled ballast (θ_{fb}) at any suction head is calculated by

$$\theta_{fb}(h) = (1 - VR)\,\theta_f(h)$$

where $\theta_{fb}(h)$ is the SWCC of the fouled ballast, V_R is the volumetric fraction of ballast aggregate in the total specimen volume, and $\theta_f(h)$ is the SWCC of the fouling material. Bareither and Benson [54] note that the Bouwer-Rice Large Particle Correction Procedure assumes the large aggregates (i.e., ballast) have negligible inter-particle moisture retention. A SWCC predicted using the Bouwer-Rice Large Particle Correction Procedure was compared and validated with SWCC of a replicate sample tested in the large TRIM.

3.4 Large-scale Direct Shear Testing

To further examine the effects of fouling and moisture on strength, direct shear testing was carried out using the University of Arkansas LSDS device capable of testing 600 mm diameter by 300 mm tall specimens (Figure 5). These dimensions satisfy the particle size to specimen size requirements of ASTM D3080 for the ballast tested. The LSDS device is a hydraulically controlled system with a horizontal shear capacity of 300 kN (67.4 kips) and a vertical capacity of 200 kN (45.0 kips), allowing for high stress conditions to be tested, although the stresses were limited in the current study to reduce the ballast degradation occurring from test to test. The samples consisted of clean granitic Class 1 acceptable ballast. The team obtained the ballast samples from a quarry and then processed them to obtain the "as delivered" gradation according to ASTM C136. Figure 6 shows the gradation used in the LSDS testing, along with the upper and lower bound limits of the Class 1 specifications and the quarry reported gradation. The percent passing the No. 200 sieve is not shown for clarity, but it was also within the specifications of Class 1 ballast. The aggregate was then separated into the various sieve sizes to allow for a new gradation to be obtained for approximately every four LSDS tests conducted.

Figure 5. University of Arkansas LSDS device (hydraulic system not shown)

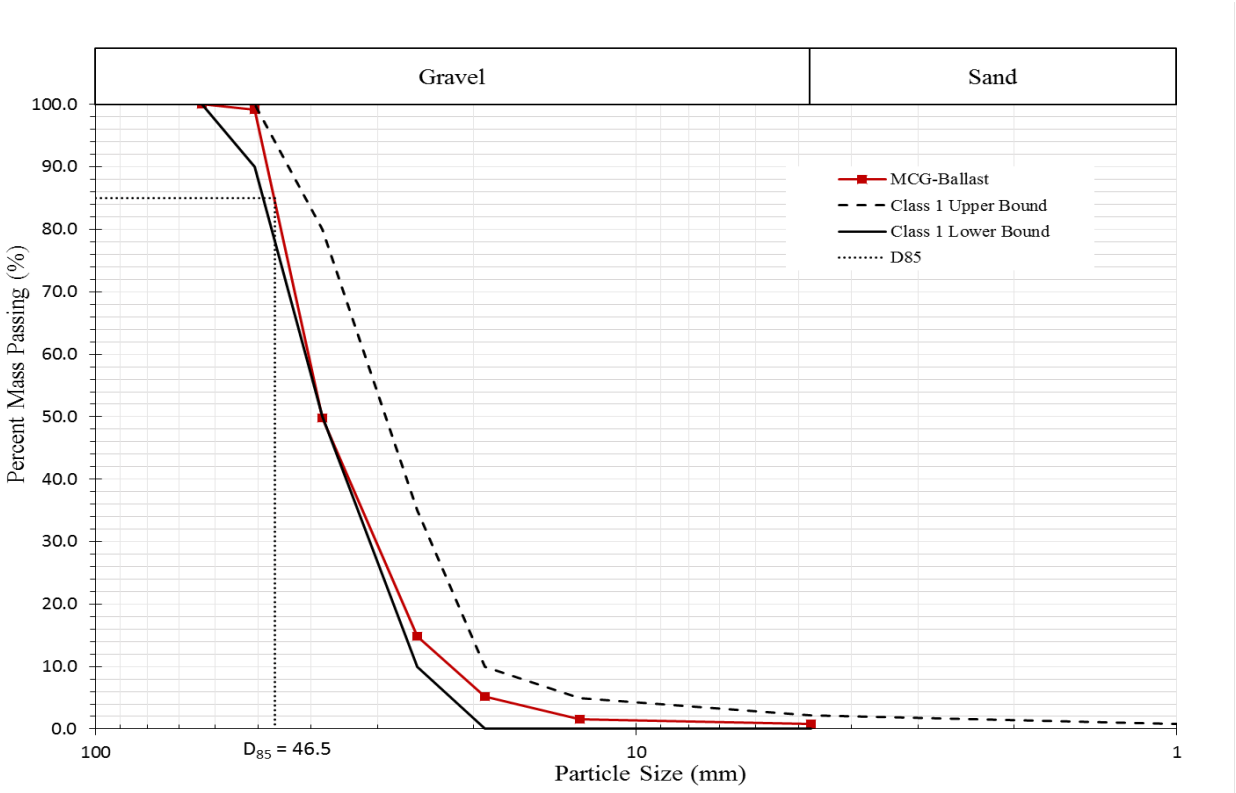

Figure 6. Particle size distribution curve for granite ballast used in LSDS testing and the particle diameter at which 85% of particles are smaller (D_{85})

Prior to LSDS testing, the minimum and maximum densities of the clean ballast were determined according to ASTM D4254 and D4253 to be 12.92 kN/m^3 (82.2 pcf) and 15.17 kN/m^3 (96.6 pcf), respectively. Two different specimen preparation methodologies/conditions were then examined to determine the most appropriate procedures for future testing of the various fouling conditions. The fouled ballast tests described herein were for a clay fouling material at 5 percent fouling

based on the total dry weight of the specimen. Phase II testing will consider the additional fouling materials described above to provide a link between the SWCCs and the fouled ballast strength and deformation responses.

3.4.1 Specimen Preparation

The clean ballast specimens were tested in a dry condition and a wet condition to provide a baseline for stress and deformation response comparisons. For the dry condition, the ballast gradation was obtained for a target weight of 127.6 kg (281.3 lbs) and was divided into three equal portions. The ballast was then placed into the shear cell and compacted in three equal lifts to ensure a uniform density across the specimen. For the wet condition, the ballast was submerged in water for 24 hours and was then drained prior to compacting. This provided a wet surface condition for the ballast where only the adsorbed (on the particle surface) and a very small amount of absorbed water were present after compacting. The gravimetric and volumetric water contents of the wet ballast were very low (0.75 and 1.13 percent, respectively) due to the fact that the ballast absorbs very little water and it has a low water holding capacity compared to its large mass. All LSDS tests targeted a relative density of 85 percent based on the ballast "matrix" only. This corresponded to a unit weight of 14.78 kN/m^3 (94.1 pcf). This relative density (based on only the ballast) was maintained for fouled ballast specimens as well to create similar packing densities and comparable results. Because only 5 percent fouling was used, it was assumed that the fouling particles were contained within the void space and did not alter the overall packing density of the ballast material.

To prepare the fouled ballast specimens, two different methodologies were used and compared. The steps in each method were similar with the main difference being whether the ballast was dry or wet when mixed with the fouling material. The target dry mass of the fouling material needed to achieve 5 percent fouling was obtained and then mixed to a target volumetric water content based on the soil's SWCC. The target water contents tested ranged from the saturated volumetric water content to the residual volumetric water content obtained from the SWCC. The fouling material was then mixed with the portions of ballast and compacted in the three lifts to achieve a relative density of 85 percent. The initial density was checked by the height of the specimen when a 10 kPa (1.45 psi) vertical stress was applied. When the fouling material was mixed with the dry ballast, a large amount of water was pulled from the fouling material by the ballast. Because these tests were to be directly compared with the SWCC data obtained and with dielectric constant in Phase II testing, a common condition needed to be established that was repeatable and consistent. Therefore, the same procedures were followed except the ballast was first submerged in water for 24 hours and then drained prior to mixing with the fouling material and compacting. This method resulted in a more consistent moisture distribution across the specimen.

3.4.2 Testing Procedure

Once the specimen was prepared to the target density, the shear cell was loaded into the University of Arkansas LSDS device and a target vertical stress was applied. A gap was then set between the upper and lower cylinders to facilitate proper shearing through the central zone as to not overestimate strength. The gap spacing is a testing parameter that is unclear in many of the previous studies on ballast and is not often mentioned or shown. It is noted here that the actual spacing requirement is not well defined or universal. As discussed in Simoni and Houlsby [55], a

small gap spacing between the upper and lower shear boxes may restrict the development of the shear band and lead to unrealistically high strengths. A large opening, however, can lead to stress reduction and material loss at the specimen edge. According to Shibuya et al. [56], the gap spacing should be maintained at a value slightly larger than the shear band thickness—approximately 10–20 times the median particle diameter, D_{50}. For the gradation tested, D_{50} was 38.1 mm, resulting in a minimum suggested gap spacing of 381 mm. Clearly this gap spacing is not a reasonable estimate for this type of testing. A systematic investigation of the effects of the gap size was outside the scope of this work, although it is a detail that will be further investigated in future testing. The gap spacing used was equal to D_{85} (i.e., diameter at which 85 percent of the particles by mass are smaller) or 46.5 mm for the gradation tested. Figure 6 illustrates how D_{85} was obtained from the particle size distribution curve. The use of D_{85} was chosen based on previous experience in aggregate testing, and similar guidance given from the Federal Highway Administration for large-scale aggregate testing. Once the gap was set, the target vertical stress was checked—and corrected if changed—and the specimens were sheared at a rate of 0.381 mm/min (0.015 in/min) to a horizontal displacement of 145 mm. This distance allowed for the peak stress, and in most cases the residual shear stress, to be determined.

Once the test was completed, the ballast was removed from the shear cell and the water content of the current condition was obtained. A new target condition was then prepared, and the ballast was compacted again in three equal lifts for the next test. For the initial set of tests, the target volumetric water content was checked, and more water was added as needed to obtain the target. This became a very tedious process and so it was determined that a more practical method would be to simply mix the specimen to the wettest condition (i.e., saturated volumetric content) and then conduct one test each day as the specimen naturally dried. The volumetric water content could then be calculated from the gravimetric moisture content obtained prior to each test, so that it could be compared to the SWCC.

Obtaining a gravimetric moisture content for these specimens was not trivial. For ballast size particles, large amounts of material (3 kg or more) are needed for a representative sample. This was not possible because the material was reused from test to test each day. Starting with a new gradation and targeted volumetric moisture content for each test was also very labor intensive and time (and space) prohibitive. It was also determined that the gravimetric water content of the fouled ballast was not as useful (due to the large mass of the ballast compared to the water) as it only varied from approximately 0.5 to 1.5 percent across the range of tested volumetric water contents. Therefore, the water content of the fouling material was tracked to make the most consistent comparison across specimens. This decision was further supported by SWCC measurements on fouled ballast specimens and the SWCC of fouling materials which appear to be the most influential on the ballast behavior in preliminary results. To obtain the water content for each test, a representative sample of the fouling material was removed from the ballast particles and oven dried to obtain the gravimetric water content. The volumetric water content was then calculated.

4. Results and Analysis

4.1 SWCC Results

4.1.1 SWCCs of Ballast Fouling Materials via the Small TRIM

SWCCs were measured and modeled on 14 ballast fouling materials. The SWCCs of seven select fouling materials are shown in Figure 7. All 14 SWCCs are available in Appendix A along with a table of all their hydraulic parameters. The seven SWCCs shown in Figure 7 were selected to represent each USCS sample available. As discussed, the USCS classifications were determined according to ASTM D2487. The range of USCS samples included poorly graded sand (SP), well graded sand (SW), silty sand (SM), low plasticity silt (ML), silty clayey sand (SC-SM), and two low plasticity clays (CL-1 and CL-2). Two CL samples were included because the SWCC results varied greatly between the two despite their similar USCS description. This was likely due to the presence of coal dust, which verified by thermogravimetry. The USCS symbols have been used as sample IDs in Figure 7 and Table 2. The van Genuchten hydraulic parameters for the SWCCs shown in Figure 7 are listed in Table 2. All samples were within 0.1 g/cm^3 of the target dry density (1.65 g/cm^3).

The sand samples in Figure 7 (i.e., SP, SW, and SM) show low resistance to drainage: the saturated phase of the SWCCs (i.e., right vertical side of the curves) transitions into a draining condition (i.e., horizontally oriented portion of the curves) at relatively low suction heads compared to the other samples. The average air entry of these materials was 1 kPa (i.e., recall that air entry is α^{-1}). The three sand samples also drained more completely compared to the other samples. The average residual volumetric water content of the sands was 6.44 percent. The results in Figure 7 and van Genuchten hydraulic parameters in Table 2 for the SM and ML samples are comparable to previous studies with the same USCS classification [24] [25].

The silty clayey sand (SC-SM) and low plasticity clay (CL-1 and CL-2) samples contained coal. The clayey-silty sands (SC-SM) with coal had a sharp (nearly horizontal) drainage phase like the well-graded and poorly-graded sands with gravel (SW and SP); however, these samples required approximately six times the suction head to initiate drainage. The average air entry for the SC-SM with coal was 6.5 kPa. They also held nearly three times more pore water than the SW and SP samples in the residual phase. The average residual volumetric water content of the SC-SM with coal was 16.5 percent. The second of the sandy lean clays (CL) with coal (CL-2 hereafter) and sandy low plasticity silt (ML) had air entry values of 20 kPa and 44.5 kPa, respectively. They did hold less residual pore water at the end of the draining phase; but only when exposed to high suction heads (15.5 and 12.1 percent at suction heads in excess of 1,000 kPa). The SWCC of CL-1 looks more like that of the clayey-silty sand (SC-SM) with coal. The CL-1 sample had an approximate coal content of 8.5 percent of material passing the No. 40 sieve whereas the CL-2 had an approximate coal content of 15 percent based on TGA. Appendix A includes the TGA results. There is limited information regarding the hydraulic properties of soil with varying percentages of coal, those found were pure coal. Additionally, no SWCC or van Genuchten parameters were found in the literature for validating results.

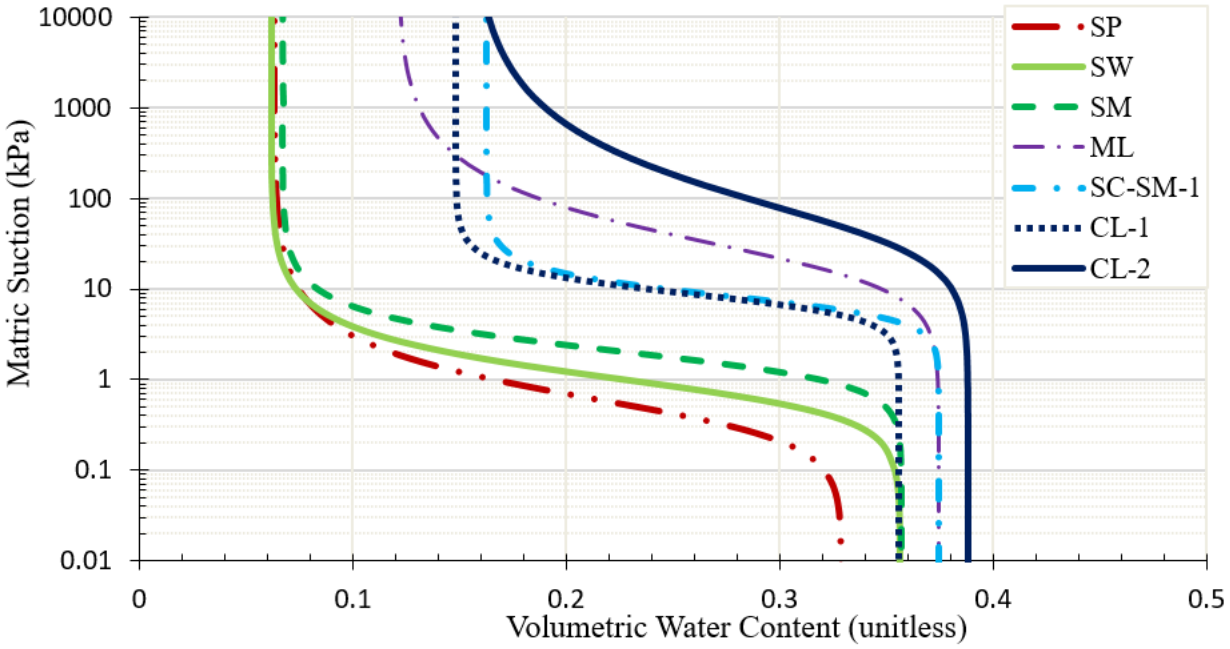

Figure 7. SWCCs of fouling materials

Table 2. Summary of hydraulic parameters of fouling materials

Sample ID	θ_r	θ_s	α (1/cm)	n	m	K_s(cm/s)	ρ_d(g/cm^3)
SP	0.063	0.329	0.238	1.98	0.496	2.56E-02	1.75
SW	0.062	0.356	0.128	2.26	0.557	6.39E-03	1.70
SM	0.067	0.357	0.0587	2.61	0.616	5.10E-04	1.70
ML	0.121	0.375	0.00492	1.82	0.451	8.70E-05	1.68
SC-SM	0.162	0.374	0.0130	3.50	0.714	9.52E-05	1.67
CL-1	0.148	0.356	0.0124	3.50	0.714	4.51E-05	1.67
CL-2	0.155	0.388	0.0022	1.61	0.379	3.50E-05	1.57

4.1.2 Theoretical SWCCs of Fouled Ballast

The seven representative fouling material SWCCs were used to create theoretical SWCCs with ballast at different fouling percentages. These calculations illustrate how the unsaturated behavior of ballast changes as the percent fouling changes. The method assumes that the finer material within each bulk sample (i.e., the fouling material in each fouled ballast) has the same suction properties as the scalped material (i.e., the fouling material tested without ballast). The primary changes are to the saturated and residual volumetric water contents and the slope of the transition phase of the SWCC. For example, Figure 8 shows the SWCCs for 35 percent fouled ballast with the same range of matric suction as Figure 7, but the corresponding volumetric water content changed. The predicted saturated volumetric water contents were between 14.0 and 19.0 percent. The ballast fouled with CL-2 had the highest saturated volumetric water content at 18.4

percent; SP had the lowest at 15.0 percent. The residual volumetric water content of all samples was less than 8.00 percent. The theoretical residual volumetric water content for ballast fouled with clean sands (i.e., SP, SW) and SM were approximately the same at 2.91 percent. Ballast that were 35 percent fouled with SC-SM and CL-2 were predicted to have a residual volumetric water content of approximately 7.50 percent.

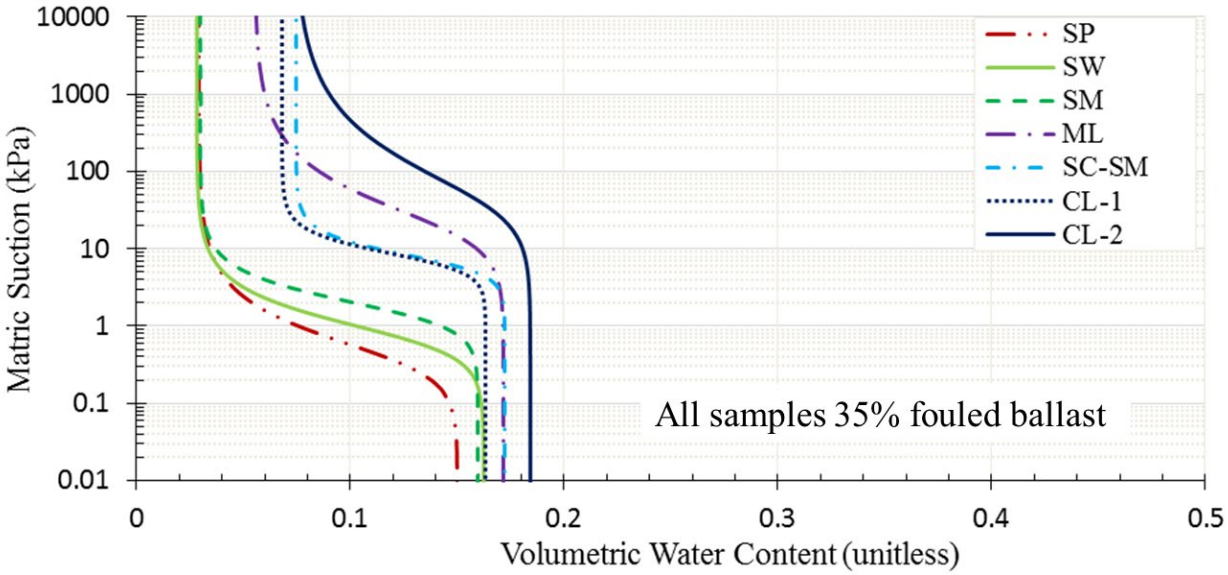

Figure 8. Theoretical SWCCs of 35% fouled ballast

The measured SWCCs (i.e., Figure 7) and predicted SWCCs (i.e., Figure 8) show that the hydraulic properties of the fouled ballast reflect that of the fouling materials. For example, the estimated SWCCs in Figure 9 show that a saturated ballast with 60 percent fouling will hold more pore water than a ballast with 35 percent fouling. The estimated SWCCs also show that when the ballast voids are completely full with fouling material and the dry density of the fouling materials is near 1.65 g/cm^3, a ballast fouled with material CL-2 (i.e., known to have coal dust) will not begin to drain until exposed to a suction head of 10 kPa regardless of the degree of fouling. Because the hydraulic properties of fouled ballast are inherited from the fouling material, the mechanisms altering SWCCs of fouling materials also influences the SWCCs of fouled ballast. The ballast fouled with SC-SM and CL, which all contained coal, had higher air entry than the sands (i.e., SP, SW, and SM). Coal affects the suction response of the fouled ballast as seen by the SWCCs of CL-1 and CL-2 fouled ballast in Figure 9. Appendix B includes all SWCCs at 35, 50, and 60 percent fouling for each fouling material.

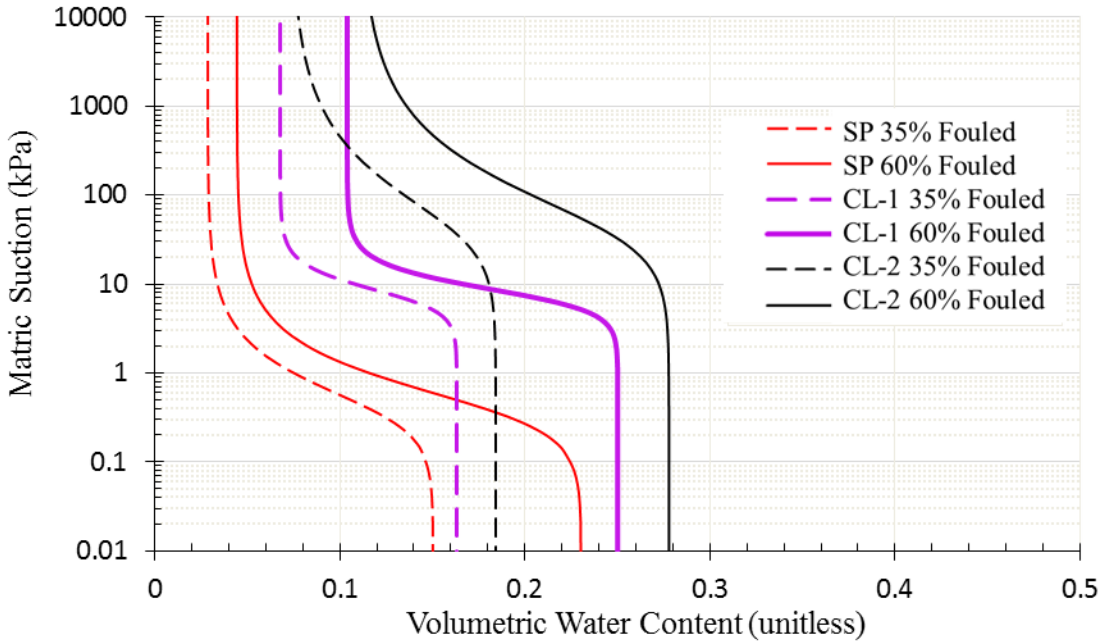

Figure 9. Influence of fouling material and percent fouling, comparing 35 and 60% fouled ballast, on SWCC

4.1.3 SWCC of Fouled Ballast

The large TRIM apparatus was validated two ways. First, by comparing a 50 percent fouled SP sample with a predicted 50 percent fouled sample. The preliminary test was conducted while also determining the best way to prepare samples in the large cell. As such, the density of fines within the ballast void space were not compacted to the same density as they were in the small TRIM when only fouling materials were tested, so results are not included herein. The two SWCCs were similar in shape with different saturated volumetric water content resulting from the different density. Following this proof of concept, the large TRIM was more thoroughly verified by comparing it to results of the small TRIM apparatus as shown in Figure 10. The green solid line is the SWCC measured using the small apparatus; the dashed black line is the SWCC measured using the large apparatus. The two SWCCs are sigmoidal in shape and have similar air entry values. The fitted parameters for the two SWCCs in Figure 10 are summarized in Table 3. The only discrepancy between the fitted parameters is the saturated hydraulic conductivity of the smaller sample was 0.0063 cm/s, whereas that of the larger sample was lower at 0.0018 cm/s. This was likely the result of reduced porosity and varied pore connectivity (i.e., increased sample density and altered particle arrangement) when preparing these samples in different devices. The difference in average density between the two samples was 0.04 g/cm^3.

Table 3. Hydraulic parameters of fouling material SW, validation of large TRIM experiment

Sample ID	θ_r	θ_s	α (1/cm)	n	m	K_s(cm/s)	ρ_d(g/cm^3)
SW Small Cell	0.062	0.357	0.128	2.26	0.557	6.39E-03	1.70
SW Large Cell	0.045	0.341	0.147	2.21	0.548	1.80E-03	1.74

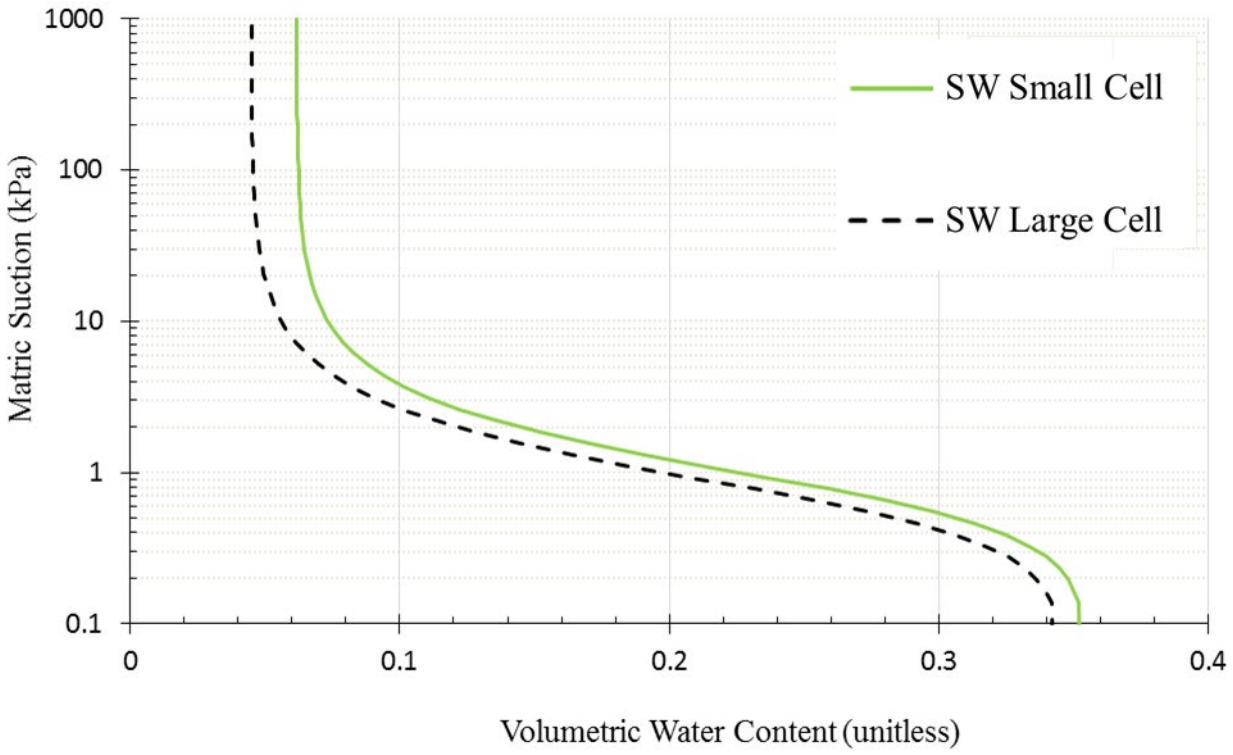

Figure 10. Validation of the large flow cell using SW specimen. SW small: original result from the standard TRIM test, SW large: the result in the larger custom cell

Three SWCCs were measured using the large apparatus and TRIM. One SWCC was for a fouling material. Two SWCCs were for fouled ballast: a 50 percent fouled ballast (SW 50% Fouled) and a 22 percent fouled ballast (SW 22% Fouled), shown in Figure 11. The three SWCCs are similar in shape; this is to be expected given that the same fouling material was used for the sample. The 22 percent fouled ballast had an air entry value of 0.34 kPa and a residual volumetric water content of 5.4 percent at approximately 2 kPa of suction head. The 50 percent fouled ballast had an air entry value of 0.80 kPa and residual volumetric water content of 5.4 percent at a 9 kPa of suction head. The fitted hydraulic parameters for the SWCCs in Figure 11 are listed in Table 4. These preliminary results are supported by the theoretical SWCCs of fouled ballast and are in agreement with Cui [21], who showed that the SWCCs of fouled ballast are different than that of the fouling material alone. Note that although Cui only included one fine-

grained material it was determined that the unsaturated behavior is controlled by the fines as water transfer occurred in the fine-grained pore network. Although the preliminary results in Figure 11 were a coarse-grained material, the shape of the SW (e.g., pure fouling material) and van Genuchten parameters in Table 4 are similar to the fouled ballast, thus highlighting the control of the fouling material on the unsaturated response.

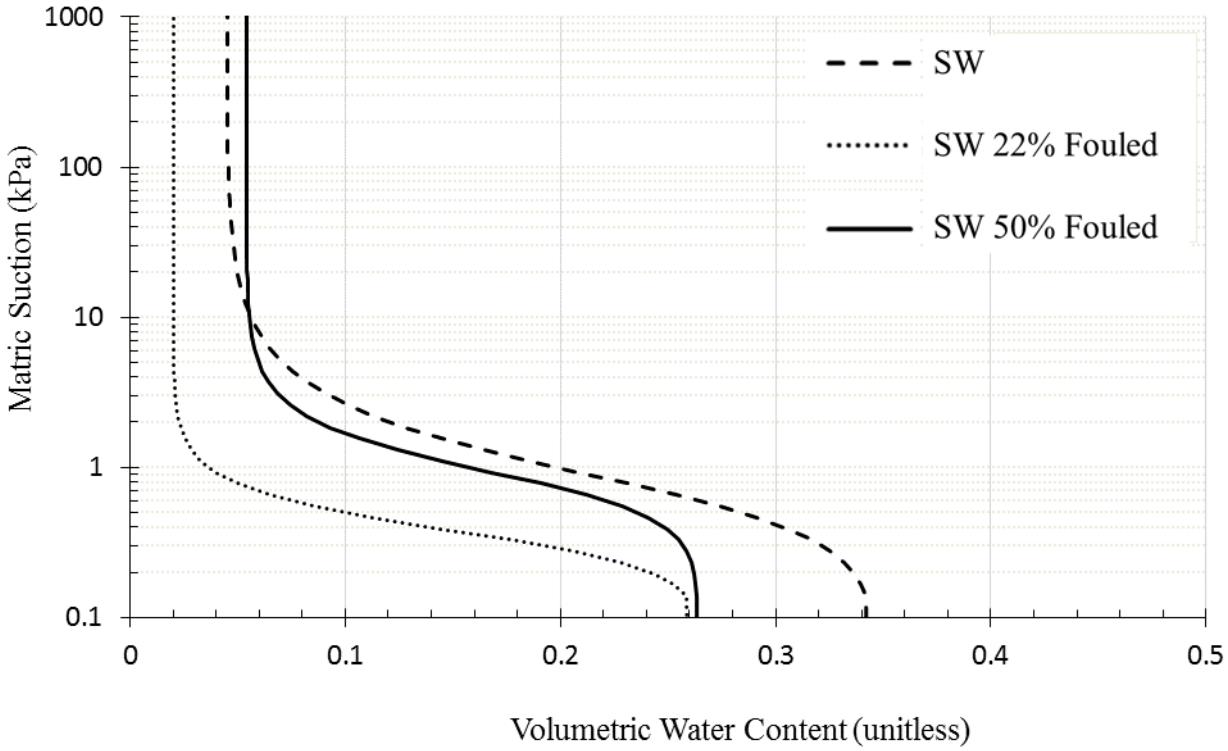

Figure 11. SWCCs of fouled ballast with SW ballast fouling material: SW is the fouling material only; SW 22% Fouled and SW 50% Fouled are fouled ballast specimen

Table 4. Hydraulic parameters of fouled ballast, results of the large TRIM experiments

Sample ID	% Fouling	FI (%)	θ_r	θ_s	$\alpha(1/\text{cm})$	n	m	$K_s(\text{cm/s})$
SW	NA	NA	0.045	0.341	0.147	2.21	0.548	1.80E-03
SW 50% Fouled	50%	36	0.054	0.264	0.122	2.97	0.664	1.14E-02
SW 22% Fouled	22%	15	0.020	0.266	0.287	3.50	0.714	8.98E-03

4.2 LSDS Results

LSDS strength testing was performed on the Class 1 granite ballast previously described and all tests were performed targeting a relative density of 85 percent. The initial LSDS testing considered dry clean ballast at a range of stresses 34.5–275.8 kPa (5–40 psi) and wet clean ballast at 68.95 kPa (10 psi) to provide a baseline strength. Table 5 summarizes the main tests

performed including the relative density achieved and the peak shear stress observed. Many tests were performed to arrive at the final methodologies but are not shown here for clarity. The relative densities were all within 1.9 percent of the targeted 85 percent which is well within the controllable variability, given that all specimen heights varied by less than 1 mm. Note it was determined while establishing the experimental methodology that a 1 mm difference in specimen height resulted in a 2 percent difference in relative density. In the case of the surface wet clean ballast test (Test No. 6), the water content data shown is for the ballast; however, for the rest of the tests where 5 percent fouling was used, the water content is of the fouling material only. As discussed, the large volume and mass of the ballast skewed this information and tracking the fouling material only provided a better comparable measure for this stage of testing.

Five tests were initially conducted on clean dry ballast to determine the linear and parabolic failure envelope and to serve as a baseline for the other comparisons. Figure 12 shows the stress-displacement and volumetric response of the specimens at the range of vertical effective stresses tested. As expected, the peak shear stresses increased with increasing vertical effective stress (Figure 12a) and the dilation decreased with increasing vertical stress (Figure 12b). The peak shear stress for each test (shown using the small circles on Figure 12a) was plotted with the corresponding vertical effective stress to obtain the Mohr-Coulomb (MC) linear and parabolic failure envelopes. Figure 13 illustrates the experimental peak stress data and the two fitted failure curves with their corresponding equations. The linear MC curve overestimates the strength at low vertical stresses while the parabolic fit or nonlinear curve captures the strength better over the full range of stresses tested.

A significant amount of ballast breakage was observed during these initial five tests (mostly at higher stresses of 137.90–275.79 kPa). Figure 14 shows the gradation curve before and after testing. Clearly, the ballast breakage results in a higher percentage of smaller particles, bringing the gradation outside of the Class 1 upper limit specification. A change in gradation of this magnitude also likely affects the strength parameters. Because the larger vertical stresses led to the highest amount of particle breakdown, obtaining the range of stresses needed to define the MC strength envelope would have required a new gradation to be used each time which would have needed a prohibitively large amount of aggregate. Therefore, the remaining testing focused on the peak stress response for tests conducted at 68.95 kPa (10 psi), so that comparisons at a single stress could be made. This would allow for moisture and percent fouling to be systematically varied, ultimately allowing for the generation of peak stress to be plotted as a function of these parameters. A new gradation was obtained for each series of tests (typically every four tests) to ensure comparable results, even at this lower stress.

Table 5. Testing summary for clean and fouled ballast LSDS tests

Test No.	Fouling Material	% Fouling by dry mass	FI (%)	Gravimetric Water Content (%)	Volumetric Water Content (%)	Vertical Effective Stress (kPa)	Relative Density (%)	Peak shear stress (kPa)
1	Clean	0	0	0	-	34.47 (5 psi)	85.2	89.23
2	Clean	0	0	0	-	68.95 (10 psi)	85.1	166.95
3	Clean	0	0	0	-	137.90 (20 psi)	85.1	282.27
4	Clean	0	0	0	-	206.84 (30 psi)	85.2	319.92

Test No.	Fouling Material	% Fouling by dry mass	FI (%)	Gravimetric Water Content (%)	Volumetric Water Content (%)	Vertical Effective Stress (kPa)	Relative Density (%)	Peak shear stress (kPa)
5	Clean	0	0	0	-	275.79 (40 psi)	85.0	379.13
6	Clean	0	0	0.75	1.13	68.95 (10 psi)	86.8	137.33
7	Clay	5	7.3	4.79	8	68.95 (10 psi)	85.3	147.34
8	Clay	5	7.3	7.19	12	68.95 (10 psi)	85.5	144.89
9	Clay	5	7.3	8.98	15	68.95 (10 psi)	84.9	129.12
10	Clay	5	7.3	23.95	40	68.95 (10 psi)	85.3	163.21
11	Clay	5	7.3	23.95	40	68.95 (10 psi)	85.6	134.56
12	Clay	5	7.3	16.65	27.81	68.95 (10 psi)	83.1	119.92
13	Clay	5	7.3	11.85	19.79	68.95 (10 psi)	83.7	195.91
14	Clay	5	7.3	11.19	18.69	68.95 (10 psi)	83.4	156.03

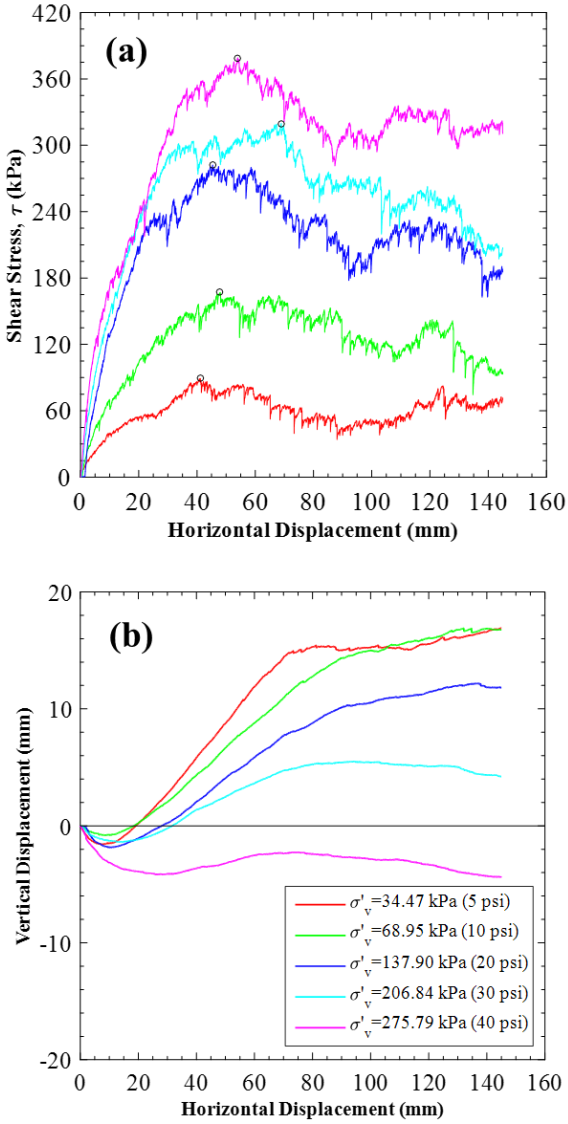

Figure 12. Shear response for clean dry ballast over a range of stresses (a) shear stress versus horizontal displacement, and (b) vertical versus horizontal displacement

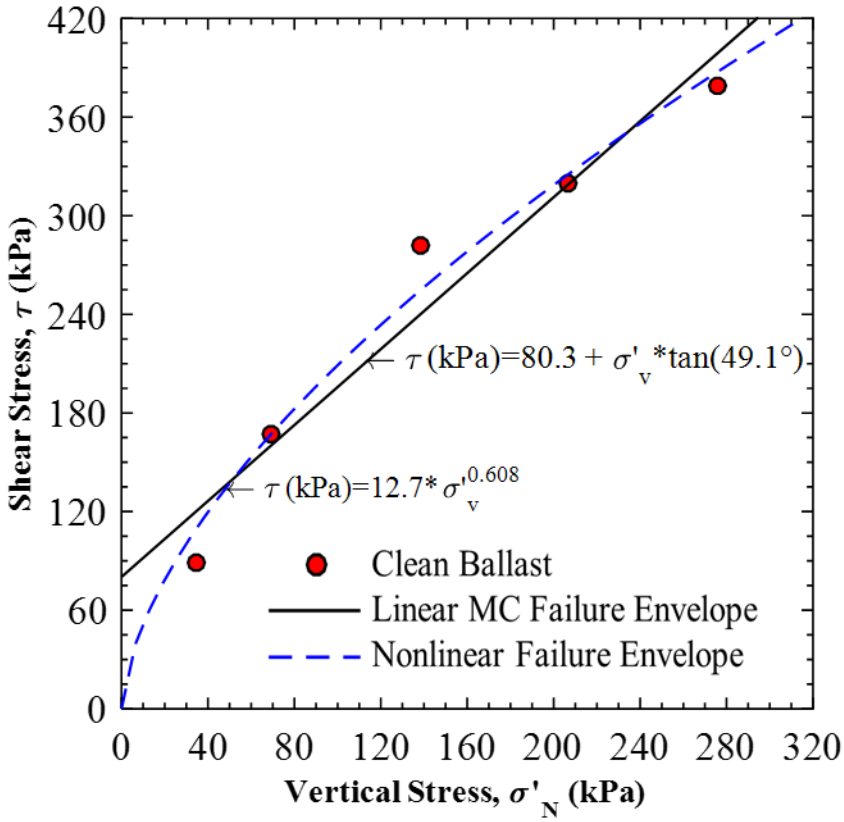

Figure 13. Linear MC failure envelope and nonlinear failure envelope for clean dry ballast over a range of vertical stresses

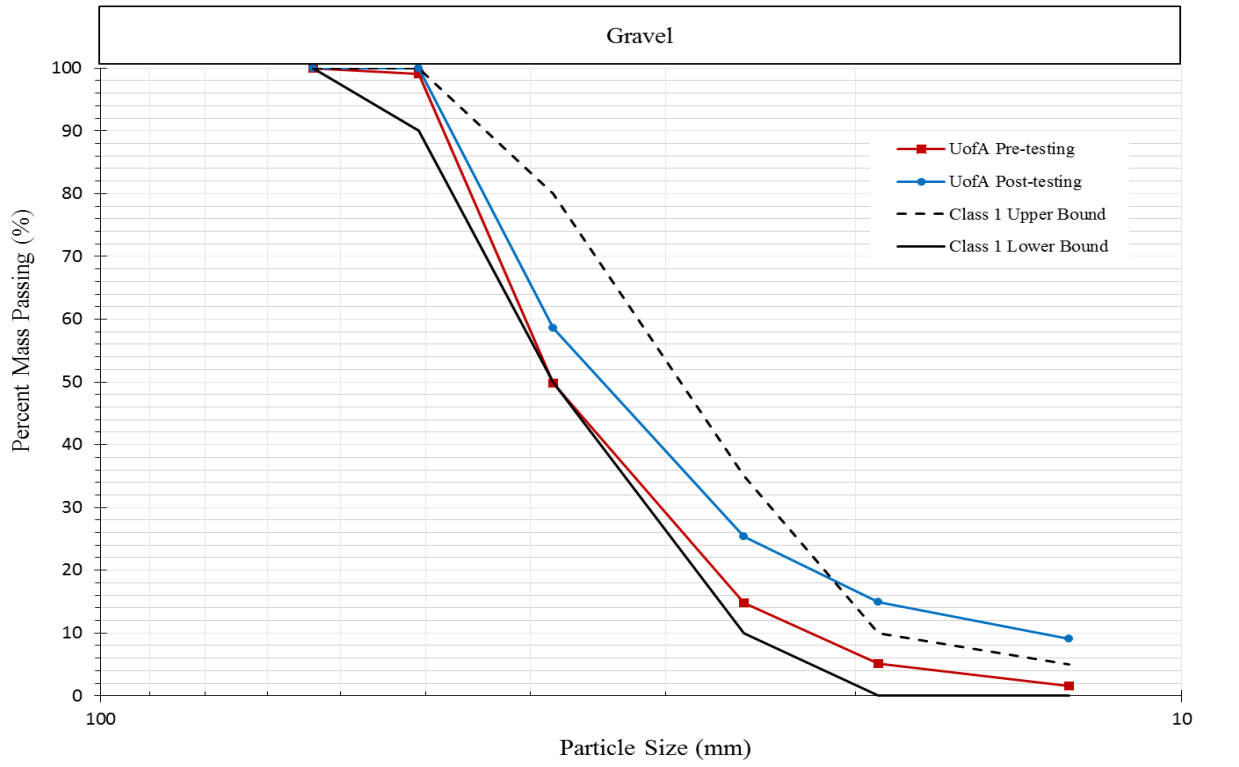

Figure 14. Particle size distribution before and after a series of five tests

Figure 15 presents a comparison of the dry and surface wet clean ballast results. The test with surface wet ballast was at a slightly higher density which likely explains the more dilative behavior, but the peak shear stress was less for the wet specimen indicating that the water is likely acting to lubricate the surface. The stress and deformation response was also obtained for clay fouled ballast specimens at 5 percent fouling for a range of moisture conditions. As previously discussed, two different sets of tests were considered in which the fouling material was mixed with either dry or surface wet ballast. Note that the discrepancies in the reported significant values for water contents are due to the fact that the volumetric water content was targeted in each of the dry fouled ballast tests while only the first target volumetric water content ($\theta_v = 40\%$) was targeted for the surface wet fouled ballast tests. In the latter experiments, the gravimetric water content was obtained before each new test to make the testing more tractable. Figure 16 presents the results of these tests. It is noted that the volumetric water content shown is for the fouling material only and the contribution from the ballast was not considered. These results are considered preliminary for Phase I of this research, where the focus was primarily on establishing the experimental procedure to connect the LSDS specimens to the large TRIM specimens. There are several inconsistencies in the responses that make drawing general conclusions difficult. In both cases, the highest volumetric water content condition resulted in the lowest overall dilation, yet it was not consistently the lowest peak stress value among the groups. It is likely that the intermediate conditions of moisture, along with the higher volumetric moisture content specimen with dry ballast, may result in specimens which exhibit some additional strength due to the presence of suction. More data are needed to confirm this; these data are planned for Phase II.

The noise in the data shows that even though the specimen size satisfies the requirements in ASTM D3080, it is likely just on the edge and a larger cell would likely provide more consistent results. A closer look at the variability among replicate tests is planned for Phase II. Issues with the rotation of the top cylinder may have also affected some of the peak responses measured. This rotation has since been fixed which will lead to more confidence in Phase II replicate results. It is clear from these results that additional testing is needed to determine the main influence of water content on ballast strength when small percentages of fouling are present. Additional tests on higher percentages of fouling are also planned to better understand how this parameter affects the ballast response.

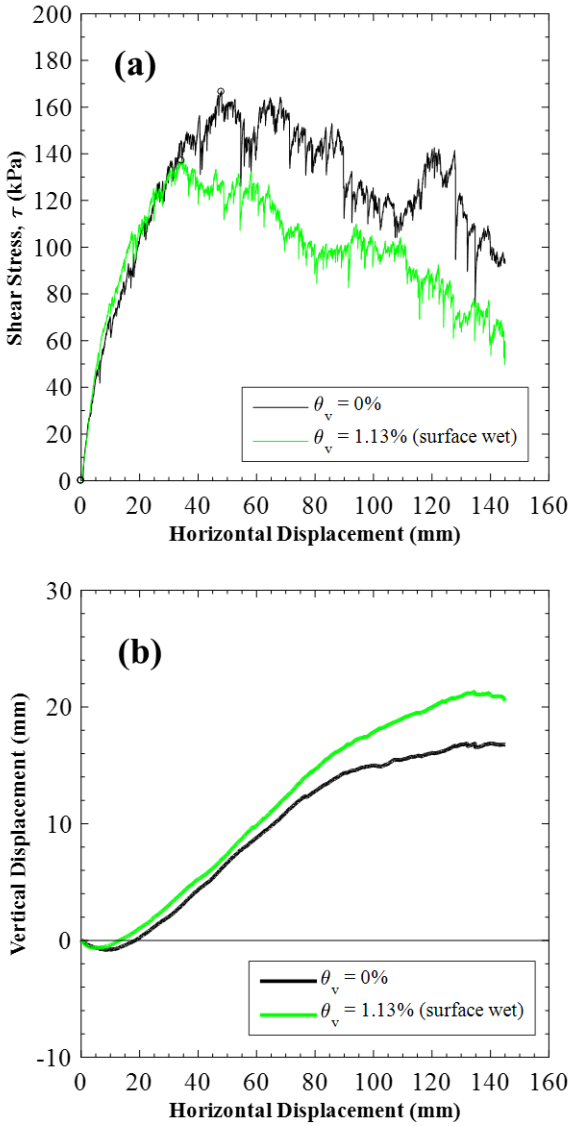

Figure 15. Stress and displacement responses for clean ballast specimens tested at 68.95 kPa (10 psi) for a dry condition and a surface wet condition

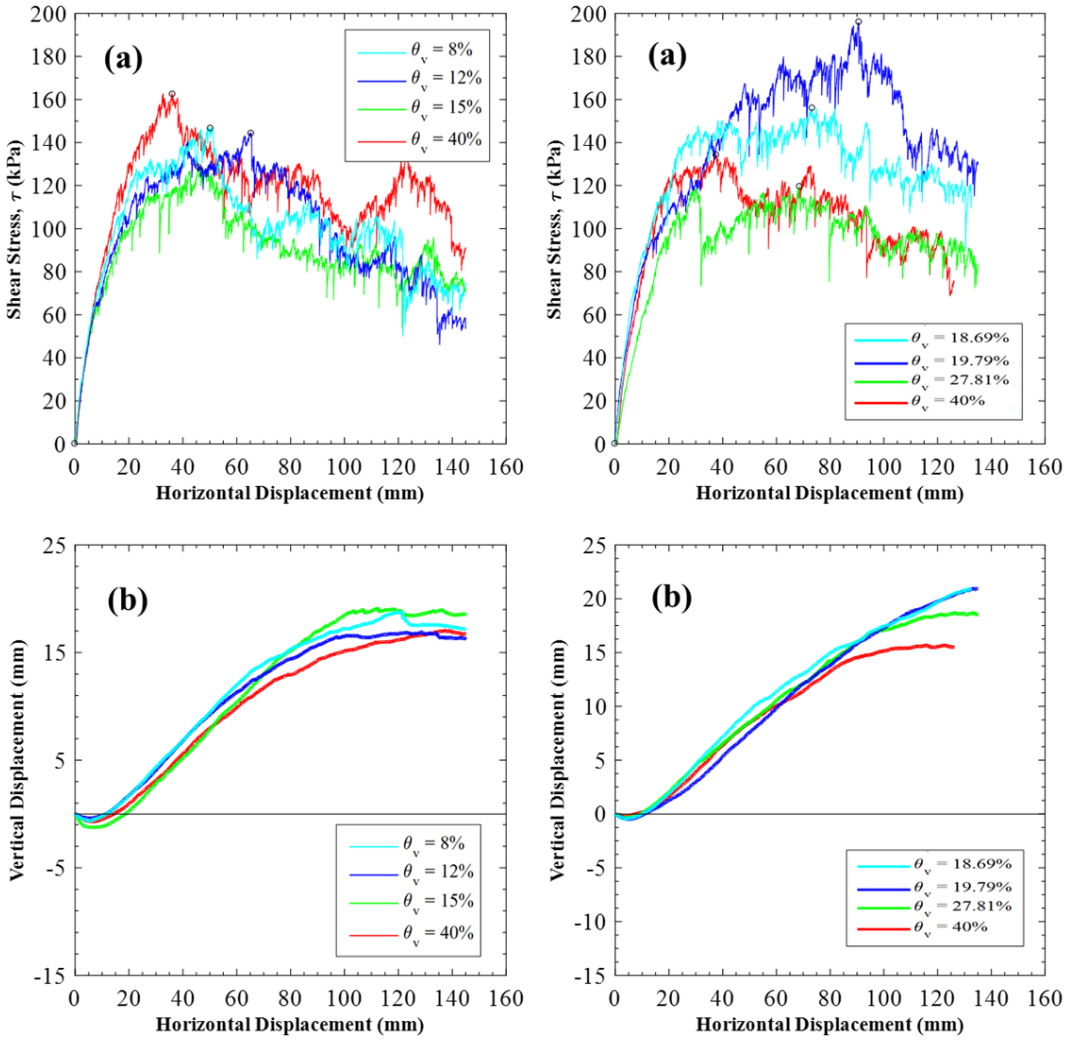

Figure 16. Shear stress and vertical displacement response for (a, b) 5% clay fouled ballast with dry ballast, and (c, d) 5% clay fouled ballast with surface wet ballast

5. Conclusion

This research seeks to identify the factors that contribute to the loss of ballast strength due to fouling and the sensitivity and extent to which they can be measured by ground penetrating radar. Phase I established how fouling materials alter the water holding capacity of ballast. This report highlighted the suction water characteristic curves (SWCCs) of seven samples of fouling material. The remaining seven samples included in Appendix A were similar to those shown herein. Specifically, the results of the three additional SW, two additional SP, and two additional SC-SM samples in the Appendix A were similar to the SP, SW, and SC-SM in the main report. First, only the fouling materials (i.e., materials passing the No 3/8 sieve) were tested to isolate the importance of the fouling material and to develop a protocol for measuring the SWCCs including the ballast aggregate. It was identified that the fouling material itself greatly impacts the water holding capacity. Although there is limited information available, this finding aligns with previous research. In general, the water holding capacity of the coarser-grained sand fouling materials (i.e., SP, SW, and SM) was quite low, as expected. The silt fouled sample (ML) had a greater water holding capacity compared to the three sands and the coal-fouled samples were more irregular. The sample with a higher coal content also held the most water at higher suction. Previous researchers have used pure coal as a fouling material; this study was unique because the samples were collected from track and contained various amounts of coal mixed with other geomaterials. The impact of fouling material characteristics was further highlighted by the numerical study. Although the range of water holding capacity was reduced for all simulated fouled ballast samples, those that contained coal dust still held a large amount of water compared to the sand. This finding has further implications for the electromagnetic and strength characteristics of fouled ballast planned in Phase II. This report also includes the development of custom equipment for measuring the water holding capacity of fouled ballast. Although the results were preliminary, they were repeatable and in agreement with the numerical simulations of SWCCs of fouled ballast and the extremely limited previous research noted in the literature. Phase II will focus on measuring the SWCCs of fouled ballast with different fouling percentages and measuring the corresponding strength and volumetric behavior during shearing.

Much of Phase I focused on sample preparation and testing methodologies between the large SWCC measurement device and the LSDS to ensure the results can be directly compared and are meaningful in Phase II. The research team determined that the maximum relative density in the SWCC cell without damaging the porous stone was 85 percent. A method for achieving a similar specimen packing density in the LSDS was determined which related to the relative density of the ballast only. It was also determined that samples should be prepared in the LSDS at the saturated volumetric water content and allowed to air dry to the residual water content, while running tests at the points in between. This will allow for comparisons of strength and volumetric behavior measurements at volumetric water contents measured with the SWCC device. Any additional points that are needed can then be targeted directly and tested. Finally, as determined in both the LSDS and SWCC, it is likely more meaningful to measure and record the water content of the fouling materials rather than the bulk of the fouled ballast. The quantity of material and time needed for measuring the water contents of the bulk fouled ballast material leaves it impractical. As previously noted, it is the SWCC characteristics of the fouling materials that influences the water holding capacity of the fouled ballast and will also likely be the main indicator of ballast strength.

The preliminary LSDS results identified that project goals can mostly be achieved at one stress level which will reduce the ballast breakdown occurring from test to test. The Mohr-Coulomb strength parameters were determined for clean ballast, however significant particle breakage was observed at higher stresses. Meaningful changes in peak stress were observed at different volumetric water contents in 5 percent fouled specimens, where the water content was bound by the SWCC measurements, although additional testing is needed to draw distinct conclusions. Phase II will continue to measure the strength at one stress for a variety of fouling materials and moisture conditions, as there is a need to establish repeatability and influences of sample variability on the results.

6. References

[1] Hyslip, J. P., Olhoeft, G. R., Selig, E. T., & Smith, S. S, "Ground Penetrating Radar for Railroad Track Substructure Evaluation," Technical Report No. DOT/FRA/ORD-05/04, U.S. Department of Tranpsortation, Federal Railroad Administration, Washington, DC, 2005.

[2] Ciampoli, L., Tosti, F., Brancadoro, M. G., D'Amico, F., Alani, A., & Benedetto, A., "A spectral analysis of ground-penetrating radar data for the assessment of the railway ballast geometric properties," *NDT & E International,* vol. 90, pp. 39–47, 2017.

[3] Al-Qadi, L., Xie, W., & Roberts, R., "Optimization of antenna configuration in multiple-frequency ground penetrating radar systems for railroad substructure assessment," *NDT & E International,* vol. 43, no. 1, pp. 20–28, 2010.

[4] Sussmann, T. R., Selig, E. T., & Hyslip, J. P., "Railway track condition indicators from ground penetrating radar," *NDT & E International,* vol. 36, no. 3, pp. 157–167, 2003.

[5] Gallagher, G. P., Leiper, Q., Williamson, R., Clark, M. R., & Forde, M. C., "The application of time domain ground penetrating radar to evaluate railway track ballast," *NDT & E International,* vol. 32, no. 8, pp. 463–468, 1999.

[6] Anbazhagan, P., Dixit, P. S. N., & Bharatha, T. P., "Identification of type and degree of railway ballast fouling using group coupled GPR antennas," *Journal of Applied Geophysics,* vol. 126, pp. 183–190, 2016.

[7] Leng, Z., & Al-Qadi, I., "Railroad ballast evaluation using ground-penetrating radar: Laboratory investigation and field validation," *Transportation Research Record: Journal of the Transportation Research Board,* vol. 2159, pp. 110–117, 2010.

[8] Sussmann, T. R., Application of ground-penetrating radar to railway track substructure maintenance management, 1999.

[9] De Chiara, F., Fontul, S., & Fortunato, E., "GPR Laboratory Tests for Railways Materials Dielectric Properties Assessment," *Remote Sensing,* vol. 6, p. 9712–9728, 2014.

[10] Sahin, H., Gu, F., Epps, J., & Lytton, R., "New method to estimate suction and moisture content of unbound aggregate base material in the field," in *Transportation Research Board 2016 Annual Meeting*, Washington, DC, 2016.

[11] Vanapalli, S. K., Sillers, W. S., & Fredlund, M. D., "The meaning and relevance of residual state to unsaturated soils," in *51st Canadian Geotechnical Conference*, 1998.

[12] Yang, H., Rahardjo, H., Leong, E. -C., & Fredlund, D. G., "Factors affecting drying and wetting soil-water characteristic curves of sandy soils," *Canadian Geotechnical Journal,* vol. 41, p. 908–920, 2004.

[13] Garven, E. A., & Vanapalli, S. K., "Evaluation of empirical procedures for predicting the shear strength of unsaturated soils," in *Unsaturated Soils 2006*, 2006, p. 2570–2592.

[14] Fredlund, D. G., & Houston, S. L., "Protocol for the assessment of unsaturated soil properties in geotechnical engineering practice," *Canadian Geotechnical Journal,* vol. 46, no. 6, p. 694–707, 2009.

[15] Bruzek, R., Stark, T. D., Wilk, Stephen T., Thompson, H. B., & Sussmann, T. R., "Fouled Ballast Definitions and Parameters," in *2016 Joint Rail Conference*, 2016.

[16] Sussmann, T. R., Ruel, M., & Chrismer, S. M., "Source of Ballast Fouling and Influence Considerations for Condition Assessment Criteria," *Transportation Research Record: Journal of the Transportation Research Board,* vol. 2289, p. 87–94, 2012.

[17] Rahardjo, H., Kim, Y., & Satyanaga, A., "Role of unsaturated soil mechanics in geotechnical engineering," *International Journal of Geo-Engineering,* vol. 10, p. 8, 2019.

[18] Khaleel, R., & Freeman, E. J., "Variability and scaling of hydraulic properties for 200 area soils, Hanford Site," Westinghouse Hanford Co., 1995.

[19] Gupta, S., Kang, D. H., & Ranaivoson, A., "Hydraulic and Mechanical Properties of Recycled Materials," Minnesota Department of Transportation, St. Paul, MN, 2009.

[20] Sherwood, R., Kulesza, S., & Bernhardt-Barry, M., "Unsaturated characteristics of fouled ballast to support in situ identification of fouling," in *Geo-Congress 2020*, Minneapolis, MN, 2020.

[21] Cui, Y. J., "Unsaturated railway trackbed materials," in *3rd European Conference on Unsaturated Soils*, Paris, France, 2016.

[22] Fredlund, D. G., & Rahardjo, H., Soil mechanics for unsaturated soils, John Wiley & Sons, 1993.

[23] Gupta, S., Ranaivoson, A., Edil, T., Benson, C., & Sawangsuriya, A., "Pavement Design Using Unsaturated Soil Technology," Minnesota Department of Transportation, Research Services Section, Technical Report No. MN/RC-2007-11, St. Paul, MN, 2007.

[24] Benson, C. H., Chiang, I., Chalermyanont, T., & Sawangsuriya, A., "Estimating van Genuchten parameters α and n for clean sands from particle size distribution data," in *From Soil Behavior Fundamentals to Innovations in Geotechnical Engineering: Honoring Roy E. Olson*, 2014.

[25] Wayllace, A., & Lu, N., "A Transient Water Release and Imbibitions Method for Rapidly Measuring Wetting and Drying Soil Water Retention and Hydraulic Conductivity Functions," *Geotechnical Testing Journal,* vol. 35, no. 1, p. 103–117, Paper No. GTJ103596. 2012.

[26] van Genuchten, M. T., "A closed-form equation for predicting the hydraulic conductivity of unsaturated soils," *Soil Science of America Journal,* vol. 44, no. 5, pp. 892–898, 1980.

[27] Hopmans, J. W., Romano, J. Š. N., & Durner, W., "Inverse Methods," in *Methods of Soil Analysis: Part 4 Physical Methods, 5.4*, Soil Science Society of America, Inc., 2002, pp. 963–1008.

[28] Tutumluer, E., Dombrow, W., & Huang, H., "Laboratory Characterization of Coal Dust Fouled Ballast Behavior," in *AREMA 2008 Annual Conference*, Salt Lake City, UT, 2008.

[29] Estaire, J., & Santana, M., "Large Direct Shear Tests Performed with Fresh Ballast," *Railroad Ballast Testing and Properties* pp. 144–161, Report No. ASTM STP1605. West Conshohocken, PA. 2018.

[30] Indraratna, B., Ionescu, D., & Christie, D., "Shear behaviour of railway ballast based on large scale triaxial testing," *Journal of Geotechnical and Geoenvironmental Engineering,* vol. 124, no. 5, pp. 439–449, 1998.

[31] Sevi, A,. Ge, L., & Take, W., "A Large-Scale Triaxial Apparatus for Prototype Railroad Ballast Testing," *Geotechnical Testing Journal,* vol. 32, no. 4, pp. 297–304, 2009.

[32] Federal Railroad Administration, "Ballast Degradation Characterized through Triaxial Testing," U.S. Department of Transportation, Research Results No. RR 16-21, Washington, DC, 2016.

[33] Jewell, R. A., "Direct shear tests on sand," *Geotechnique,* vol. 39, no. 2, pp. 309–322, 1989.

[34] Lings, M. L., & Dietz, M. S., "An improved direct shear apparatus for sand," *Geotechnique,* vol. 54, no. 4, pp. 245–256, 2004.

[35] Indraratna, B., Ngo, N., Rujikiatkamjorn, C., & Vinod, J. S., "Behavior of fresh and fouled railway ballast subjected to direct shear testing: discrete element simulation," *International Journal of Geomechanics,* vol. 14, no. 1, pp. 34–44, 2014.

[36] Dowbrow, W., Huang, H., & Tutumluer, E., "Comparison of coal dust fouled railroad ballast behavior - Granite vs. limestone," in *8th International Conference on Bearing Capacity of Roads and Airfields*, Urbana-Champaign, IL, 2009.

[37] Wnek, M. A., Tutumluer, E., Moaveni, M., & Gehringer, E., "Investigation of aggregate properties influencing railroad ballast performance," *Transporation Research Record: Journal of the Transportation Research Board,* vol. 2374, pp. 180-189, 2013.

[38] Huang, H., Tutumluer, E., & Dombrow W., "Laboratory characterization of fouled railroad ballast behavior," in *88th Annual Meeting of the Transportation Research Board*, Washington, DC, 2009.

[39] Stark, T. D., Swan, R. H., & Yuan, Z., "Ballast Direct Shear Testing," in *ASME/IEEE 2014 Joint Rail Conference*, Colorado Springs, CO, 2014.

[40] Selig, E. T., & Waters, J. M., Track geotechnology and substructure management, Thomas Telford, 1994.

[41] ASTM_D6913M-17, *Standard Test Methods for Particle-Size Distribution (Gradation) of Soils Using Sieve Analysis,* West Conshohocken, PA, 2017.

[42] ASTM_D7928-17, *Standard Test Method for Particle-Size Distribution (Gradation) of Fine-Grained Soils Using the Sedimentation (Hydrometer) Analysis,* West Conshohocken, PA, 2017.

[43] ASTM_D4318-17e1, *Standard Test Methods for Liquid Limit, Plastic Limit, and Plasticity Index of Soils,* West Conshohocken, PA: www.astm.org, 2017.

[44] ASTM_D854-14, *Standard Test Methods for Specific Gravity of Soil Solids by Water Pycnometer,* West Conshohocken, PA: www.astm.org, 2014.

[45] ASTM_D5084-16a, *Standard Test Methods for Measurement of Hydraulic Conductivity of Saturated Porous Materials Using a Flexible Wall Permeameter,* West Conshohocken, PA, 2016.

[46] ASTM_D5856-15, *Standard Test Method for Measurement of Hydraulic Conductivity of Porous Material Using a Rigid-Wall, Compaction-Mold Permeameter,* West Conshohocken, PA: www.astm.org, 2016.

[47] AREMA, "Chapter 1 Railway and Ballast," in *AREMA Manual for Railway Engineering*, American Railway Engineering and Maintenance-of-Way Association, 2019.

[48] Zhang, W., Jiang, S., Hardacre, C., Goodrich, P., Wang, K., Shao, H., & Wu, Z., "A combined Raman spectroscopic and thermogravimetric analysis study on oxidation of coal with different ranks," *Journal of Analytical Methods in Chemistry,* vol. 2015, no. 306874, 2015.

[49] Hu, W., Dano, C., Hicher, P. -Y., Le Touzo, J. -Y., Derkx, F., & Merliot, E., "Effect of sample size on the behavior of granular materials," *Geotechnical Testing Journal,* vol. 34, pp. 186–197, 2011.

[50] Soilmoisture Equipment Corp., "Porous Ceramics," 3 June 2020. [Online].

[51] Richards, L. A., "Capillary conduction of liquids in porous mediums," *Physics,* vol. 1, pp. 318–333, 1931.

[52] Bouwer, H., Rice, R. C., "Hydraulic Properties of Stony Vadose Zones[a]," *Groundwater,* vol. 22, p. 696–705, 1984.

[53] C.-1. ASTM, *Standard Test Method for Bulk Density ("Unit Weight") and Voids in Aggregate,* West Conshohocken, PA: www.astm.org, 2017.

[54] Bareither, C. A., & Benson, C. H., "Evaluation of Bouwer-Rice large-particle correction procedure for soil water characteristic curves," *Geotechnical Testing Journal,* vol. 36, no. 5, p. 680–694, 2013.

[55] Simoni, A., & Houlsby, G. T., "The direct shear strength and dilatancy of sand-gravel mixtures," *Geotechnical and Geological Engineering,* vol. 24, pp. 523–549, 2006.

[56] Shibuya, S., Mitachi, T., & Tamate, S., "Interpretation of direct shear box testing of sands as quasi-simple shear," *Geotechnique,* vol. 47, no. 4, pp. 769–790, 1997.

[57] U.S. Department of the Interior, U.S. Geological Survey, "USGS Groundwater Ingormation," 18 December 2017. [Online].

[58] SoilWater Retention LLC, *Transient Release and Imbibitions Method (TRIM),* SoilWater Retention LLC, 2018.

[59] Hay, W. W., Railroad engineering, vol. 1, John Wiley & Sons, 1982.

[60] Armstrong, J. H., The Railroad: What it is, What it Does. The Introduction to Railroading, 1990.

[61] Russo, D., "Determining soil hydraulic properties by parameter estimation: On the selection of a model for the hydraulic properties," *Water resources research,* vol. 24, p. 453–459, 1988.

[62] Brooks, R. H., & Corey, A. T., "Properties of porous media affecting fluid flow," *Journal of the Irrigation and Drainage Division,* vol. 92, p. 61–90, 1966.

[63] Sapko, M. J., Cashdollar, K. L., & Green, G. M., "Coal dust particle size survey of US mines," *Journal of Loss Prevention in the Process Industries,* vol. 20, p. 616–620, Pittsburgh Research Laboratory, National Institute for Occupational Safety and Health, 2007.

[64] Eching, S. O., & Hopmans, J. W., "Optimization of hydraulic functions from transient outflow and soil water pressure data," *Soil Science Society of America Journal,* vol. 57, p. 1167–1175, 1993.

[65] Wallace, A. J., "Permeability of fouled rail ballast," *UG Thesis, School of Civil, Mining and Environmental Engineering, University of Wollongong,* 2003.

[66] Azam, A. M., Cameron, D. A., Gabr, A. G., & Rahman, M. M., "Matric suction in recycled unbound granular materials," in *Geo-Congress 2014: Geo-characterization and Modeling for Sustainability*, 2014.

[67] Indraratna, B., Su, L.-J., & Rujikiatkamjorn, C., "A new parameter for classification and evaluation of railway ballast fouling," *Canadian Geotechnical Journal,* vol. 48, p. 322–326, 2011.

[68] Hollenbeck, K.-J., & Jensen, K. H., "Experimental evidence of randomness and nonuniqueness in unsaturated outflow experiments designed for hydraulic parameter estimation," *Water Resources Research,* vol. 34, no. 4, p. 595–602, 1998.

[69] Ba, M., Nokkaew, K., Fall, M., & Tinjum, J. M., "Effect of matric suction on resilient modulus of compacted aggregate base courses," *Geotechnical and Geological Engineering,* vol. 31, p. 1497–1510, 2013.

[70] Russo, D., Bresler, E., Shani, U., & Parker, J. C., "Analyses of infiltration events in relation to determining soil hydraulic properties by inverse problem methodology," *Water Resources Research,* vol. 27, no. 6, 1991.

[71] Simunek, J., Sejna, M., van Genuchten, M. Th., Šimunek, J., Šejna, M., Jacques, D., Šimunek, J., Mallants, D., Saito, H., & Sakai, M., "The HYDRUS-1D Softare Package for Simulating the One-Dimensional Movement of Water, Heat, and Multiple Solutes in Variably-Saturated Media," Department of Environmental Sciences, University of California Riverside, Riverside, CA, 1998.

Appendix A.
Ballast Fouling Samples

Table A.1: Gradation characteristics of fouling samples

No.	Percent Gravel	Percent Sand	Percent Fines	D_{10} (mm)	D_{50} (mm)	LL	PI	Cc	Cu	USCS	Gs
1	47.2	51.7	1.10	0.31	4.39	-	-	1.16	18.5	SW	2.66
2	44.8	54.3	0.90	0.30	4.11	-	-	1.88	17.6	SW	2.63
3	41.3	57.7	1.00	0.27	3.36	-	-	1.38	17.9	SW	2.63
4	42.3	56.8	0.90	0.33	3.82	-	-	1.52	15.3	SW	2.60
5	41.3	56.7	2.00	0.20	3.26	-	-	0.697	24.7	SP	2.62
6	25.4	72.3	2.30	0.12	1.31	-	-	0.416	19.5	SP	2.62
7	33.7	65.0	1.30	0.16	2.23	-	-	0.634	24.0	SP	2.63
8	26.8	55.7	17.5	0.03	0.80	20	2	1.07	75.3	SM	2.60
9	9.80	35.3	54.9	0.002	0.046	38	27	2.12	50.1	ML	2.70
10	16.7	43.0	40.3	0.002	0.24	24	6	0.340	380	SC-SM	2.67
11	16.7	44.1	39.2	0.001	0.25	24	6	0.334	524	SC-SM	2.58
12	15.7	38.5	45.8	0.002	0.13	24	6	0.318	170	SC-SM	2.66
13	11.0	33.5	55.5	0.001	0.028	27	7	0.287	199	CL	2.60
14	10.8	30.5	58.7	0.001	0.018	28	8	0.393	160	CL	2.56

D_{10} – Particle size for which 10% of particles by mass are smaller
D_{50} – Median particle size, or for which 50% of particles by mass are smaller
LL – Liquid Limit
PI – Plasticity Index
Cc – Coefficient of curvature
Cu – Coefficient of uniformity
USCS – Unified Soil Classification System
G_s – Specific gravity of solids

Table A.2: Measured saturated hydraulic conductivity

Sample ID	K_s(cm/s)	ρ_d(g/cm^3)
SP	6.90E-02	1.66
SC-SM	1.47E-04	1.68
CL	2.69E-05	1.67

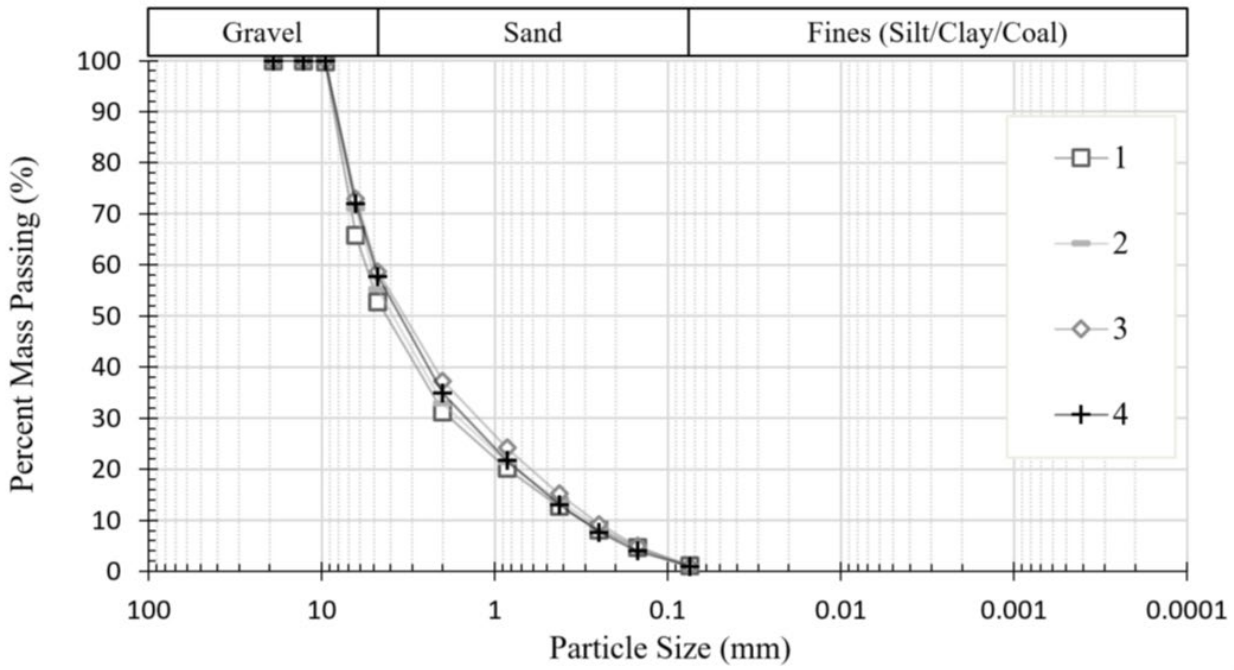

Figure A.1: GSD of SW fouling samples

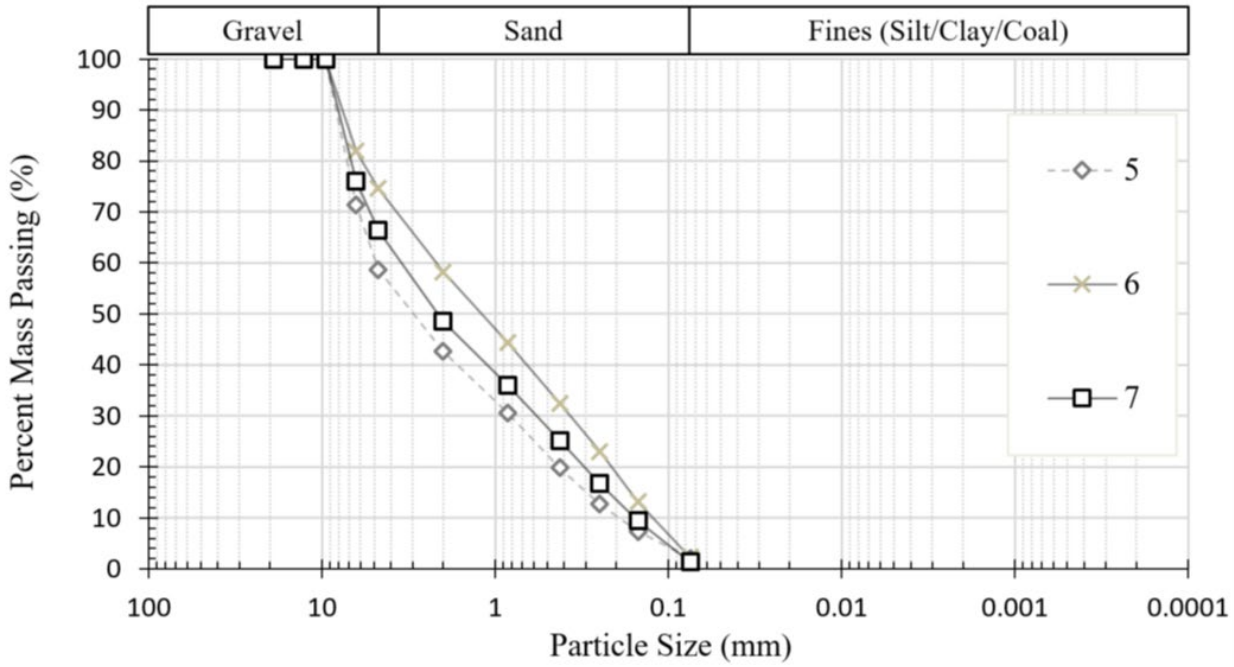

Figure A.2: GSD of SP fouling samples

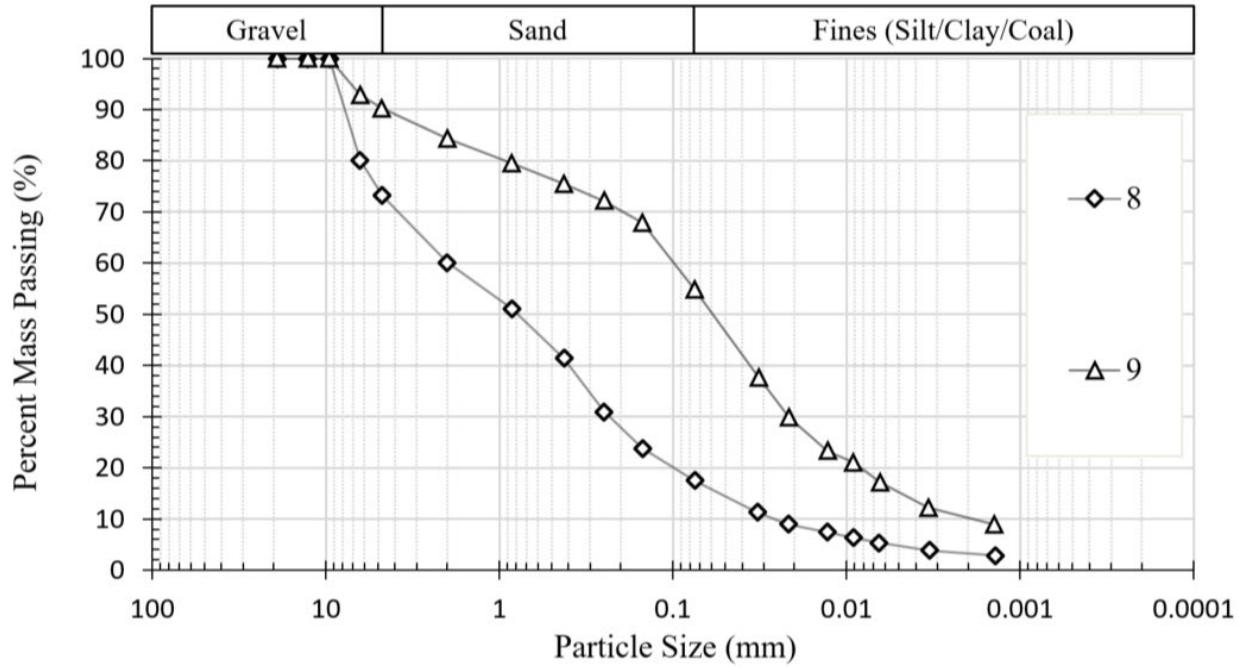

Figure A.3: GSD of SM (No. 8) and ML (No. 9) fouling samples

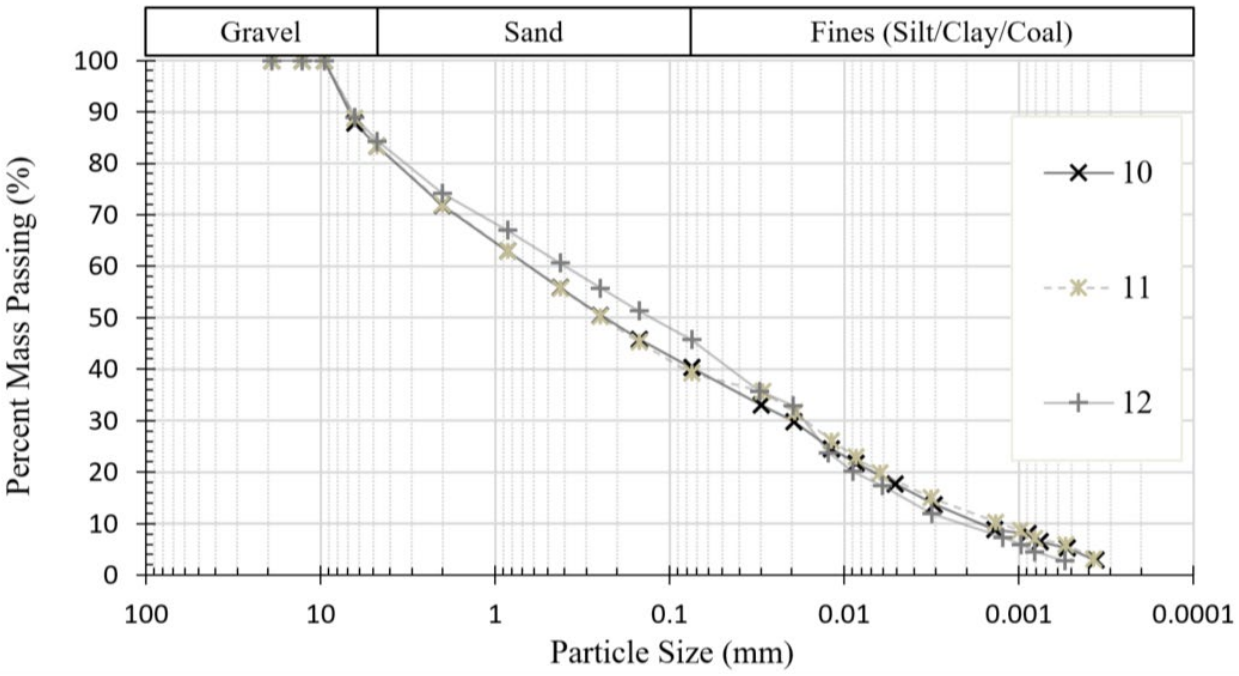

Figure A.4: GSD of SC-SM fouling samples with coal dust

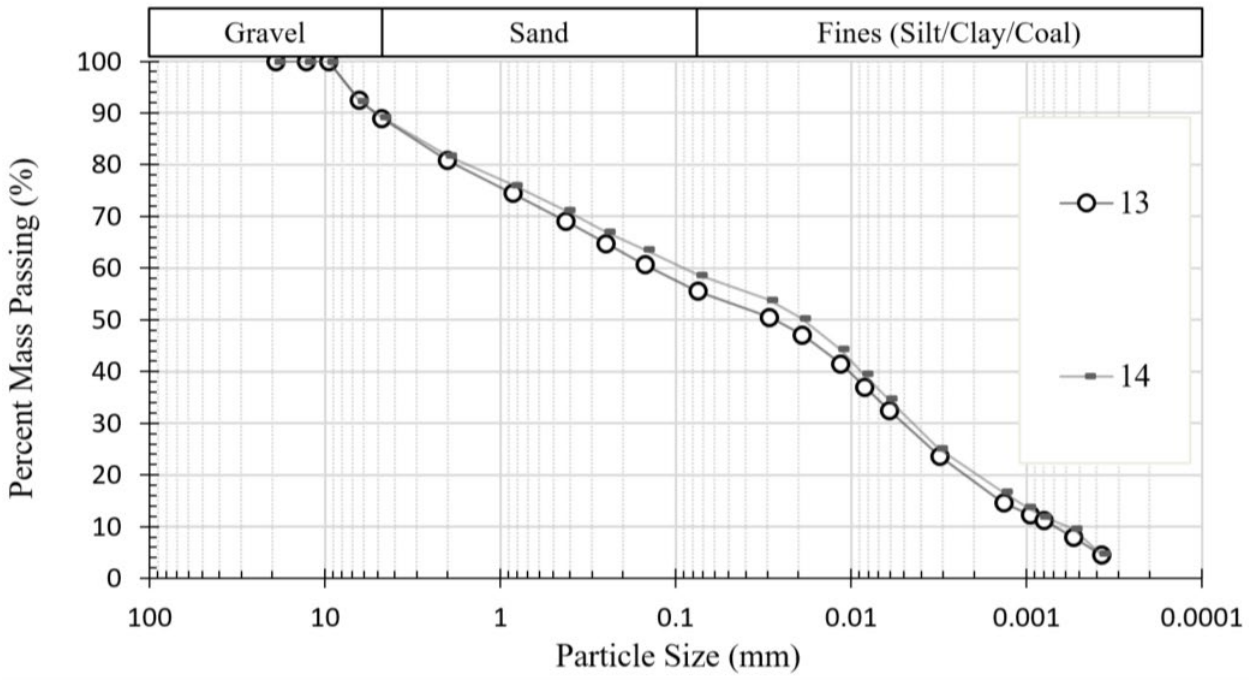

Figure A.5: GSD of CL fouling samples with coal dust

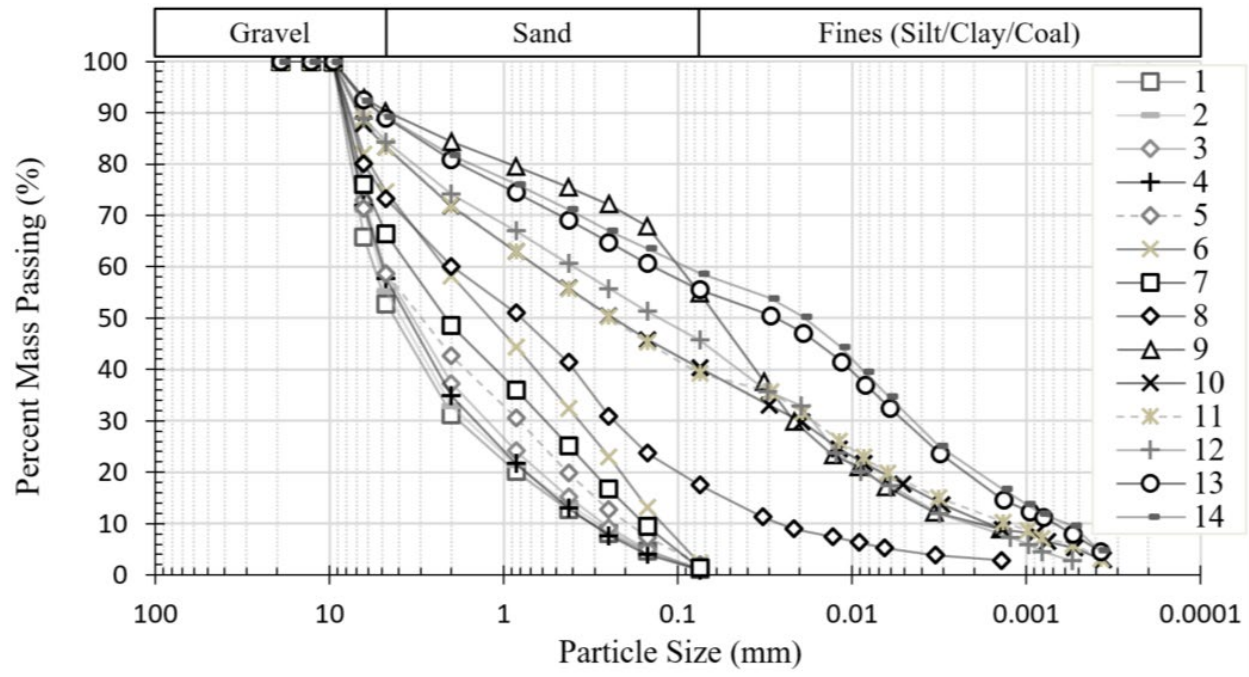

Figure A.6: GSD of all fouling samples

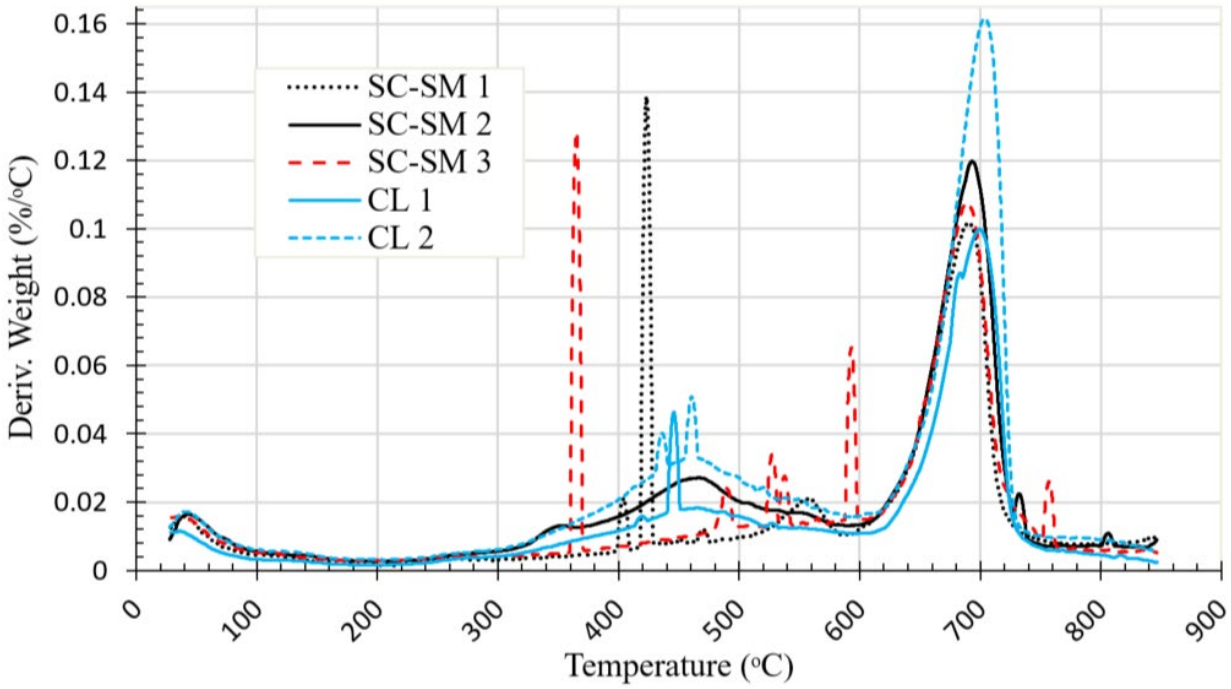

Figure A.7: TGA, deriv. weight (%/°C) vs. temp. (°C) for the fouling samples with coal dust

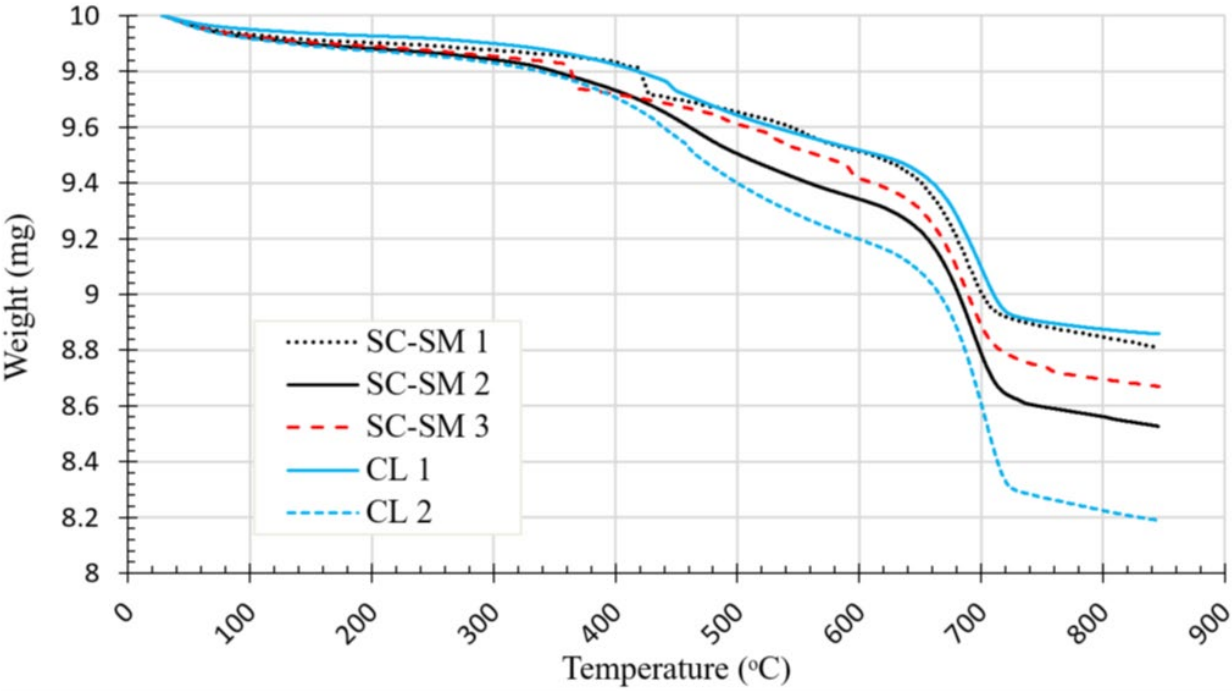

Figure A.8: TGA, weight (mg) vs. temp. (°C) for the fouling samples with coal dust

Table A.3: van Genuchten hydraulic parameters and experimental density

No.	USCS	θ_r	$\alpha(1/\mathrm{cm})$	n	m	$K_s(\mathrm{cm/s})$	$\rho_d(\mathrm{g/cm^3})$
1	SW	0.056	0.069	3.50	0.714	1.71E-02	1.56
2	SW	0.059	0.190	3.33	0.700	1.12E-02	1.64
3	SW	0.063	0.164	5.00	0.800	1.60E-03	1.76
4	SW	0.063	0.238	1.98	0.496	2.56E-02	1.66
5	SP	0.063	0.107	4.06	0.754	8.14E-03	1.56
6	SP	0.082	0.066	6.73	0.851	7.36E-04	1.65
7	SP	0.062	0.128	2.26	0.557	6.39E-03	1.70
8	SM	0.067	0.0587	2.61	0.616	5.10E-04	1.70
9	ML	0.121	0.00492	1.82	0.451	8.70E-05	1.68
10	SC-SM	0.162	0.0130	3.50	0.714	9.52E-05	1.67
11	SC-SM	0.169	0.0128	3.50	0.714	2.01E-04	1.64
12	SC-SM	0.180	0.0217	3.50	0.714	1.18E-04	1.68
13	CL	0.148	0.0124	3.50	0.714	4.51E-05	1.67
14	CL	0.155	0.0022	1.61	0.379	3.50E-05	1.57

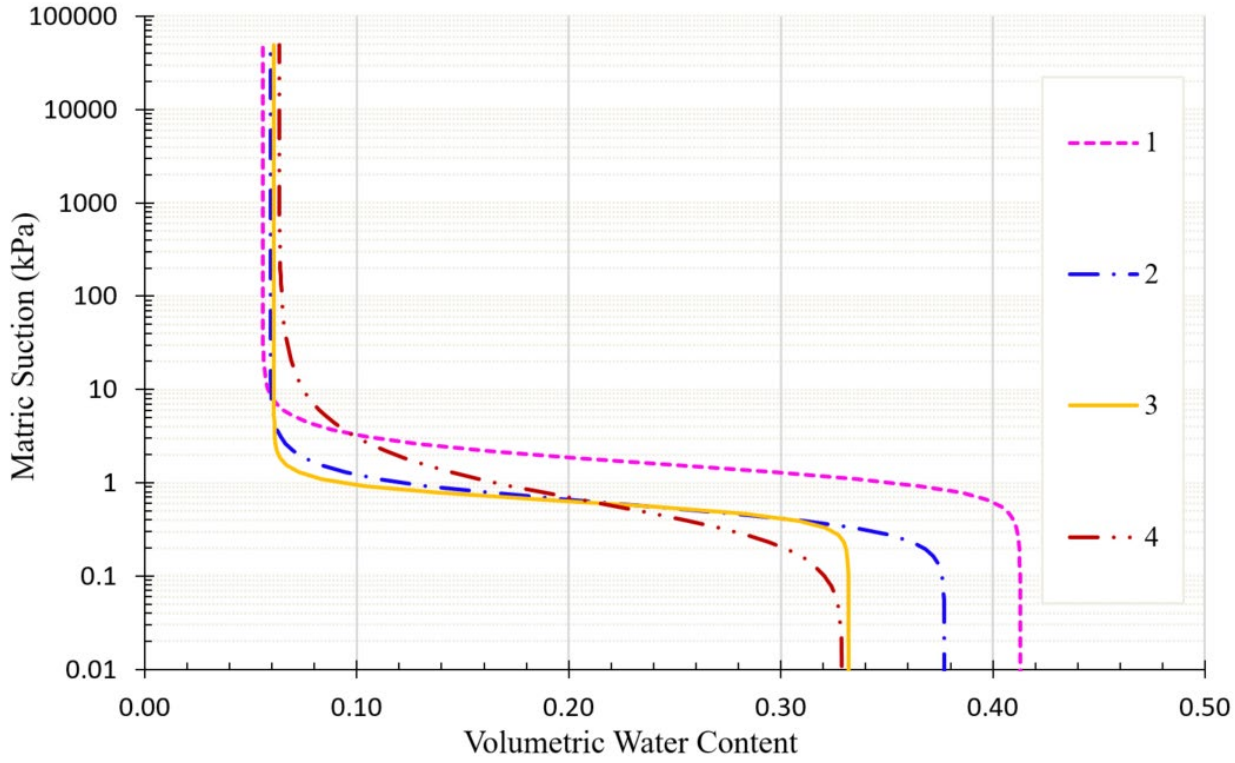

Figure A.9: SWCCs of SW fouling samples

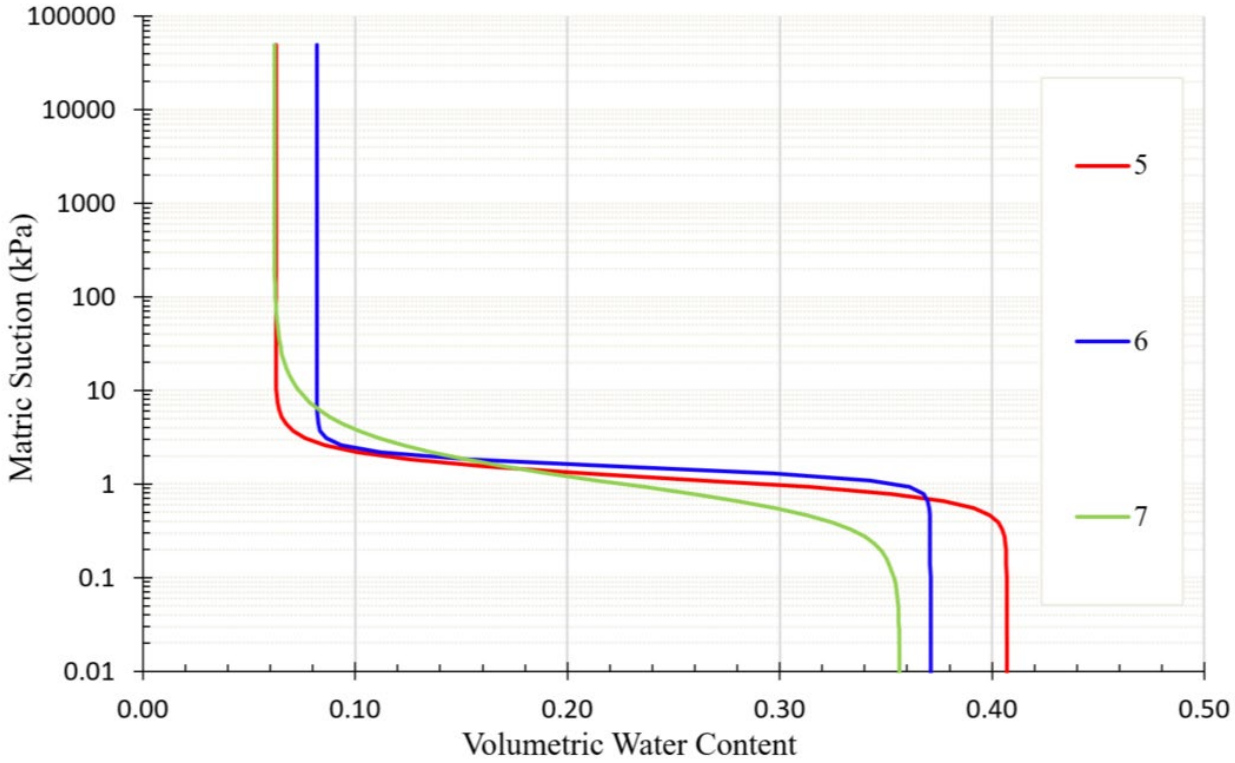

Figure A.10: SWCCs of SP fouling samples

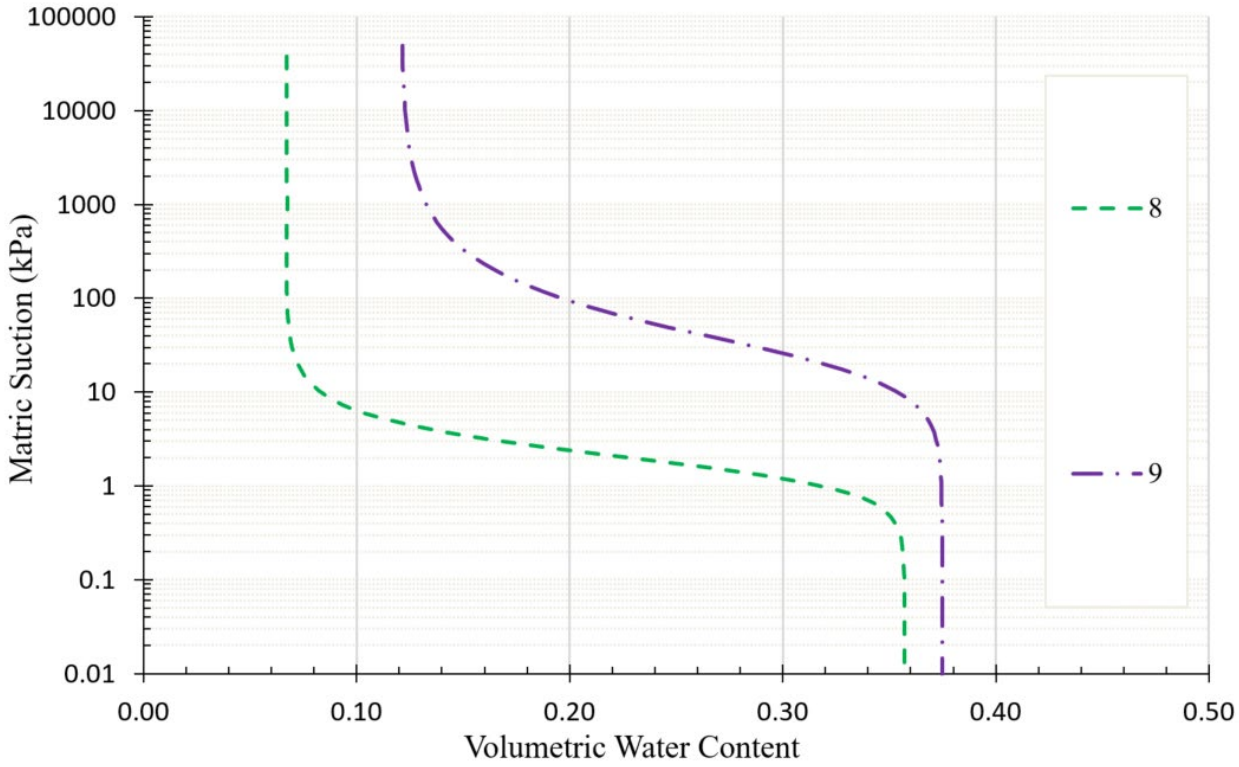

Figure A.11: SWCCs of SM (8) and ML (9) fouling samples

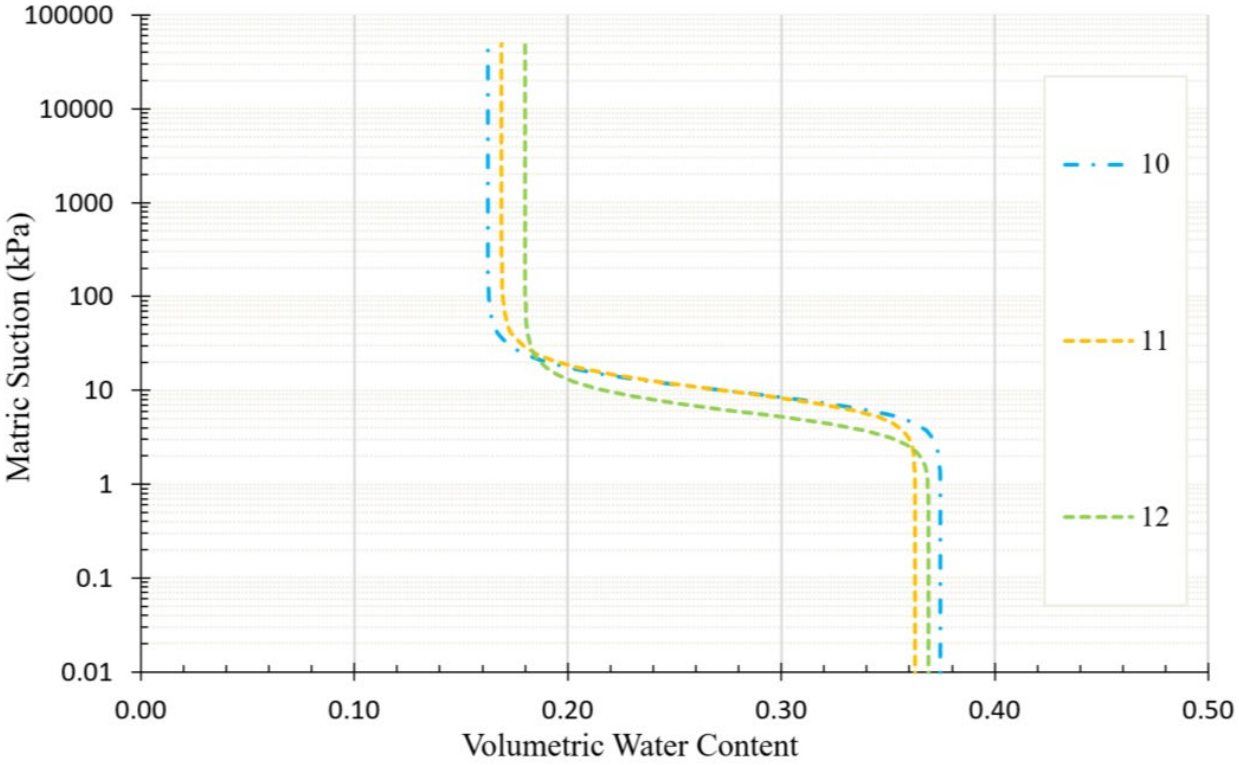

Figure A.12: SWCCs of SC-SM fouling samples with coal dust

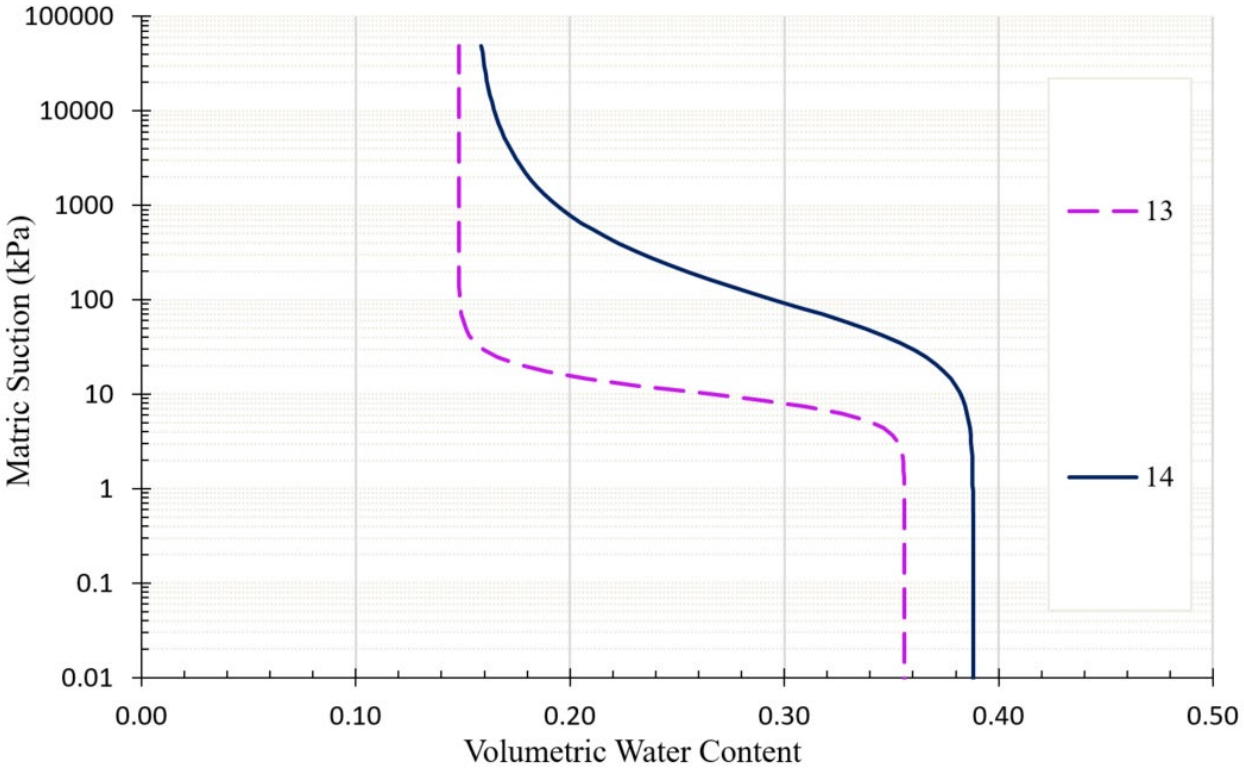

Figure A.13: SWCCs for CL fouling samples with coal dust

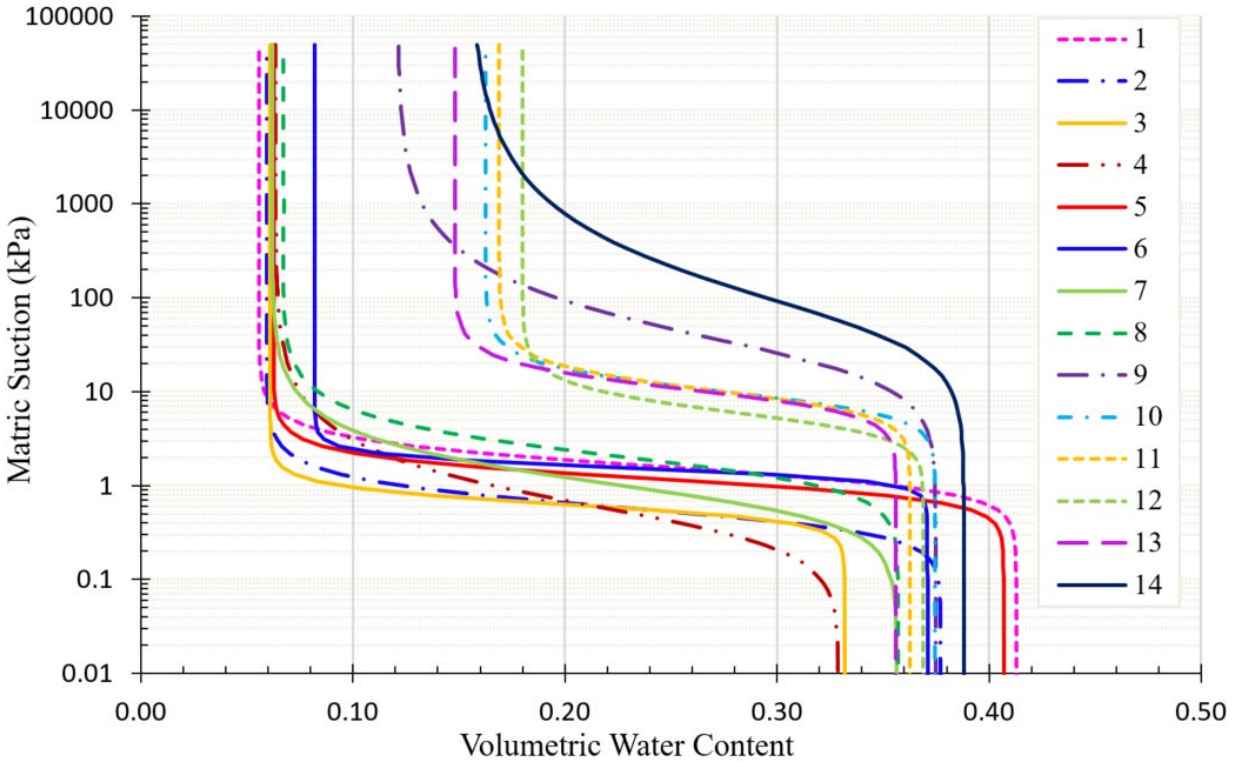

Figure A.14: SWCCs of all fouling samples

Appendix B.
Fouled Ballast Specimens

Table B.1: Gradation characteristics of fouled ballast specimens

Specimen ID	Percent Gravel	Percent Sand	Percent Fines	D_{10} (mm)	D_{50} (mm)	Cc	Cu	FI (%)	G_s
SP-22	85.3	14.4	0.3	1.69	27.5	8.33	17.8	15	2.64
SP-35	76.8	22.7	0.5	0.558	24.9	3.72	50.3	24	2.64
SP-50	66.7	32.7	0.6	0.315	8.60	1.86	75.2	34	2.64
SP-60	60.2	39.0	0.8	0.248	7.33	2.07	39.0	41	2.64
SW-35	79.8	19.9	0.3	1.45	24.8	1.50	19.9	21	2.63
SW-50	71.1	28.4	0.5	0.699	17.2	1.47	34.6	29	2.62
SW-60	65.3	34.1	0.6	0.602	7.63	2.60	15.5	35	2.62
SM-35	74.4	19.5	6.1	0.217	24.8	8.41	132	32	2.63
SM-50	63.4	27.9	8.7	0.105	9.84	1.56	226	45	2.62
SM-60	56.0	33.5	10.5	0.0653	6.86	1.06	142	54	2.62
ML-35	68.4	12.3	19.2	0.0172	24.9	14.4	1670	51	2.66
ML-50	54.9	17.6	27.4	0.00774	9.60	0.0592	3080	73	2.67
ML-60	45.9	21.2	33.0	0.00577	1.77	0.0697	1650	87	2.67
SC-SM-35	70.9	15.0	14.1	0.00151	24.8	72.9	1910	43	2.65
SC-SM-50	58.4	21.5	20.1	0.00737	9.58	2.58	3240	62	2.65
SC-SM-60	50.1	25.8	24.2	0.00531	4.78	1.07	1850	74	2.66
CL1-35	68.9	11.7	19.4	0.00478	24.9	98.2	6015	51	2.62
CL1-50	55.5	16.7	27.7	0.00242	9.54	0.345	9864	72	2.62
CL1-60	46.6	50.1	33.3	0.00176	2.85	0.0464	5402	87	2.61
CL2-35	68.8	10.7	20.5	0.00418	24.8	101	6880	52	2.61
CL2-50	55.4	15.2	29.4	0.00203	9.65	0.188	1170	74	2.60
CL2-60	46.5	18.3	35.2	0.00140	2.58	0.0270	6800	89	2.59

D_{10} – Particle size for which 10% of particles by mass are smaller
D_{50} – Median particle size, or for which 50% of particles by mass are smaller
Cc – Coefficient of curvature
Cu – Coefficient of uniformity
FI – Selig Index
G_s – Specific gravity of solids

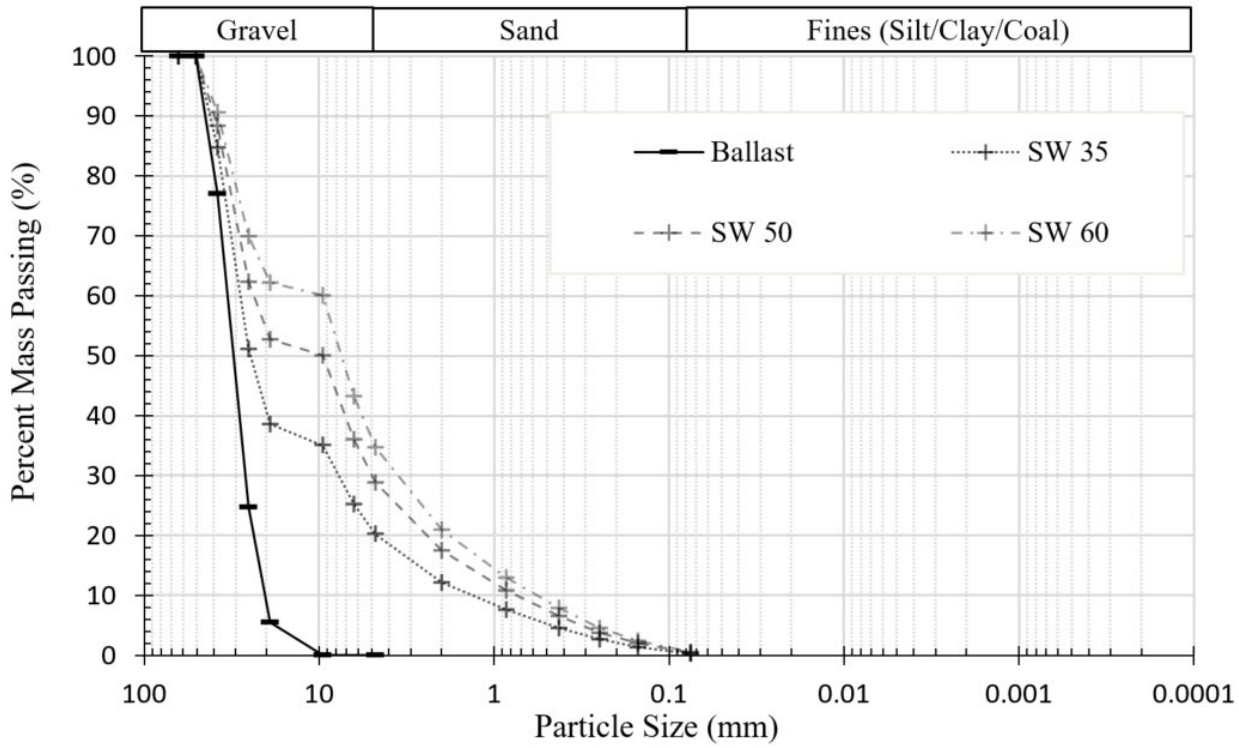

Figure B.1: GSD of SW fouled ballast specimens

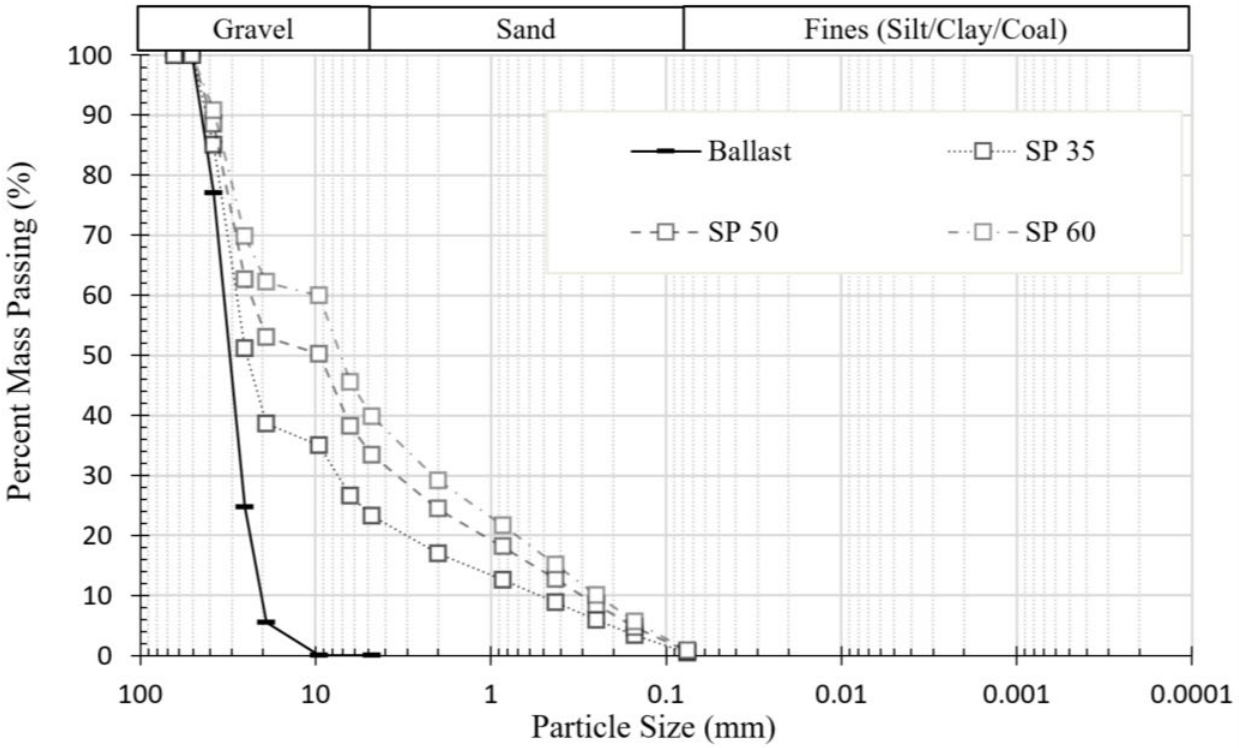

Figure B.2: GSD of SP fouled ballast specimens

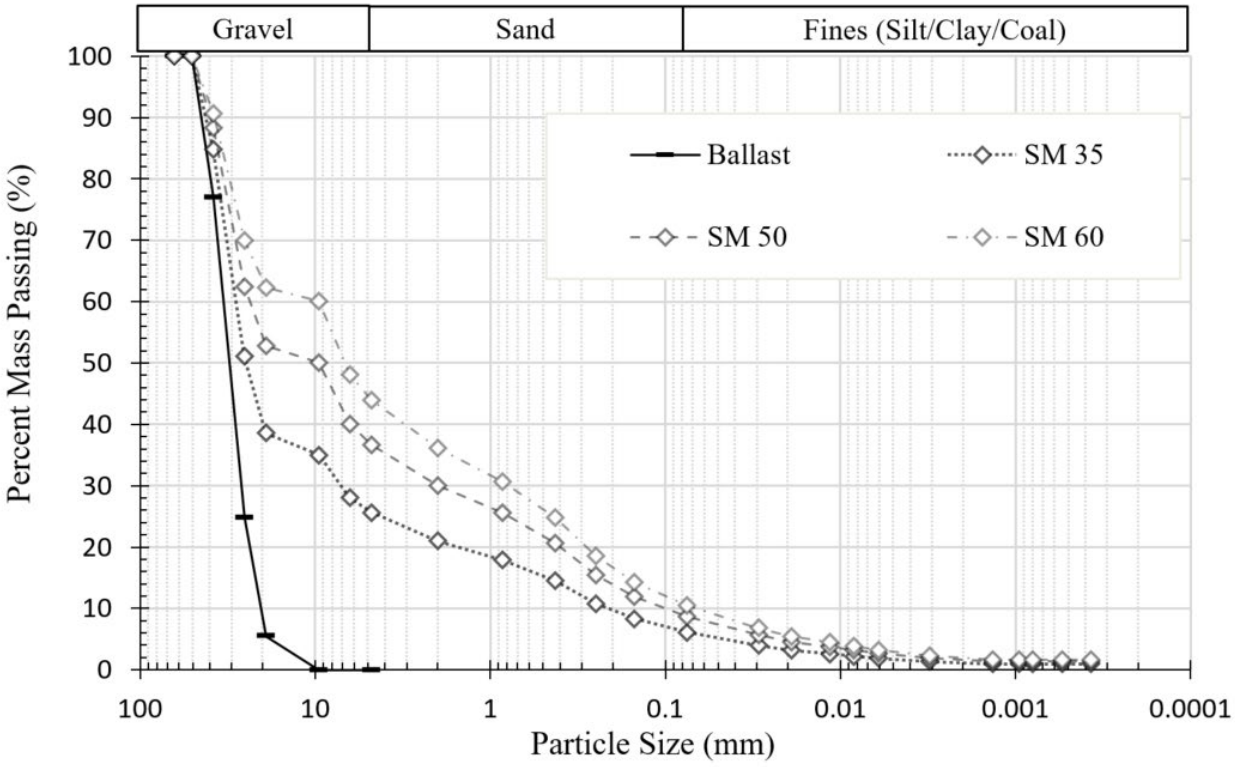

Figure B.3: GSD of SM fouled ballast specimens

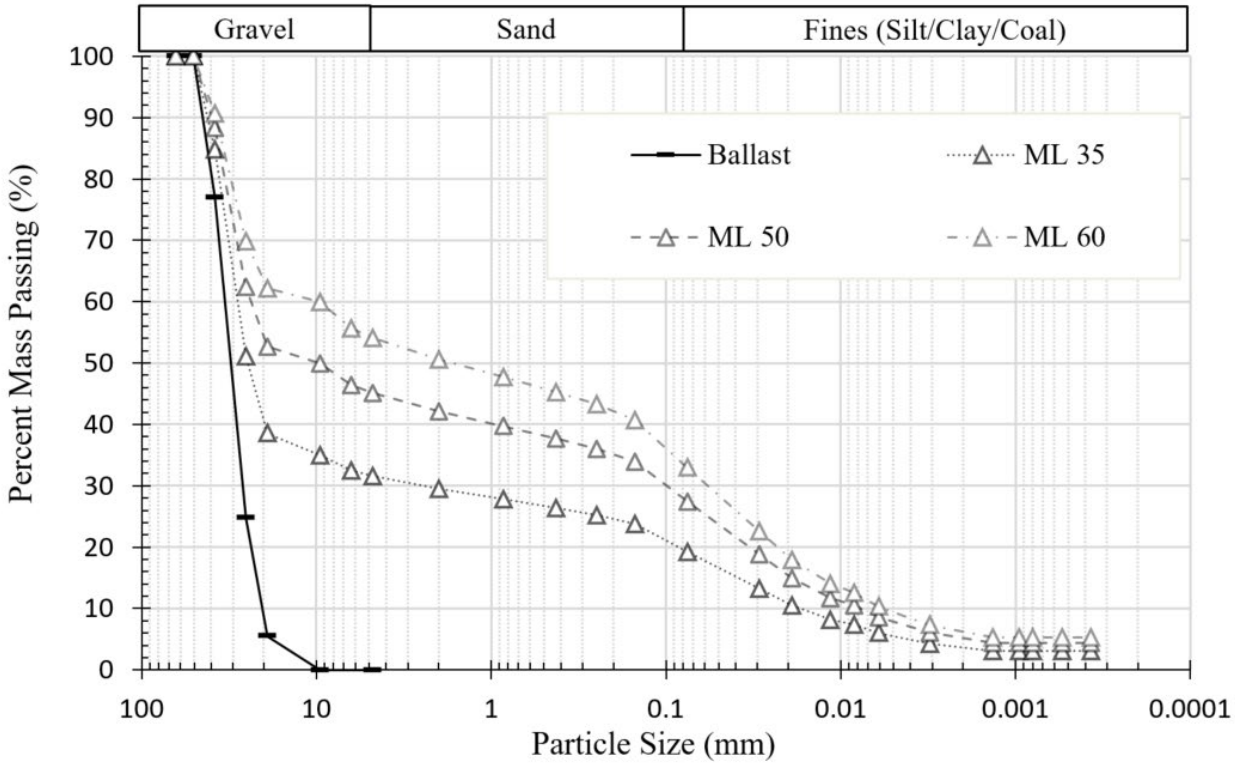

Figure B.4: GSD of ML fouled ballast specimens

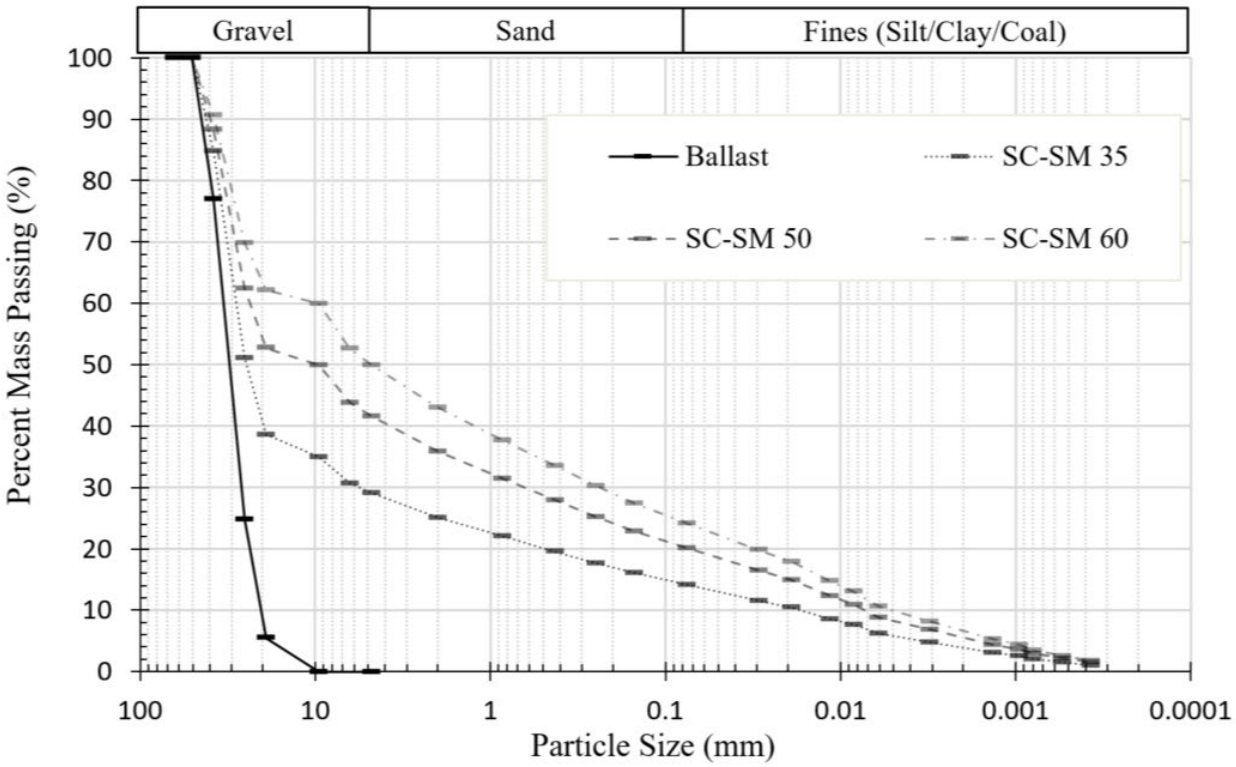

Figure B.5: GSD of SC-CM fouled ballast specimens

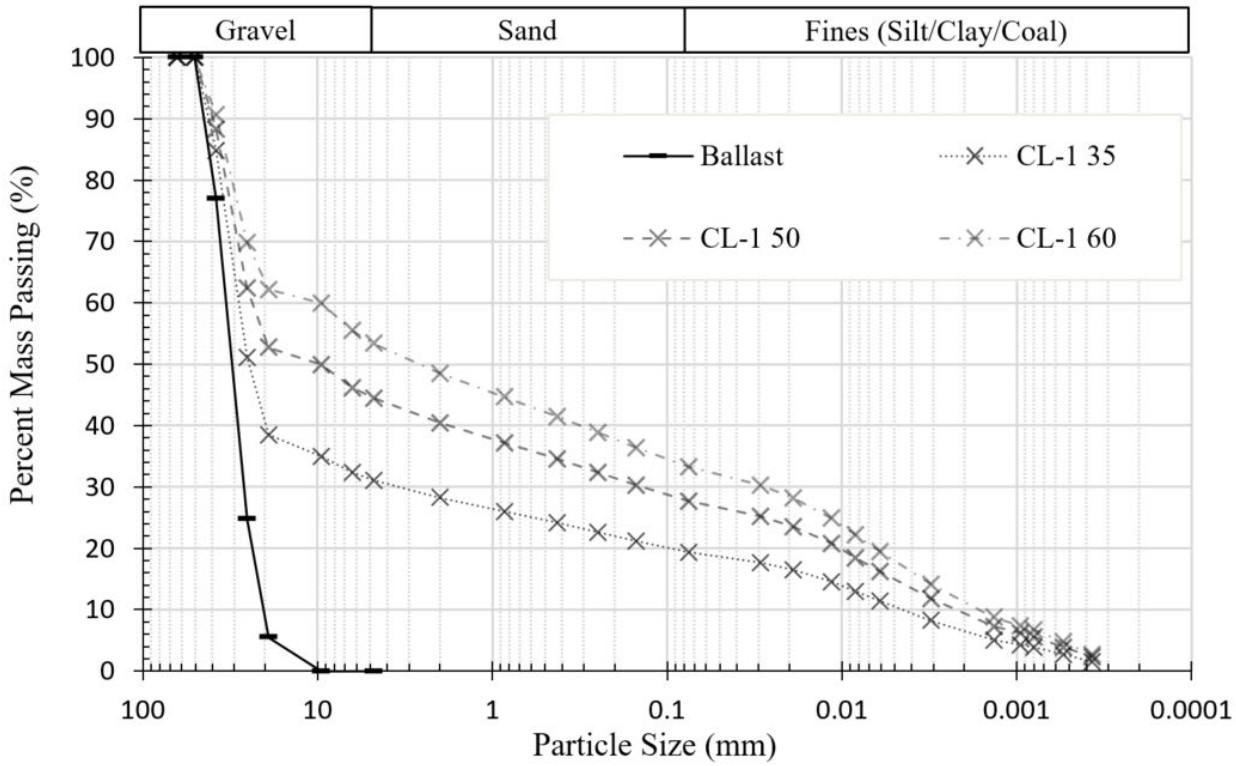

Figure B.6: GSD of CL-1 fouled ballast specimens

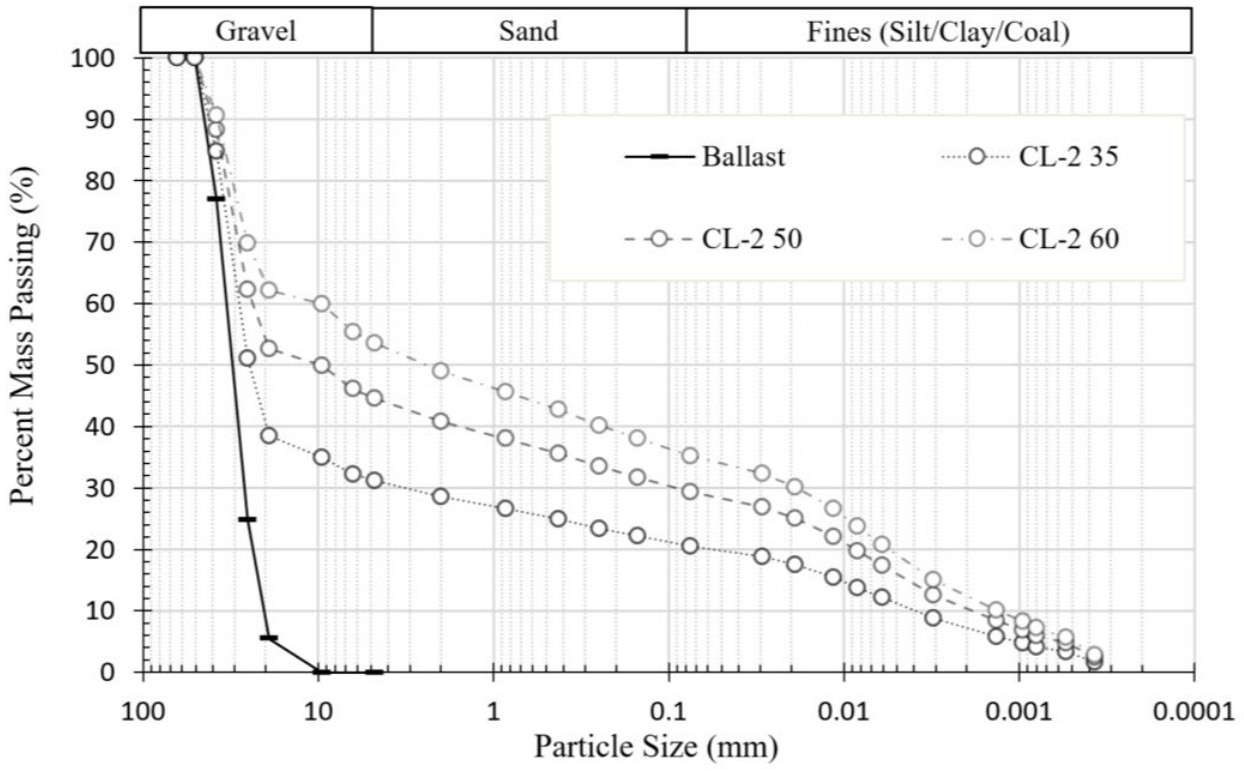

Figure B.7: GSD of CL-2 fouled ballast specimens

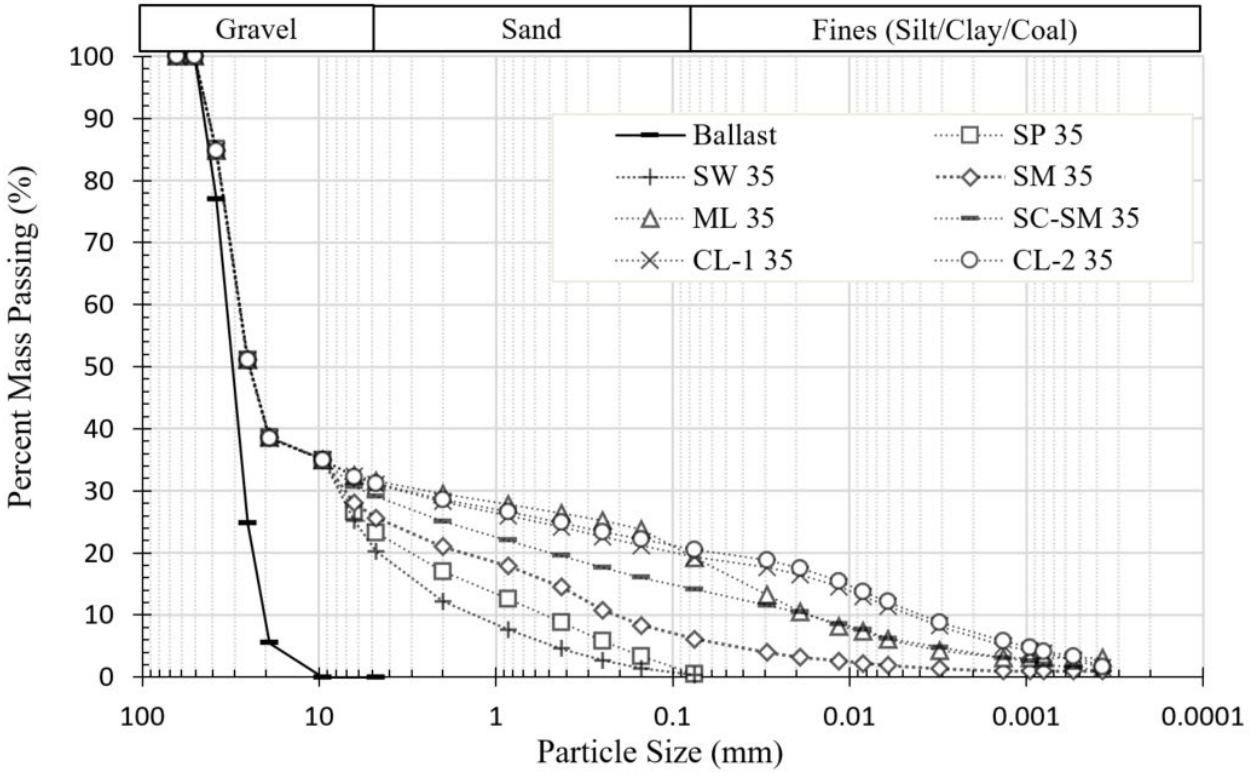

Figure B.8: GSD summary of 35% fouled ballast specimens

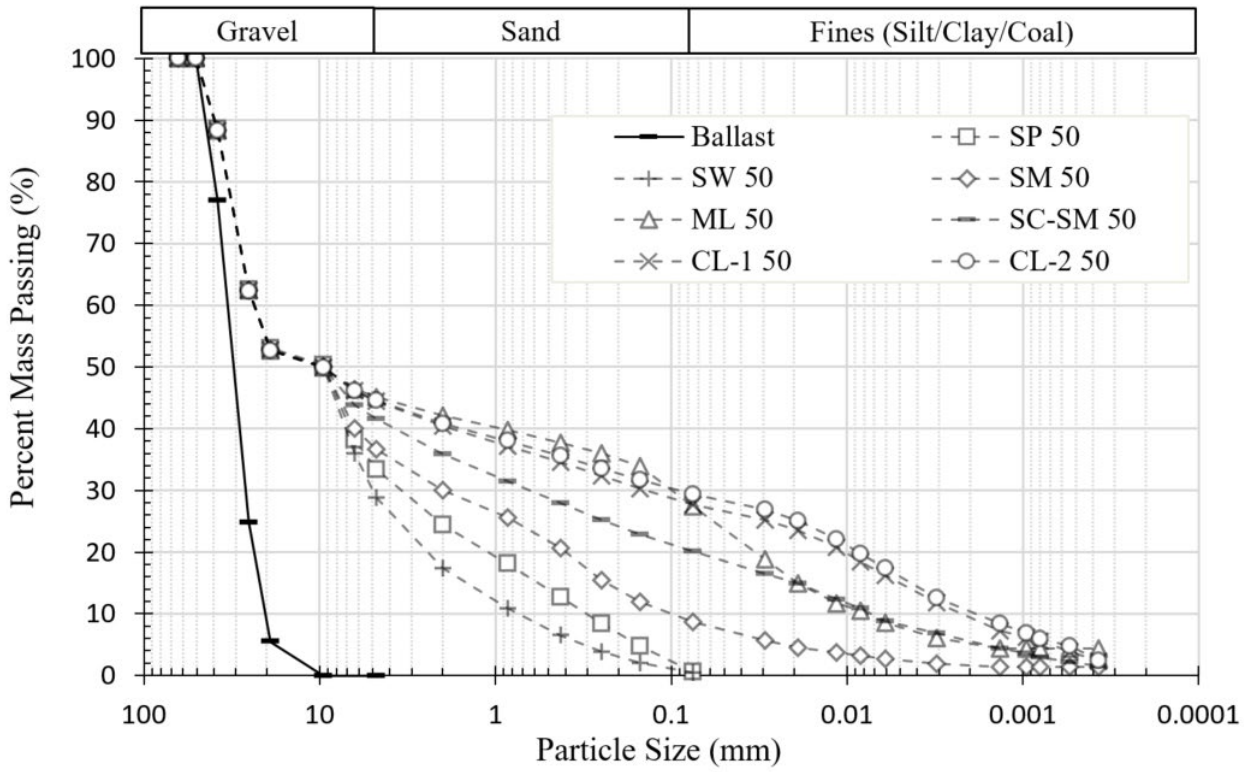

Figure B.9: GSD summary of 50% fouled ballast specimens

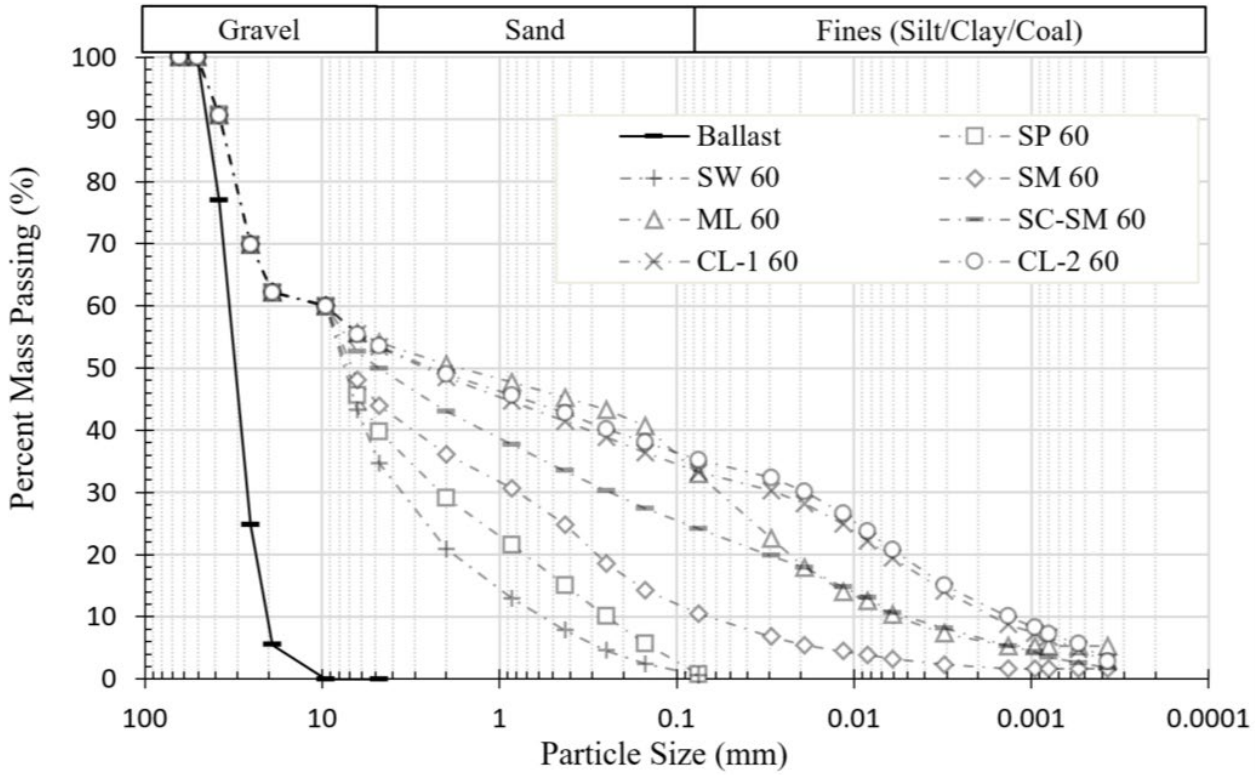

Figure B.10: GSD summary of 60% fouled ballast specimens

Table B.2: van Genuchten hydraulic parameters and bulk/fines density of fouled ballast specimens

Sample ID	θ_r	θ_s	$\alpha(1/\mathrm{cm})$	n	m	$\rho_{d,fb}(\mathrm{g/cm^3})$	$\rho_{d,f}(\mathrm{g/cm^3})$
SW 35	0.03	0.15	0.238	1.98	0.496	2.21	1.66
SW 50	0.04	0.20				2.06	1.66
SW 60	0.04	0.23				1.97	1.66
SP 35	0.03	0.16	0.128	2.26	0.557	2.21	1.70
SP 50	0.04	0.22				2.07	1.70
SP 60	0.04	0.25				1.98	1.70
SM 35	0.03	0.16	0.0587	2.61	0.616	2.25	1.75
SM 50	0.04	0.21				2.11	1.75
SM 60	0.05	0.25				2.03	1.75
ML 35	0.06	0.17	0.00492	1.82	0.451	2.20	1.68
ML 50	0.07	0.23				2.06	1.68
ML 60	0.09	0.26				1.97	1.68
SC-SM 35	0.09	0.20	0.0130	3.50	0.714	2.19	1.67
SC-SM 50	0.10	0.23				2.04	1.67
SC-SM 60	0.10	0.24				1.96	1.67
CL-1 35	0.07	0.16	0.124	3.50	0.714	2.19	1.67
CL-1 50	0.09	0.22				2.05	1.67
CL-1 60	0.10	0.25				1.96	1.67
CL-2 35	0.08	0.18	0.0022	1.61	0.379	2.13	1.57
CL-2 50	0.10	0.24				1.97	1.57
CL-2 60	0.11	0.28				1.87	1.57

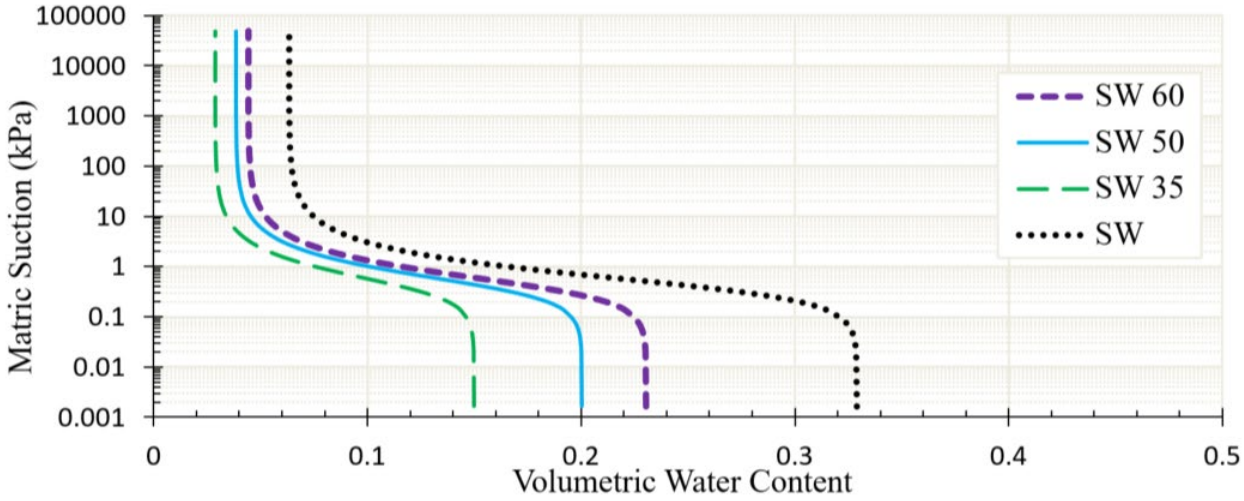

Figure B.11: Predicted SWCCs for SW fouled ballast specimens

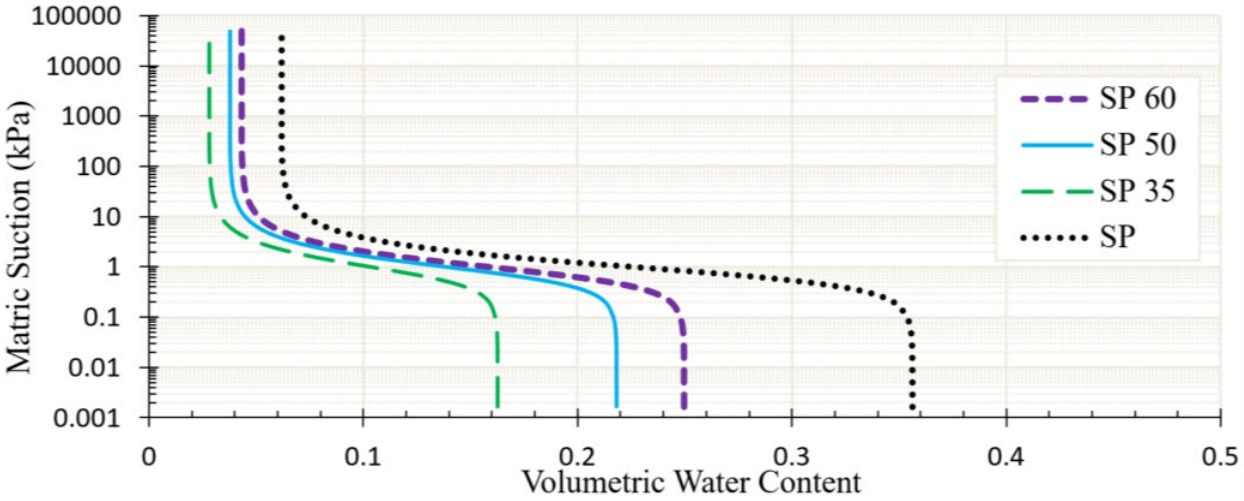

Figure B.12: Predicted SWCCs for SP fouled ballast specimens

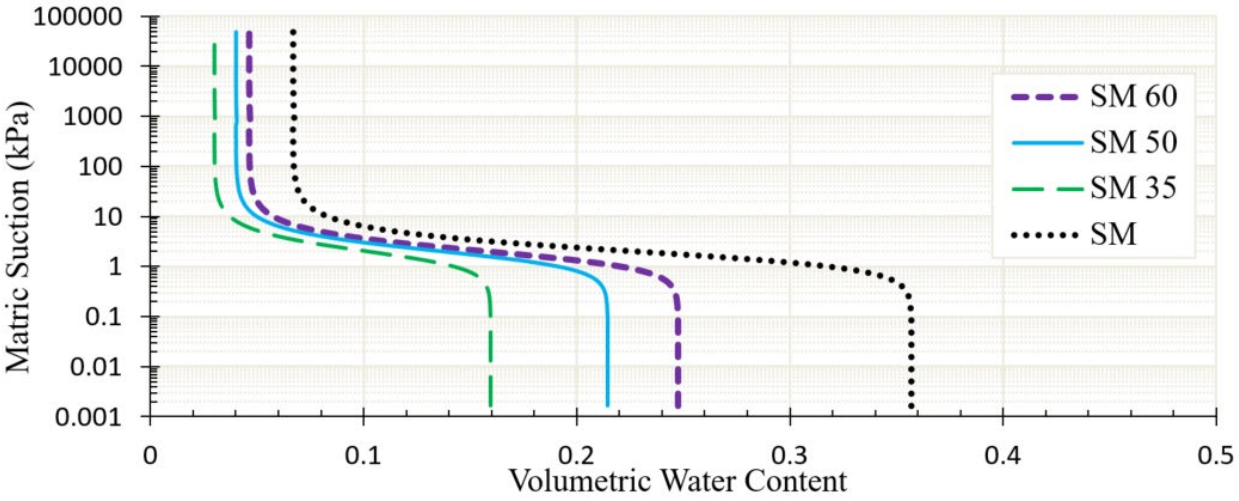

Figure B.13: Predicted SWCCs for SM fouled ballast specimens

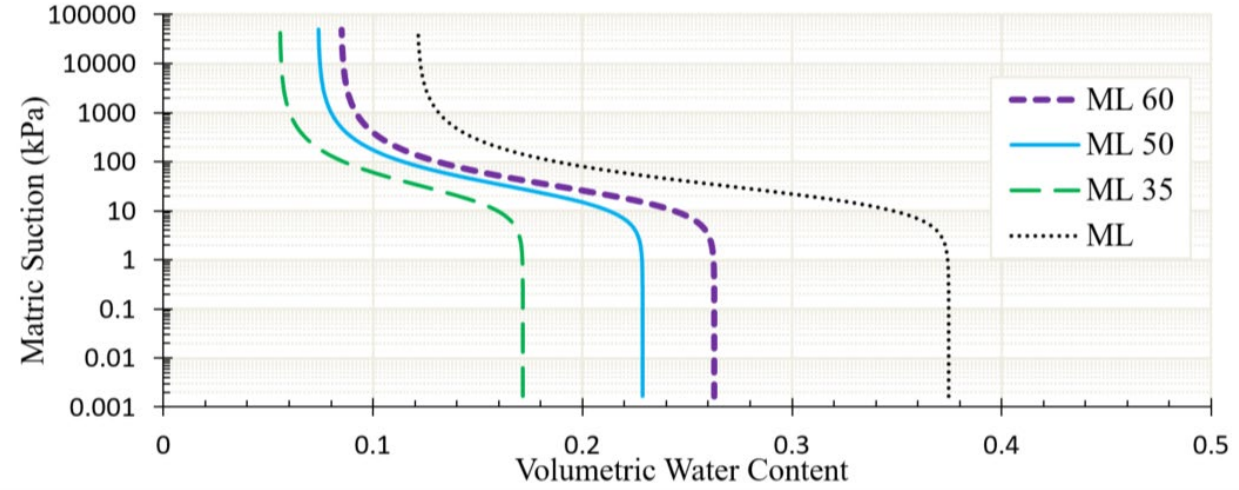

Figure B.14: Predicted SWCCs for ML fouled ballast specimens

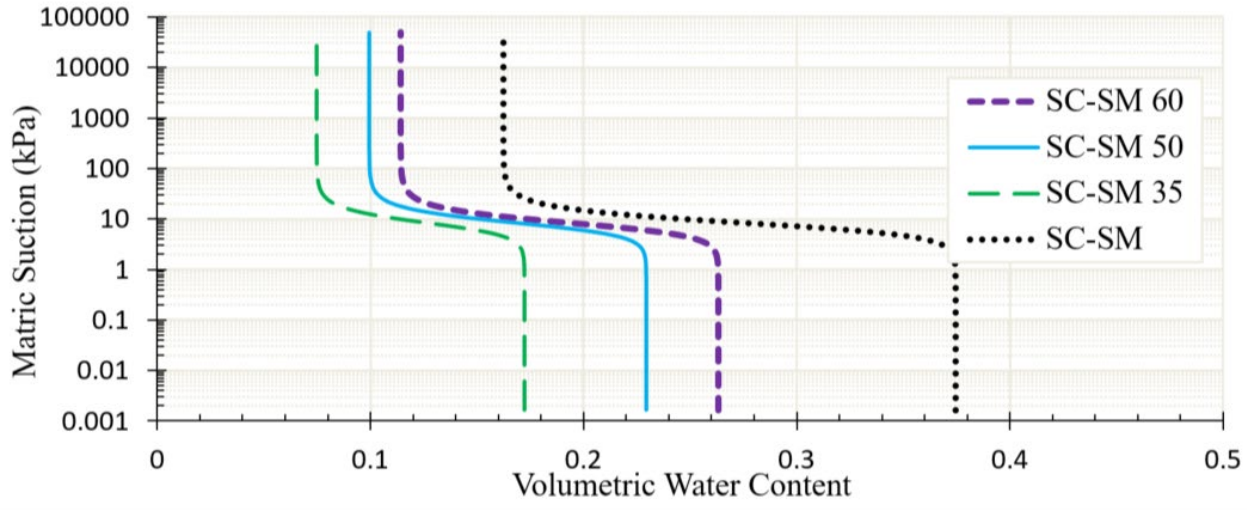

Figure B.15: Predicted SWCCs for SC-SM fouled ballast specimens

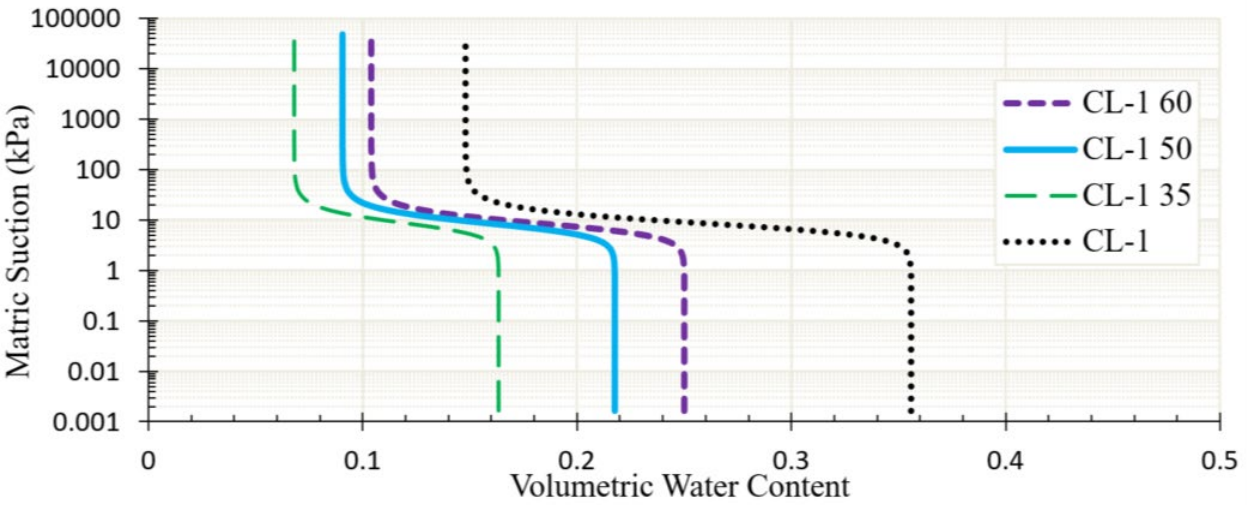

Figure B.16: Predicted SWCCs for CL-1 fouled ballast specimens

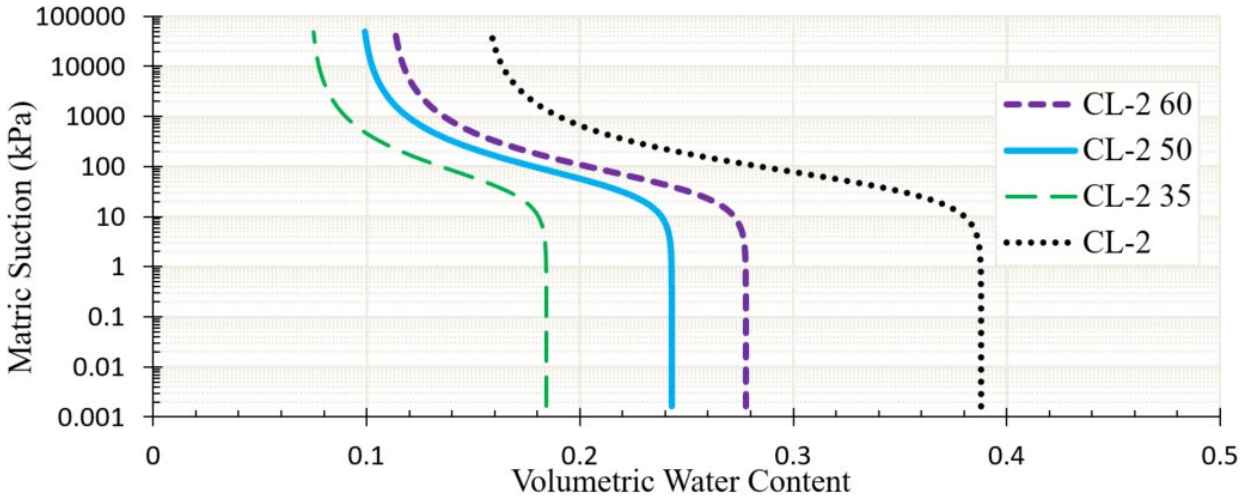

Figure B.17: Predicted SWCCs for CL-2 fouled ballast specimens

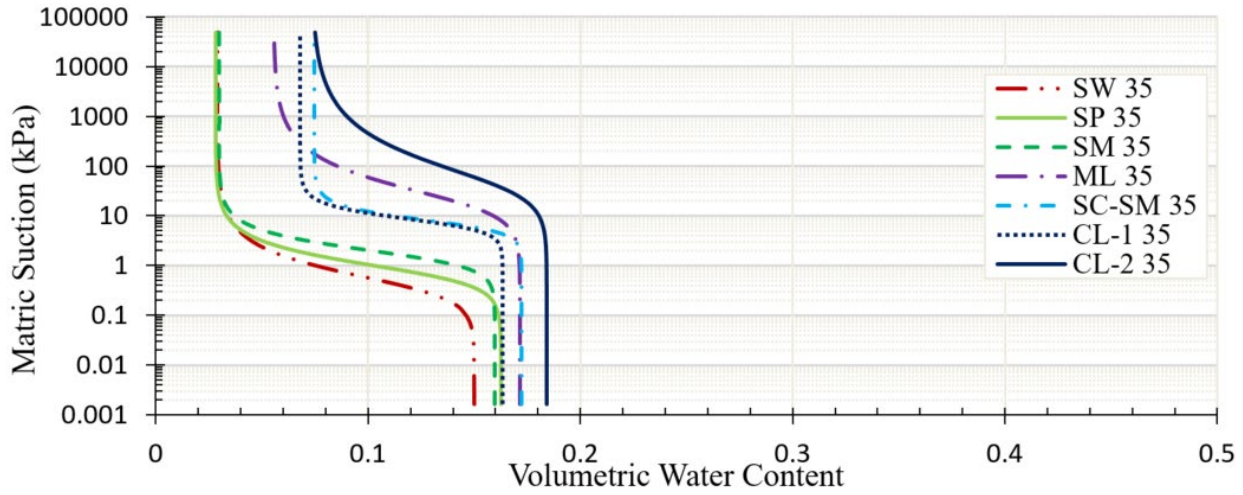

Figure B.18: SWCC summary for 35% fouled ballast specimens

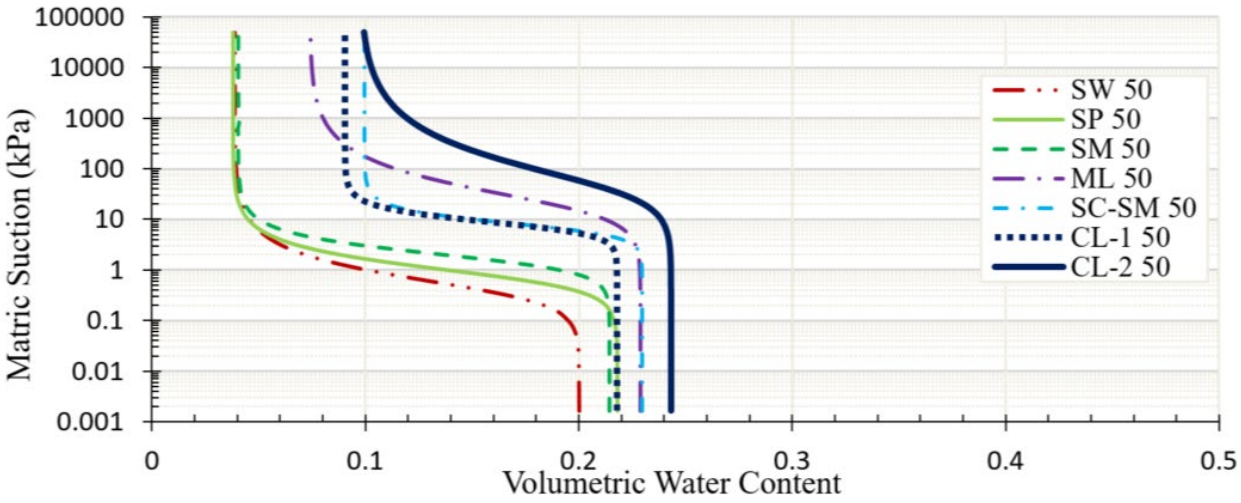

Figure B.19: SWCC summary for 50% fouled ballast specimens

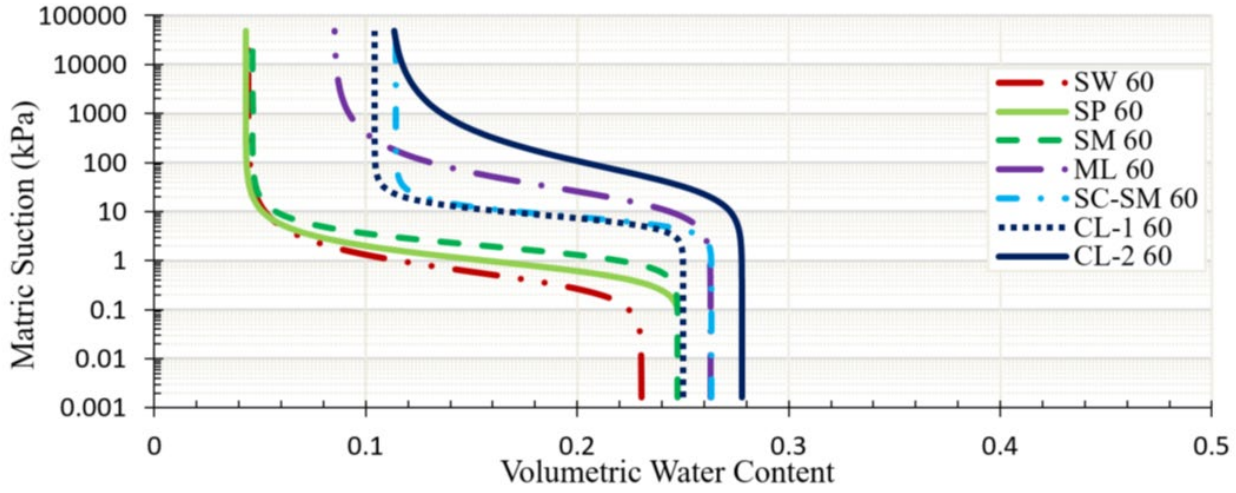

Figure B.20: SWCC summary for 60% fouled ballast specimens

Table B.3: Large TRIM Specimens Properties

Sample ID	FI	ρ_d(g/cm^3)	Porosity (%)	Gs
SP	-	1.74	34	2.64
SP 50	36	1.94	26	2.64
SP 22	15	1.94	27	2.64

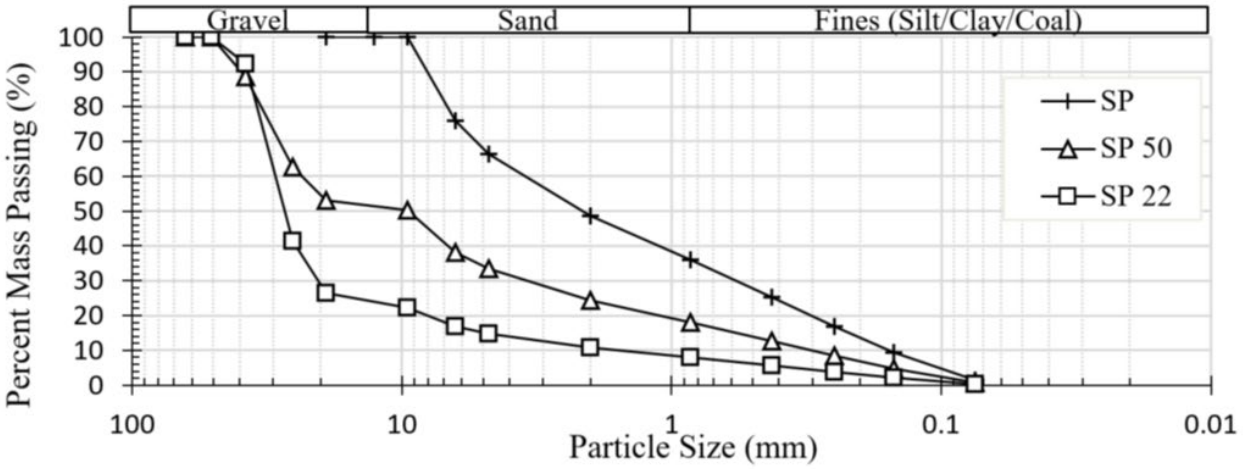

Figure B.21: GSD of fouled ballast specimen tested in the large TRIM

Table B.4: van Genuchten hydraulic parameters of large TRIM specimens

Sample ID	θ_r	$\alpha(1/\text{cm})$	n	m	$K_s(\text{cm/s})$
SP	0.045	0.147	2.21	0.548	1.80E-03
SP 50	0.054	0.122	2.97	0.664	1.14E-02
SP 22	0.020	0.287	3.50	0.714	8.98E-03

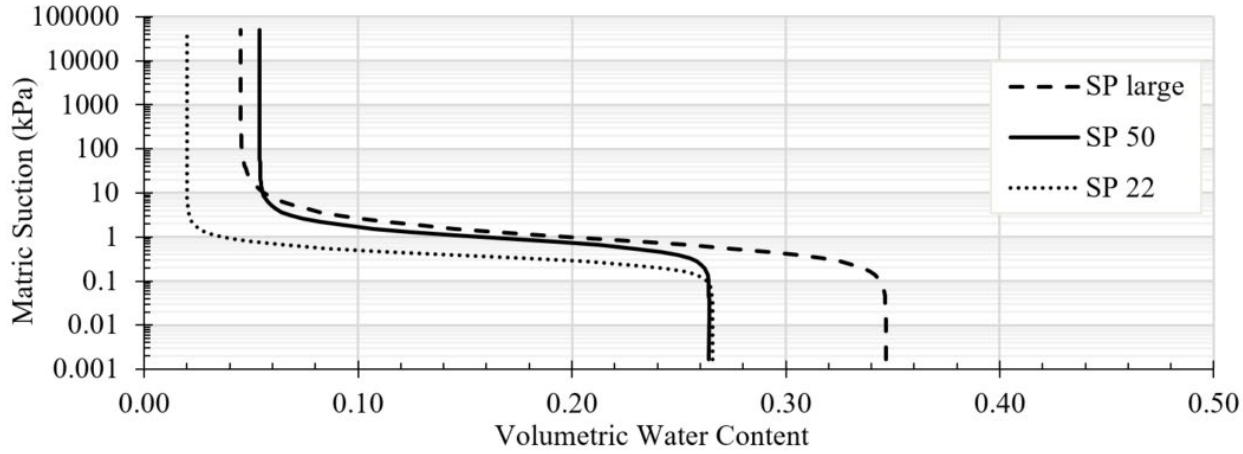

Figure B.22: SWCCs of specimens tested using the large TRIM

Abbreviations and Acronyms

ACRONYMS	EXPLANATION
AREMA	American Railway Engineering and Maintenance-of-Way Association
ASTM	American Society for Testing and Materials
FRA	Federal Railroad Administration
GPR	Ground Penetrating Radar
HAE	High Air Entry
LSDSS	Large-scale Direct Simple Shear
LSDS	Large-scale Direct Shear
CL	Low Plasticity Clay, according to the USCS
ML	Low Plasticity Silt, according to the USCS
MC	Mohr-Coulomb
SP	Poorly Graded Sand, according to the USCS
SC-SM	Silty, Clayey Sand, according to the USCS
SM	Silty Sand, according to the USCS
SWCC	Suction Water Characteristic Curves
TGA	Thermogravimetric Analysis
TRIM	Transient Water Release and Imbibition Method
USCS	Unified Soil Classification System
SW	Well Graded Sand, according to the USCS